



Comparative feasibility study of a
30 MW disruptive floater solution
with a 15 MW PivotBuoy and a
benchmark 15 MW
semi-submersible floater in the Bay
of Biscay

Multidisciplinary Project

Technical University Delft
TotalEnergies

Authors

Dimitri Tijdeman
Jan Stevens
Lukas Teuber
Mark Lonissen
Niels Roeders
Robbert Lip
November 9, 2023

CEGM3000

MULTIDISCIPLINARY PROJECT

**Comparative feasibility study of a 30 MW
disruptive floater solution with a 15 MW PivotBuoy
and a benchmark 15 MW semi-submersible floater
in the Bay of Biscay**

Authors:

Dimitri Tijdeman (4599020)
Jan Stevens (5647258)
Lukas Teuber (4922263)
Mark Lonissen (4448685)
Niels Roeders (4871006)
Robbert Lip (4906098)

Supervisors from TotalEnergies:

Marianna Rondon
Mattéo Capaldo
Arsim Ahmedi
Frédéric Gentil

Supervisors from Technical University Delft:

Frank Lange
Jeroen Hoving
Alex Kirichek

November 9, 2023

Abstract

This paper investigates the technical, life cycle, and economic feasibility of a 30 MW upscaled downwind turbine, comparing it to a 15 MW X1 Wind PivotBuoy downwind turbine and a benchmark 15 MW IEA Umaine VolturnUS-S upwind turbine in the 450 MW Sud de la Bretagne I wind farm site. The study is significant due to the rising energy demand, the potential for decreasing the levelized cost of energy with increased turbine size, and the optimized use of space. The size limit of current upwind turbine designs could be addressed using a downwind turbine solution.

The research is conducted by modelling the global dynamic response of the structure using **OpenFAST** and computing the natural frequencies and stresses using a finite element model. A lifecycle analysis is performed to identify potential pitfalls and bottlenecks by analysing the individual lifecycle phases. The economic feasibility is assessed by simulating the annual energy production using **TOPFARM** and utilizing structural analysis and lifecycle assessment to quantify capital, operational, and abandonment expenditures. Based on the annual energy production and the performance indicators the levelized cost of energy is calculated.

The findings indicate that while the global stability is within boundaries, the stress in members is too high with a simple scale-up of the proposed design. Bottlenecks are found in lifting operations and supply chain readiness. The levelized cost of energy and capital expenditure increased due to substructure self-weight, rendering the proposed 30 MW scale-up currently unfeasible when compared to the other two wind farms.

These findings are important as they demonstrate that the 15 MW X1 Wind PivotBuoy is not scalable without design changes. The levelized cost of energy does not decrease with an increased floater solution. The 15 MW X1 Wind PivotBuoy downwind turbine seems more economically viable, making it a more interesting option for future development.

Contents

Nomenclature	vii
1 Project description	1
1.1 Introduction	1
1.2 Upwind vs Downwind	1
1.3 Research Objective	2
1.4 Regional analysis	3
1.5 Methodology	4
1.6 Software	5
1.6.1 TOPFARM	5
1.6.2 PyWake	5
1.6.3 OpenFAST	5
1.7 Structure of Report	5
2 Wind Turbines	7
2.1 15 MW IEA VoltturnUS-S	7
2.2 15 MW X1 Wind PivotBuoy	8
2.3 30 MW solution	11
3 Environmental conditions	13
3.1 Wind	13
3.2 Waves	14
3.2.1 Significant wave height	15
3.2.2 Zero crossing period	16
3.3 Current	17
4 Structural analysis 30 MW solution	19
4.1 Introduction	19
4.2 Preliminary design	19
4.3 Global stability response	25
4.3.1 Method	25
4.3.2 Movement boundaries	26
4.3.3 Design load cases (DLC)	26
4.3.4 Dimensions from initial design tool	27
4.3.5 Assumptions and potential model improvements	28
4.3.6 Axial and member hydrodynamic drag coefficients	29
4.3.7 Heave plates	30
4.3.8 Final dimensions	31
4.3.9 Final design performance (DLC's applied)	32
4.3.10 Comparison to L. Trezza's model	33
4.4 Finite Element Analysis	33
4.4.1 Approach	33
4.4.2 Assumptions	33

4.4.3	Consequences and Limitations	35
4.4.4	Model set-up	35
4.4.5	Frequency spectrum	39
4.5	Detailed member design	42
4.5.1	Environmental loads	42
4.5.2	Deflections	45
4.5.3	Stresses	46
4.5.4	Ultimate limit state criteria	47
4.5.5	Structural improvements	48
4.6	Weight reduction	49
4.7	Turret: yaw system with elastic coupling	50
4.7.1	Selection of bearing type	51
4.7.2	Design Loads Cases	51
4.7.3	Bearing calculation - Static analysis following ISO 76	52
4.7.4	Bearing calculation - Fatigue analysis following ISO 281	52
4.7.5	Failure modes	53
4.8	Conclusion	54
5	Lifecycle Assessment	55
5.1	Supply chain	55
5.1.1	Wind turbine generator	56
5.1.2	Main columns	57
5.1.3	Pontoons	57
5.1.4	Damping plates	57
5.1.5	Pivot mast	57
5.1.6	Pivot top	58
5.1.7	Tower top adapter	58
5.1.8	Pivot bottom	58
5.1.9	Tethers	59
5.1.10	Anchors	59
5.1.11	Summary	59
5.2	Construction	60
5.2.1	Construction steps	60
5.2.2	Construction yards	61
5.3	Transport	64
5.3.1	Marshalling anchorages	64
5.3.2	Emergency anchorages	65
5.3.3	Transportation vessels	66
5.3.4	Distances	66
5.4	Installation	67
5.5	Operation & Maintenance	68
5.5.1	Maintenance strategies	68
5.5.2	Failure rates	69
5.5.3	Applied maintenance strategy	70
5.6	Decommissioning	71
5.7	Weather window	71
5.8	Conclusion	73
6	Economic Evaluation	75
6.1	AEP	75
6.1.1	Price of Energy	75
6.1.2	Wind farm optimization	76
6.1.3	Yaw Misalignment	78
6.1.4	Results	81

6.2	CAPEX	82
6.2.1	CAPEX 15 MW IEA	83
6.2.2	CAPEX 15 MW X1 Wind PivotBuoy	85
6.2.3	CAPEX 30 MW solution	91
6.2.4	CAPEX Comparison	96
6.2.5	CAPEX Uncertainties	97
6.3	OPEX	99
6.3.1	OPEX 15 MW IEA	99
6.3.2	OPEX 15 MW X1 Wind PivotBuoy	100
6.3.3	OPEX 30 MW solution	101
6.3.4	OPEX Comparison	102
6.3.5	OPEX Uncertainties	102
6.4	ABEX	103
6.4.1	ABEX 15 MW IEA	103
6.4.2	ABEX 15 MW X1 Wind PivotBuoy	104
6.4.3	ABEX 30 MW solution	104
6.4.4	ABEX Comparison	105
6.5	LCOE	105
6.6	Conclusion	107
7	Summary of results	109
7.1	Structural analysis	109
7.1.1	Preliminary design	109
7.1.2	Global stability analysis	109
7.1.3	FEM analysis	110
7.1.4	Turret analysis	110
7.2	Lifecycle assessment	111
7.2.1	Supply chain	111
7.2.2	Construction	111
7.2.3	Transport	111
7.2.4	Installation	111
7.2.5	Operation & Maintenance	111
7.2.6	Decommissioning	112
7.3	Economic Analysis	112
7.3.1	CAPEX OPEX ABEX	112
7.3.2	AEP	112
7.3.3	Wind-current misalignment effect on AEP	112
7.3.4	LCOE	112
8	Discussion and conclusion	114
8.1	Project outline	114
8.2	Discussion	114
8.2.1	Structural analysis	114
8.2.2	Life cycle assessment	115
8.2.3	Economic evaluation	115
8.3	Conclusion	116
8.4	Opportunities	117
A	TOPFARM and PyWake	119
A.1	Wind Farm Optimization	119
A.1.1	Wind turbine	119
A.1.2	Site	119
A.1.3	Constraints	119
A.1.4	Driver	120

A.1.5	Cost-model	120
A.1.6	Wake-model	120
A.1.7	Optimizing the farm level	122
B	Numerical modelling	123
B.1	Approach	123
B.2	Results	124
B.2.1	Pontoon left	124
B.2.2	Pontoon right	126
B.2.3	Pontoon front	128
B.2.4	Mast front right	130
B.2.5	Mast front left	132
B.2.6	Pivot mast (diagonal)	134
B.2.7	TLP	136
C	Turret failure modes	138
D	30 MW details OpenFAST	140

Nomenclature

Acronyms and Abbreviations

ABEX	Abandonment Expenditure
AEP	Annual Energy Production
AHV	Anchor Handling Vessel
ANEMOC	Atlas Numérique d'États de Mer Océaniques et Côtiers
BoP	Balance of Plant
CAPEX	Capital Expenditure
CFD	Computational Fluid Dynamics
CTV	Crew Transport Vessel
DLC	Design Load Case
DOF	Degree of Freedom
DTU	Danmarks Tekniske Universitet
DWT	Downwind Turbine
ECN	Energy research Centre of the Netherlands
EPEX	European Power Exchange
EMR	Énergies Marines Renouvelables
EWM	Extreme Wind Model
FCR	Fixed Charge Rate
FEM	Finite Element Method
FOWF	Floating Offshore Wind Farm
FOWT	Floating Offshore Wind Turbine
GW	Gigawatt
GWh	Gigawatt hour
HAWT	Horizontal-axis turbine
Hyd	Hydraulic systems
I&C	Installation & Commissioning
IEA	International Energy Agency
IRR	Internal Rate of Return
kW	kilowatt
kWh	kilowatt hour
LCOE	Levelized Cost Of Energy
MRE	Marine Renewable Energies
MW	Megawatt
MWh	Megawatt hour
NPV	Net Present Value

n_{wt}	Number of wind turbines
OEM	Original Equipment Manufacturer
OPEX	Operational Expenditure
RNA	Rotor Nacelle Assembly
SEM-REV	Site d'expérimentation en Mer pour la Récupération de l'Energie des Vagues
SPM	Single-Point-Mooring
TLP	Tension-Legged Platform
UWT	Upwind Turbine
VAWT	Vertical-axis turbine
WTG	Wind Turbine Generator
l&v	Logistics and Vessels

Chapter 1

Project description

1.1 Introduction

The current demand for renewable energy is unprecedented, with TotalEnergies setting the goal of increasing their renewable energy production to 50% of their total in 2050 [1]. To meet this target, a significant portion of this energy will need to be generated through offshore wind turbines. The emergence of floating wind technology in recent years has revolutionized offshore wind energy, allowing for the installation of turbines in deeper waters. This innovation opens up greater possibilities and expanses for offshore wind farms. Floating offshore wind turbines (FOWTs) offer a solution by enabling energy generation further from the shore, ultimately expanding available space for the industry and reducing conflicts in space-limited near-shore areas. The industry is pushing the boundaries of wind turbine sizes in the next decade predicting a reduction in per-megawatt project costs [2]. This leads to a trend towards larger turbines in the industry. These needs and trends are the underlying motivation for this project. The primary objective of this project is to assess the viability of a 450 MW floating offshore wind farm, consisting of fifteen 30 MW floating wind turbines, in the Bay of Biscay. The limits of the industry are investigated in the process.

Installing a 30 MW wind turbine with a 200-meter hub height and a 340-meter rotor diameter presents unique challenges, as this scale of installation has not been previously attempted. This report aims to identify and emphasize the challenges, pinpoint potential bottlenecks, and assess the economic and technical viability of installing such a turbine.

1.2 Upwind vs Downwind

The majority of wind turbines are designed as horizontal-axis turbines (HAWT), which offer greater efficiency and longer lifespans compared to their vertical-axis counterparts (VAWT). HAWT can have different setups based on the position of the rotor, resulting in two distinct configurations: upwind (UWT) and downwind (DWT) pictured in Figure 1.1. In the upwind configuration, the turbine blades face directly into the wind, allowing for maximum exposure to the airflow. Conversely, in the downwind configuration, the blades are positioned facing away from the wind. Advantages for downwind turbines are that they could potentially passively align with the wind, and the blades can be made less stiff [3].

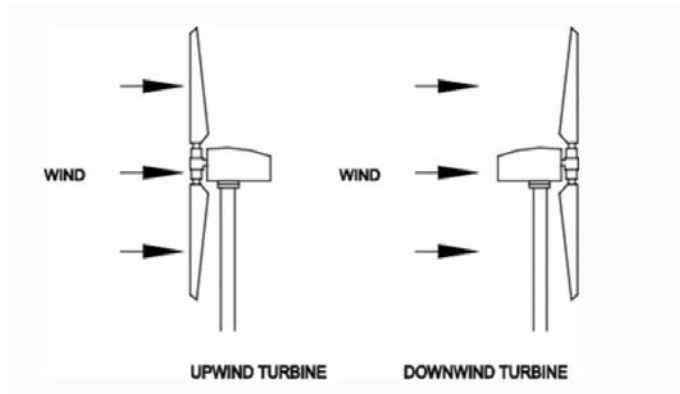


Figure 1.1: Schematic of UWT and DWT [4].

1.3 Research Objective

The offshore wind industry is reaching its limit with conventional tower-type structures because the first natural frequency is getting close to the 3P excitation with an increased rotor diameter. This created the development need for different tower structures. X1 Wind (founded in 2017) proposes a pyramid structure to replace conventional towers [5] with a downwind nacelle on top. With this concept X1 Wind also introduces the PivotBuoy, allowing the floater to weathervane around a single point. This enables the turbine to passively align with the wind, foregoing an active yaw system (more on that in chapter 2).

Based on the prior described trends and needs there is an interest from TotalEnergies to assess the structural and economic feasibility of a 30 MW disruptive floating solution. This results in the following research objective:

“Evaluate the feasibility of a 30 MW upscaled DWT and compare it economically to a 15 MW X1 Wind PivotBuoy DWT and a benchmark 15 MW IEA Umaine VoltturnUS-S UWT in the Bay of Biscay based on a 450 MW wind farm.”

Both the 15 MW IEA Umaine VoltturnUS-S UWT and a 15 MW X1 Wind PivotBuoy DWT are considered feasible for this study. This research is performed to create a first feasibility study on a 30 MW turbine upscale. It gives insight into the technical and economical difficulties and states the upsides and downsides of the project. The specific types of turbines are explained further in the research (see chapter 2).

To arrive at the research objective three distinct assessments are performed:

1. **Assess the direct scalability of the 15 MW X1 Wind PivotBuoy to a 30 MW solution.**
2. **Evaluate the feasibility of the supply chain, construction, transport, installation, operations, maintenance and decommissioning of the proposed 30 MW solution.**
3. **Compare the economic feasibility of the proposed 30 MW solution to the benchmark 15 MW IEA Umaine VoltturnUS-S and 15 MW X1 Wind PivotBuoy based on industry performance indicators.**

Figure 1.2 gives an overview of the project structure.

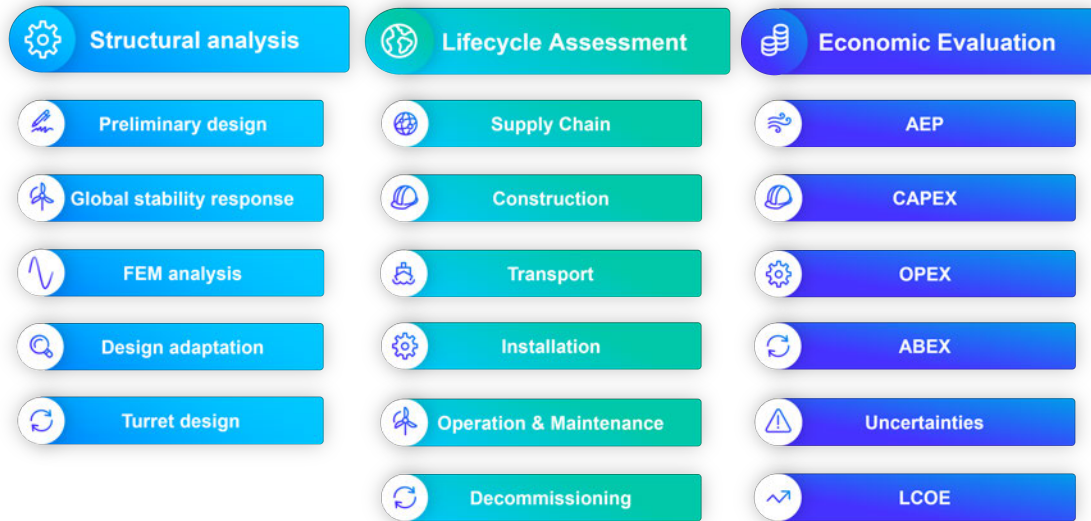


Figure 1.2: Overview of project structure.

1.4 Regional analysis

For this study, a wind farm situated in the Bay of Biscay is used. The Bay of Biscay is a gulf of the northeast Atlantic Ocean located south of the Celtic Sea. It lies on the western coast of France. In Figure 1.3 the location of the wind farm is marked with a red dot.



Figure 1.3: Overview of location, adapted from 4C offshore [6].

In terms of renewable energy, the Bay of Biscay is home to France's first offshore wind farm, Saint-Nazaire [7]. Located about 12 km off the coast, on top of the Banc de Guérande seabed formation in the northern part of the Bay of Biscay, this wind farm has a total capacity of 480 MW and

consists of 80 units of 6 MW Wind Turbine Generators. Given the depth of the Bay of Biscay, fixed wind turbines may not be suitable, but floating offshore wind turbines are a viable option. Bretagne has ambitious plans for offshore wind, with over 6 GW of wind parks in the pipeline [8]. Of this 6 GW, a significant portion is designated to be floating offshore wind farms (FOWF). One of these planned wind farms is Sud de la Bretagne I. An area in the Bay of Biscay specifically appointed for floating offshore wind, due to the high water depth. In Figure 1.4, the location of this area relative to Bretagne is shown in red.



Figure 1.4: Location of wind farm relative to Bretagne, adapted from 4C offshore [6].

1.5 Methodology

This section describes the methods used in this study to reach the end results. In order to derive a meaningful conclusion about the 30 MW solution, first a technical and life cycle feasibility will be performed specifically for the 30 MW solution. Then an economical comparison with a 15 MW IEA and 15 MW X1 Wind PivotBuoy is carried out. This leads to three distinct phases or analyses, shown in Figure 1.2.

The structural analysis involves a preliminary design of the substructure to arrive at the initial dimensions of the substructure; a global stability analysis to assess the dynamic response of the substructure; a Finite Element Method (FEM) model to evaluate the natural frequencies, modal shapes, displacements and stresses in the structure; a local stability check of the members; and a technical verification of the PivotBuoy.

The life cycle assessment evaluates the possibilities of the individual life cycle stages. This is done by comparing current industry standards with the proposed 30 MW design for the supply chain, construction, transport, installation, operations, maintenance and decommissioning. This is carried out to find bottlenecks and pitfalls in the up-scaled design.

The economic evaluation compares the three different designs based on their annual energy production (AEP), capital expenditures (CAPEX), operational expenditures (OPEX), and abandonment expenditure (ABEX), and uses these values to calculate the levelized cost of energy (LCOE). The lower this value is, the cheaper the energy and the more competitive the production method is.

For the 15MW X1 Wind PivotBuoy, a comparison is made to the claims made by X1, to see if their predictions on cost savings are right.

1.6 Software

This report comes with the enclosed software, code, and notebooks created during the project. For further information, refer to the `README` file. The following Python and MATLAB-based software tools were used in the process of creating this report.

1.6.1 TOPFARM

TOPFARM, developed by DTU Wind Energy, is a versatile Python package for optimizing wind farms, applicable to both onshore and offshore settings [9]. It utilizes `OpenMDAO` for optimization and interfaces with `PyWake` to efficiently compute a wind farm's AEP. Over the course of its development, TOPFARM has grown into a highly adaptable tool capable of addressing a variety of optimization challenges. It can handle different design variables and objective functions, making it a valuable asset for a wide range of optimization scenarios. Furthermore, the objective function `TopFarmProblem` can incorporate economic considerations, including various financial factors inherent in wind farm design. These factors cover financial balance, foundation costs, electrical costs (such as cabling), turbine component fatigue degradation, and Operation & Maintenance costs.

The optimization process is underpinned by `PyWake`, which computes wake losses and power production for individual turbines and entire wind farms using engineering wake models. In TOPFARM, the cost model component evaluates the objective function, which can be framed in terms of either power production or financial goals.

1.6.2 PyWake

`PyWake` is an open-source, Python-based wind farm simulation tool developed at DTU [10]. This adaptable tool is capable of performing a wide range of computations, including flow field analysis, power generation predictions for individual turbines, and the calculation of the AEP for entire wind farms.

`PyWake` is primarily designed to efficiently compute wake interactions within a wind farm across a range of steady-state conditions. Its application is particularly pertinent in assessing the power output of a wind farm, accounting for wake-induced losses within a specified layout configuration. Further information on the use of TOPFARM and `PyWake` is provided in Appendix A.

1.6.3 OpenFAST

“OpenFAST is a multi-physics, multi-fidelity tool for simulating the coupled dynamic response of wind turbines. Practically speaking, OpenFAST is the framework (or glue code) that couples computational modules for aerodynamics, hydrodynamics for offshore structures, control and electrical system (servo) dynamics, and structural dynamics to enable coupled nonlinear aero-hydro-servo-elastic simulation in the time domain.” OpenFAST uses many different modules; it uses `AeroDyn`, `HydroDyn`, `ElastoDyn`, `MoorDyn`, `InflowWind` and `ServoDyn`. [11] OpenFAST allows the user to model, besides upwind configuration turbines, downwind rotor floating wind turbines. The members are defined in `HydroDyn`, meaning that for the hydrodynamics, the Morison equation is applied.

1.7 Structure of Report

First, in chapter 2, the different turbines used in this report are described. Then, in chapter 3, the wind, wave, and current conditions used in this report are elaborated. After describing the

conditions, the three analyses are performed; chapter 4 shows the structural analysis, chapter 5 the life cycle assessment, and chapter 6 the economic evaluation. Each of these chapters closes with a sub-conclusion of the separate analysis. The three analyses are followed by a short summary of the results in chapter 7. Finally, in chapter 8, the results are discussed, final conclusions are drawn, and opportunities are given.

Chapter 2

Wind Turbines

2.1 15 MW IEA VoltornUS-S

The 15 MW IEA turbine, as defined by the International Energy Agency (IEA) [12], currently represents the largest publicly available reference turbine. The turbine design serves as a benchmark for future development in the offshore wind research and industry. The design is a collaboration between the National Renewable Energy Laboratory (NREL) and the Technical University of Denmark (DTU) as part of the IEA Wind Task 37. The turbine is supported by VoltornUS-S, a semi-submersible floater solution for the 15 MW IEA designed at the University of Maine (UMaine) [13]. In Table 2.1 the properties of the UMAINE 15 MW IEA turbine are defined. Figure 2.1 exhibits the 15 MW IEA reference turbine with the reference semi-sub floating platform.

Table 2.1: 15 MW IEA Reference Wind Turbine Parameters [13, 12].

Parameter	Value
Power rating [MW]	15.0
Rotor diameter [m]	250.0
Rotor orientation	UWT
Number of blades	3
Cut-in wind speed [m/s]	3.0
Rated wind speed [m/s]	10.59
Cut-out wind speed [m/s]	25.0
Hub height [m]	150.0
Tower base diameter [m]	10.0
Transition piece height [m]	15.0
Excursion (Length, Width, Height) [m]	90.1, 102.1, 290.0
Platform Type	semisubmersible
Mooring System	Three-line chain catenary
Freeboard [m]	15.0
Draft [m]	20.0
Substructure Mass [t]	3914
Tower Mass [t]	1263
RNA Mass [t]	991

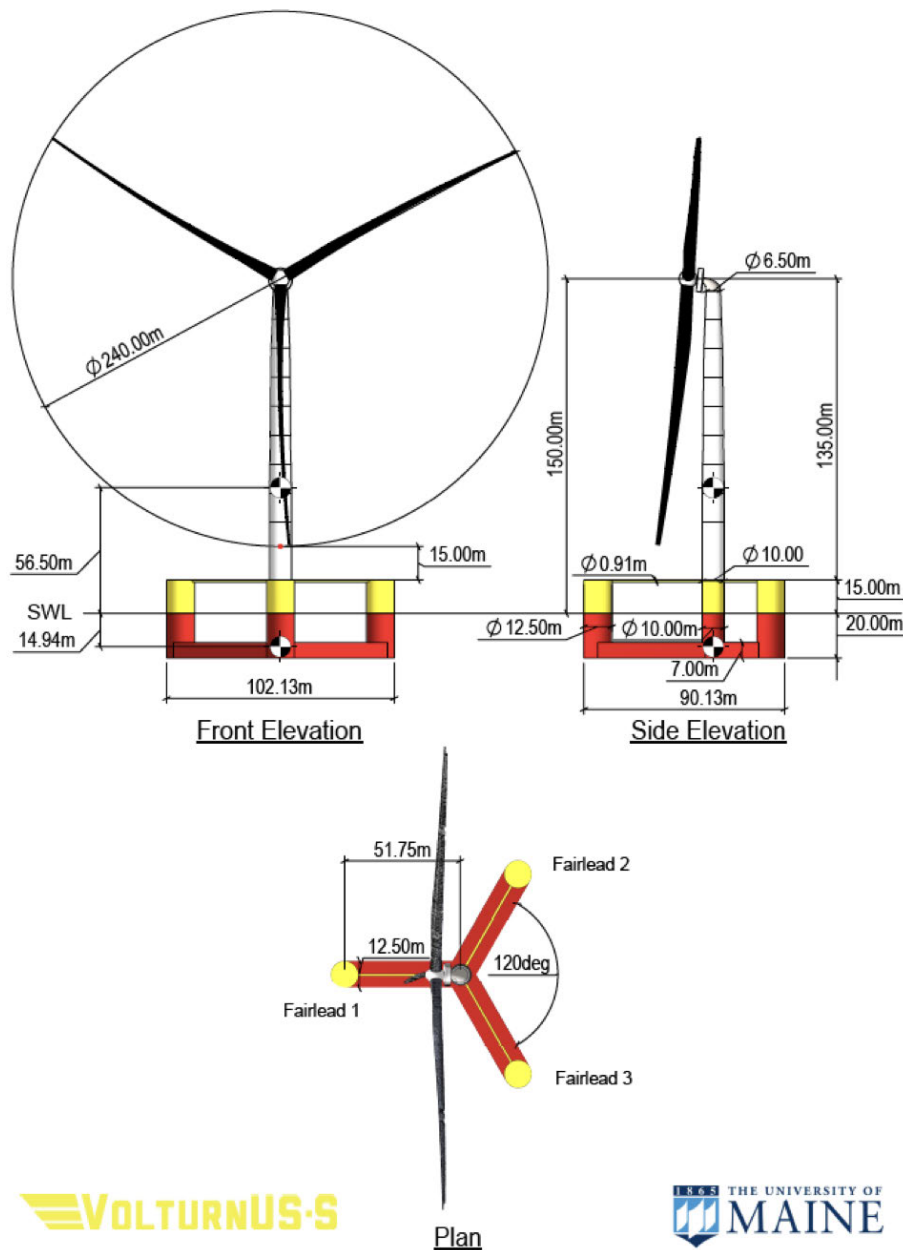


Figure 2.1: UMaine IEA 15 MW turbine with VoltturnUS-S semi-submersible floating platform [13].

2.2 15 MW X1 Wind PivotBuoy

The X1 Wind PivotBuoy is a wind turbine concept that is composed of a floating substructure with a DWT (X1 Wind), and a submerged tension-legged platform (TLP) with a single-point-mooring (SPM) attachment point (PivotBuoy) [5]. Figure 2.2 shows the X1 Wind PivotBuoy concept. The substructure supports the rotor nacelle assembly (RNA) through a triangular beam structure. This design is supposed to address the limits of conventional Wind turbines. Using this isostatic design X1 Wind claims to be more efficient than traditional tower designs, allowing for a significant weight reduction. One of the three columns of the substructure (Pivot Column) acts as a pivot point. This Pivot Column is linked to the underwater TLP mooring system. This,

in combination with the downwind turbine, allows the X1 Wind PivotBuoy to self-align in the wind. The X1 Wind PivotBuoy is equipped with a 15 MW downwind turbine. This turbine is modified from the 15 MW IEA reference turbine. The main modifications include the lack of an active yaw system, which would be redundant in a self-aligning configuration, and a downwind rotor configuration. The downwind rotor configuration allows the blades to be less stiff since they can bend away from the structure. This is supposed to create a weight reduction in the rotors of about 5% [14]. Figure 2.3 shows a schematic representation of the X1 Wind floating downwind platform wherein the PivotBuoy is integrated.



Figure 2.2: X1 Wind PivotBuoy concept.

The PivotBuoy combines the cables, mooring and anchoring systems into a single point. This enables a quick-connect system for faster connections between the floating platform and its mooring [5]. The SPM system, including a turret, ensures the PivotBuoy can freely revolve around this point, enabling the passive alignment with the wind. The PivotBuoy combines this SPM system with a TLP, allowing for an even higher reduction in weight when compared to catenary mooring solutions, since these solutions need a weighty active ballast system. PivotBuoy claim that weight reduction can be between 50 and 90% when compared to spar and semi-submerged structures, whilst also making installation easier when compared to current TLP solutions [5]. Note that these dimensions do not reflect the actual design by X1 Wind and PivotBuoy, as these are not published.

Table 2.2: 15 MW X1 Wind PivotBuoy Wind Turbine Parameters [5], [15].

Parameter	Value
Power rating [MW]	15.0
Rotor diameter [m]	250.0
Rotor orientation	DWT
Number of blades	3
Cut-in wind speed [m/s]	3.0
Rated wind speed [m/s]	10.59
Cut-out wind speed [m/s]	25.0
Hub height [m]	150.0
Tower base diameter [m]	-
Transition piece height [m]	-
Excursion (Length, Width, Height) [m]	100.0, 96.0, 290.0
Platform Type	pyramid floater
Mooring System	Tension Leg Platform
Freeboard [m]	15.0
Draft [m]	20.0
Substructure Mass [t]	2519.2
Tower Mass [t]	-
RNA Mass [t]	921.0

Table 2.3: 30 MW DWT Parameters, dimensions determined in section 4.1.

Parameter	Value
Power rating [MW]	30.0
Rotor diameter [m]	358.0
Rotor orientation	DWT
Number of blades	3
Cut-in wind speed [m/s]	3.0
Rated wind speed [m/s]	10.59
Cut-out wind speed [m/s]	25.0
Hub height [m]	204.4
Tower base diameter [m]	-
Transition piece height [m]	-
Excursion (Length, Width, Height) [m]	174.6, 207.0, 383.4
Platform Type	Pyramid floater
Mooring System	Tension Leg Platform
Freeboard [m]	10.0
Draft [m]	8.0
Substructure Mass [t]	8757.6
Tower Mass [t]	-
RNA Mass [t]	2306.1

Chapter 3

Environmental conditions

This chapter represents the relevant environmental conditions used for the design of the 30 MW upscale solution. The concerning data includes the data regarding wind, significant wave height, zero-crossing period and the current data. The data is used for different purposes, multiple sources are used to obtain the relevant data.

3.1 Wind

For the wind data, two data resources are used. The first data is extracted from a master thesis performed on the 15 MW X1 Wind PivotBuoy [15]. These values are utilized to make a comparison to the prior research by Trezza, chapter 4 will elaborate on the used data and conditions.

Further data from the Copernicus Climate Change Service is utilized. The data covers the period from 2003 to 2022 and measures the wind speed at 100 meters above sea level. The data is an hourly average from the original measurements. From this data, a time series and joint frequency table is created.

The average wind speed is at around 8 m/s and the directional maximum wind speed lies at around 30 m/s. The wind has two clearly dominant directions, from where the wind is most strong and most frequently occurring, namely around 270°N and around 60°N.

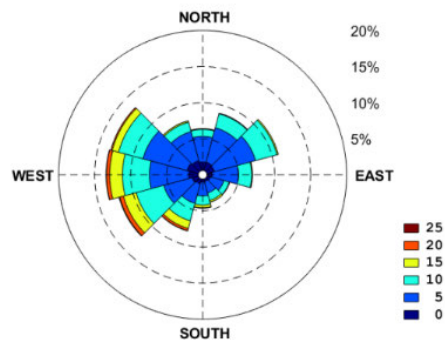


Figure 3.1: Annual wind rose at 100 meter height [16].

Table 3.1: Annual direction of sample distribution (%) [16].

Wind (m/s)	0°	30°	60°	90°	120°	150°	180°	210°	240°	270°	300°	330°	Omni
<2	0.27	0.23	0.22	0.20	0.20	0.19	0.20	0.23	0.23	0.27	0.28	0.28	2.80
2 ≤ U < 4	0.87	0.86	0.80	0.64	0.53	0.48	0.52	0.61	0.73	0.92	1.08	0.99	9.02
4 ≤ U < 6	1.45	1.62	1.59	1.07	0.77	0.62	0.70	0.94	1.21	1.73	2.02	1.63	15.34
6 ≤ U < 8	1.60	2.12	2.35	1.48	0.82	0.71	0.78	1.11	1.65	2.26	2.68	1.86	19.43
8 ≤ U < 10	1.12	1.91	2.64	1.54	0.72	0.61	0.74	1.20	1.76	2.21	2.53	1.43	18.43
10 ≤ U < 12	0.64	1.32	1.96	1.16	0.46	0.57	0.64	1.12	1.81	1.79	1.89	0.83	14.18
12 ≤ U < 14	0.28	0.58	0.95	0.58	0.25	0.38	0.44	1.00	1.52	1.42	1.23	0.42	9.04
14 ≤ U < 16	0.11	0.17	0.31	0.21	0.11	0.21	0.30	0.73	1.17	1.02	0.71	0.19	5.23
16 ≤ U < 18	0.04	0.04	0.06	0.04	0.02	0.13	0.17	0.47	0.80	0.82	0.39	0.08	3.05
18 ≤ U < 20	0.01	0.00	0.01	0.01	0.01	0.03	0.08	0.29	0.50	0.47	0.22	0.03	1.66
20 ≤ U < 22	0.00	0.00	0.00		0.00	0.01	0.04	0.17	0.33	0.28	0.12	0.01	0.97
22 ≤ U < 24	0.00				0.00	0.00	0.02	0.11	0.18	0.13	0.04	0.00	0.50
24 ≤ U < 26	0.00					0.00	0.00	0.05	0.08	0.07	0.01	0.00	0.22
26 ≤ U < 28	0.00					0.00	0.00	0.03	0.04	0.02	0.00	0.00	0.10
28 ≤ U < 30	0.00						0.00	0.01	0.01	0.00	0.00	0.00	0.03
30 ≤ U							0.00	0.00	0.01	0.00	0.00	0.00	0.01
Total (%)	6.40	8.86	10.88	6.93	3.89	3.94	4.63	8.06	12.03	13.42	13.21	7.76	100.00
Mean (m/s)	6.99	7.71	8.32	8.06	7.28	8.31	8.77	10.35	10.88	10.07	8.90	7.37	8.85
Max (m/s)	28.40	20.65	20.79	19.76	23.24	27.36	30.49	36.49	36.30	37.69	32.64	35.84	37.69

3.2 Waves

For the first case, the wave data obtained is again from [15]. The wave values for the different design load cases are used from this master thesis to compare the 30 MW solution. These values will be explained in chapter 4.

The second situation uses wave data from the Copernicus Climate Change Service. The data covers the period from 2003 to 2022 and measures the wave height and zero-crossing period. The data is hourly averaged from the original measurements.

The extreme conditions are computed in terms of return values obtained by means of extreme value analyses. This is done by means of a detailed analysis of the available hourly reanalysis ERA5 data (The data was downloaded from the Copernicus Climate Change Service). The considered data are 1-hour average values from 2003 until 2022 to give a representative size to perform an extreme value analysis.

The following steps are taken to ensure a reliable extreme value analysis. (1) The threshold of the data set is selected by determining the mean excesses and using the Peak Over Threshold method to guarantee that the chosen extremes are independent, (2) the extremes are fitted to a Generalized Pareto distribution and using a QQ (Quantile-Quantile plot) and the PP-plot (Probability-Probability plot) the goodness of fit of the distribution is assessed, (3) the return period is plotted.

The return period for the wave conditions in the case of an offshore wind substructure is defined to be 50 years. The values for the wave data can be extracted from the graph created, these values will later on be used to determine the JONSWAP spectrum.

3.2.1 Significant wave height

As explained above, the first step is to determine the threshold for the extreme value analysis (see Figure 3.2). To determine a reliable value, the threshold number should be picked until the line stops behaving linearly.

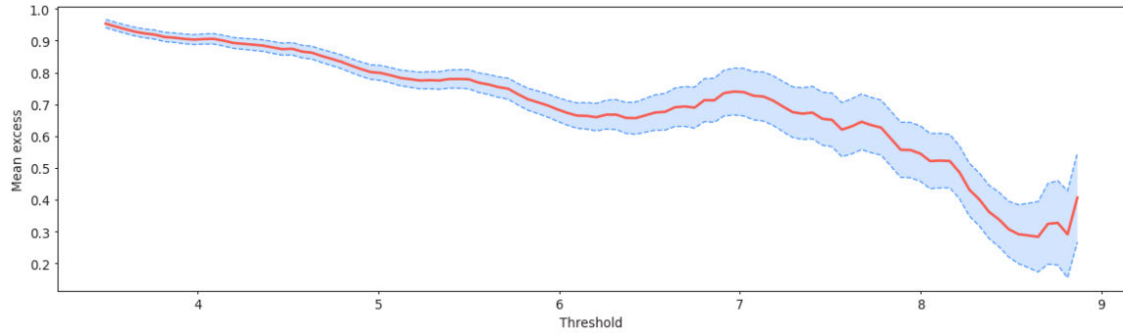


Figure 3.2: Threshold significant wave height.

In this case, the chosen threshold is 5.2 m/s. Now the extreme value analysis can be done with peak over threshold where the declustering time is 48 hours to ensure the wave heights are independent of each other.

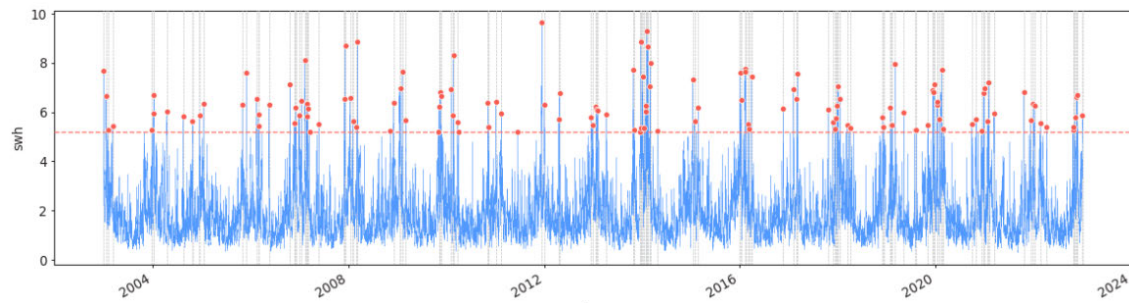


Figure 3.3: Extreme value significant wave height.

The last step is to fit the extreme values into a distribution. With this information, a prediction can be made for the return period of 50 years (see Figure 3.4)

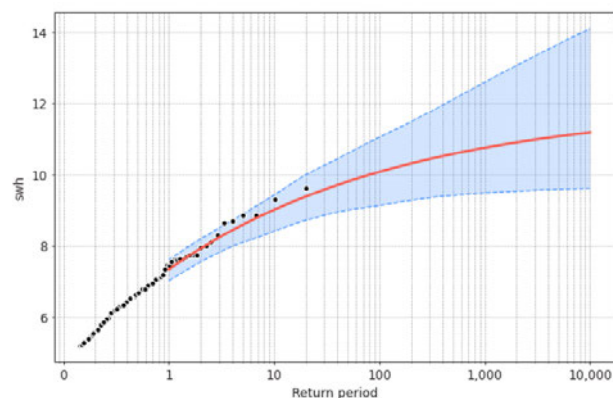


Table 3.2: Return period of significant wave height.

Return period [y]	Return value [m]
1	7.3
5	8.6
10	9.0
25	9.5
50	9.8

Figure 3.4: Return period significant wave height.

3.2.2 Zero crossing period

The threshold for the zero crossing period is chosen as 10 sec. Now the extreme value analysis can be done with a peak over threshold where the declustering time is 48 hours to ensure the zero crossing periods are independent of each other (see Figure 3.6).

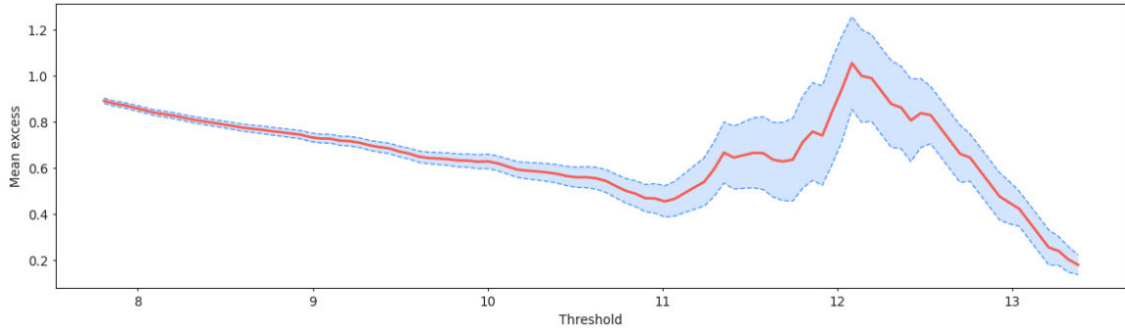


Figure 3.5: Threshold zero-crossing wave period.

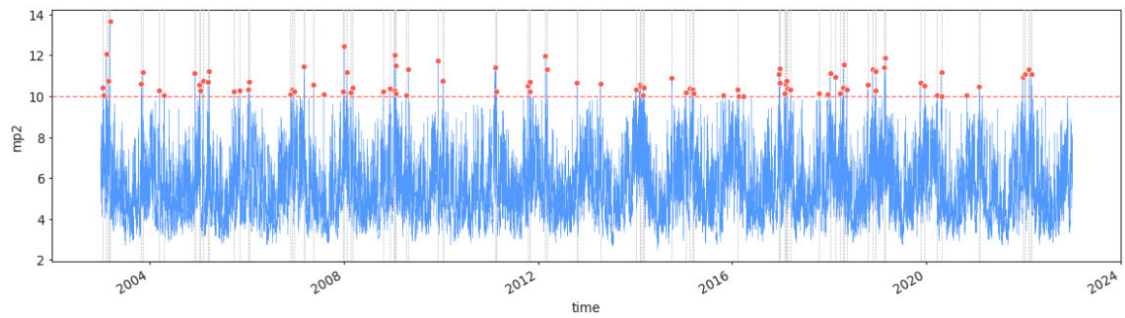


Figure 3.6: Extreme values zero-crossing wave period.

The last step is to fit the extreme values into a distribution. With this information, a prediction can be made for the return period of 50 years (see Figure 3.7).

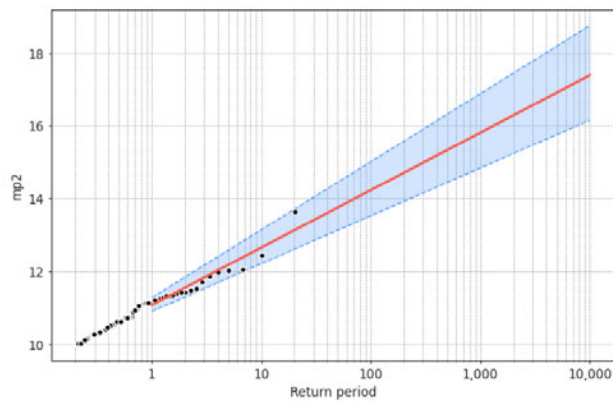


Table 3.3: Return period of zero-crossing period.

Return period [y]	Return value [s]
1	11.1
5	12.2
10	12.7
25	13.3
50	13.8

Figure 3.7: Extreme values zero-crossing wave period.

3.3 Current

Due to the limited availability of current velocity data at the site location, data from the SEM-REV report [16] is utilized to obtain reliable results. This report consists of the environmental conditions of a site 40 kilometres from the Sud de la Bretagne I site Figure 3.8. In the case of this preliminary study, the conditions are considered to be sufficient.

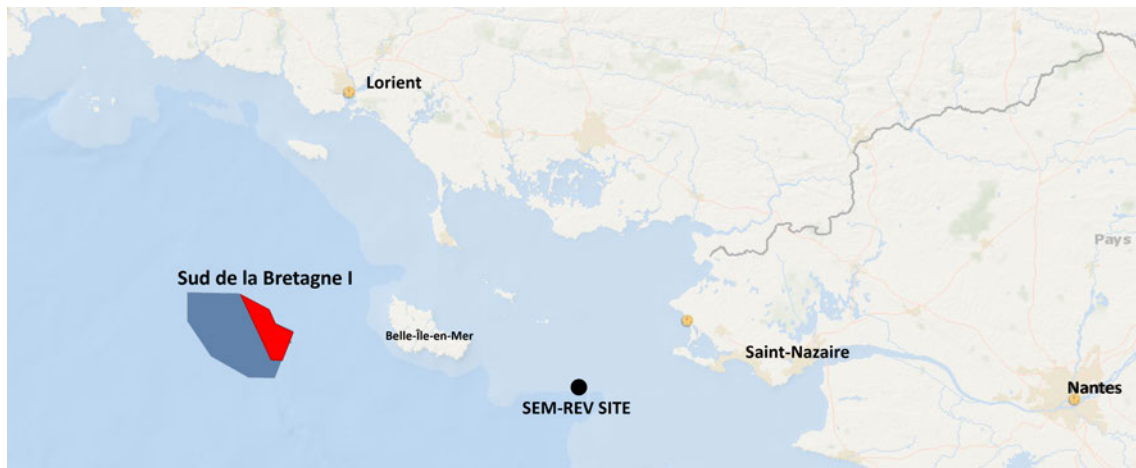


Figure 3.8: Location of Sud de la Bretagne I and SEM-REV Site [6].

Predominantly, the currents originate from two primary directions: the southwest (210°N) and the northeast (45°N). This current data serves a dual purpose: firstly, it is employed to calculate the misalignment, and secondly, it plays a pivotal role in determining various loading scenarios.

In Figure 3.9 and Table 3.4, a visual representation of the data is given. The first graph illustrates the distribution of current velocities, while the second showcases an annual sample distribution, highlighting the correlation between currents and their respective directions.

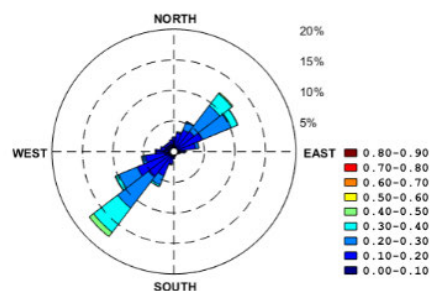


Figure 3.9: Current velocity distribution [16].

Table 3.4: Annual direction of sample distribution (%) [16].

Current U (m/s)	0°	15°	30°	45°	60°	75°	90°	105°	120°	135°	150°	165°	180°	195°	210°	225°	240°	255°	270°	285°	300°	315°	330°	345°	Omni	
0 <= U < 0.1	1.12	0.92	0.72	0.61	0.62	0.88	0.89	0.74	0.64	0.58	0.59	0.65	0.78	0.88	0.93	0.84	1.13	1.48	1.53	1.43	1.31	1.27	1.23	1.24	23.02	
0.1 <= U < 0.2	1.24	2.17	3.15	3.53	4.45	2.71	0.87	0.28	0.12	0.07	0.08	0.13	0.36	1.19	3.34	4.40	5.38	3.27	1.41	0.76	0.50	0.44	0.48	0.72	41.03	
0.2 <= U < 0.3	0.05	0.19	1.36	5.35	5.10	0.54	0.07	0.01	0.01	0.00	0.00	0.01	0.03	0.13	1.63	6.39	3.27	0.54	0.13	0.04	0.01	0.01	0.01	0.01	0.02	24.91
0.3 <= U < 0.4	0.00	0.00	0.11	2.47	1.14	0.02	0.01						0.00	0.00	0.02	0.31	4.99	0.60	0.07	0.01						9.76
0.4 <= U < 0.5		0.00	0.01	0.22	0.05	0.00									0.00	0.02	0.89	0.08	0.00							1.27
0.5 <= U < 0.6			0.00		0.00											0.01	0.00									0.01
0.6 <= U < 0.7																										
0.7 <= U < 0.8																										
0.8 <= U < 0.9																										
0.9 <= U < 1																										
Total (%)	2.40	3.29	5.34	12.18	11.37	4.15	1.85	1.03	0.77	0.65	0.67	0.79	1.17	2.22	6.23	17.52	10.46	5.37	3.09	2.23	1.82	1.72	1.72	1.98	100.00	
Mean (m/s)	0.11	0.13	0.17	0.23	0.21	0.14	0.11	0.08	0.07	0.07	0.07	0.07	0.09	0.12	0.17	0.25	0.18	0.13	0.11	0.09	0.09	0.08	0.09	0.09	0.18	
Max (m/s)	0.31	0.42	0.50	0.50	0.50	0.40	0.36	0.30	0.30	0.26	0.26	0.30	0.39	0.40	0.47	0.56	0.57	0.46	0.38	0.29	0.25	0.24	0.23	0.27	0.57	

Chapter 4

Structural analysis 30 MW solution

4.1 Introduction

The goal of the structural analysis is to investigate whether the direct scalability of the X1 Wind PivotBuoy concept is feasible as a 30 MW solution. This is done by the following analyses. Firstly, a model defining the preliminary dimensions of the substructure is set up. With this, it is possible to dimension the floaters, horizontal and diagonal elements that together form the substructure. These dimensions are found through Euler buckling rules and moment equilibrium, ensuring no tension in the pivot connector system. The preliminary design tool will give a multitude of design variants that can be checked in the upcoming analysis which ensure no tension in the turret system.

With the preliminary global design options, it is possible to move forward into the global stability analysis using openFAST. The previously synthesized global design options are loaded into openFAST, where the wind, wave, and current forces are dynamically modelled on the structure. As an output, the pitch and heave characteristics are of great importance. For a design to suffice, these characteristics need to fall under a certain threshold for different design load cases. When a design proposed by the preliminary Python model does not suffice these demands, another design variant is picked with different floater diameters and spacing. This finally gives a validated preliminary design with global stability of the turbine upscale solution.

With the validated preliminary design, it is possible to move into a deeper, more detailed, design. For this, a FEM model is set up to first perform a modal analysis. From this, the eigenfrequencies of the solution can be found. These are checked towards the wave spectrum, wind spectrum, and dynamic rotor regions. These eigenfrequencies can not align with these frequency spectra and range to counteract resonance. After the natural frequencies analysis, wave forces are put on the model and the deflections and stresses in the members are checked. Finally, the occurring stresses in all the members are checked with the steel strength and given a unity check.

4.2 Preliminary design

To determine the preliminary design of the substructure of the floater for the 30 MW wind turbine, a Python notebook created by the TU Delft, is adapted. This notebook allows for the calculation of the buoyancy of a system in a static situation. The model includes classes where rectangular and circular shapes can be created. Subsequently, the weight and buoyancy forces of these elements can be calculated.

In Equation 4.1 the equation that is used to determine the weight of the different elements of the floater is elaborated. In Equation 4.2 the equation to calculate the buoyancy force is shown. In the

model, a more elaborated function is set up. In this model, the finite difference method is used. The midpoint of a certain structural component is defined. hereafter, it creates multiple points in the shape that is determined in the class. All these points are connected by elements. These elements together establish the structural component from which the buoyancy and weight can be calculated with the equation mentioned below.

$$F_{weight} = \rho\pi(r_o - r_i)^2h \quad (4.1)$$

Where:

r_o = outer diameter

r_i = inner diameter

h = height

ρ = material density

$$F_{buoyancy} = \rho\pi r_o^2 h_d g \quad (4.2)$$

Where:

r_o = outer diameter

g = gravity

h_d = draft

ρ = fluid density

The benefit of this method is that a certain draft can be assigned to this structure. Which allows the option to take the spacing and the diameter of the floater as variables.

One of the main design issues with the PivotBuoy system is that the pivot connection will endure high fatigue if exposed to alternating tension and compression forces. This will dramatically shorten the lifetime of the system and, thus is highly unwanted. For this reason, it is chosen to optimize the spacing between the floaters and the floater diameter based on a reaction force that is close to zero in the pivot connector during maximum thrust force. This ensures that there will always be a compressive force in this connector and tension will never occur. In order to find the force in the connector floater the following steps are executed:

- The moment in the pivot connector is calculated, which incorporates maximum thrust force, buoyancy forces, and self-weight.
- This moment is counteracted in the pivot floater (floater A) by finding the extra buoyancy necessary in the floaters B.
- Through a vertical equilibrium of the entire system, the vertical force in floater A can be found.

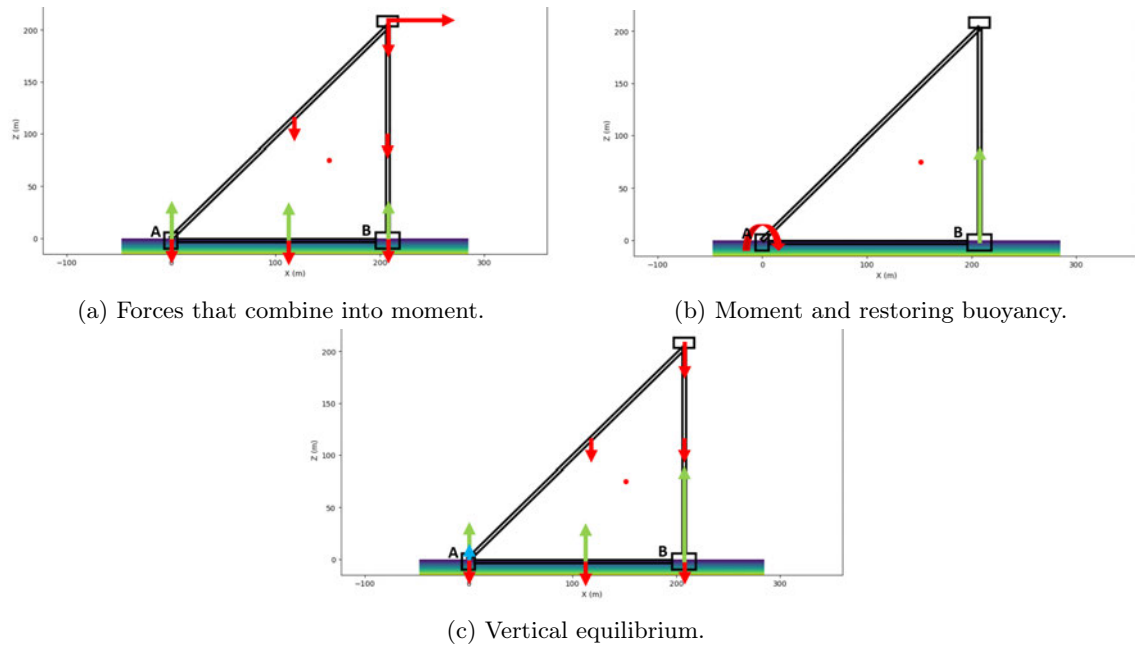


Figure 4.1: Forces and moments.

In Figure 4.1a the forces that are taken into account for this moment equilibrium are displayed. Here, the red forces are due to the weights and thrust force and the green forces are the Buoyancy forces. The moment is taken around floater A. Figure 4.1b shows the moment around floater A in red and the restoring buoyancy force in floater B in green. Finally, Figure 4.1c shows the vertical equilibrium. The restoring force in floater B is shown in green, all the weights and buoyancies are shown in blue and the force in floater A is shown in red.

With these three steps, an optimization can be run to find the optimal trade-off between the spacing of the floaters and their diameters. In Table 4.1 an overview is given which distinguishes the fixed and optimized parameters.

Table 4.1: Overview parameters.

Fixed parameters	Variables
Draft	Floater spacing
Height pontoon	Diameter floater B
Hub height	Diameter connectors
Diameter floater A	Thickness connectors

Important to mention is that the diameter and thickness of the connectors depend on the length of the connectors. In the model, two rules are applied to determine this. The first rule is Euler-Buckling (see Equation 4.3 and the second one is a rule of thumb provided by the TU Delft specifically for offshore structures (see Equation 4.4 & Equation 4.5. By comparing the results of these methods, the most critical one is determined to be the most sufficient.

$$F_{cr} = \frac{\pi^2 EI}{L^2} \quad (4.3)$$

$$D = 0.018L \quad (4.4)$$

$$t = \frac{D}{40} \quad (4.5)$$

This is done by recalculating this force in floater A for numerous different combinations of spacing and diameter. This is made visibly in Figure 4.2, where the x-axis is the floater diameter in meters, the y-axis is the force in the connector in Newton, where a negative number is tension and a positive is compressive. Finally, the different line colours depict the different spacings between the floaters. With this, all possible design variants which ensure no tension can be found. These are denoted as the black dots in the optimization graph. The design that was eventually deemed globally stable is the green one, which has a diameter of 27.5 m and a spacing of 230 m.

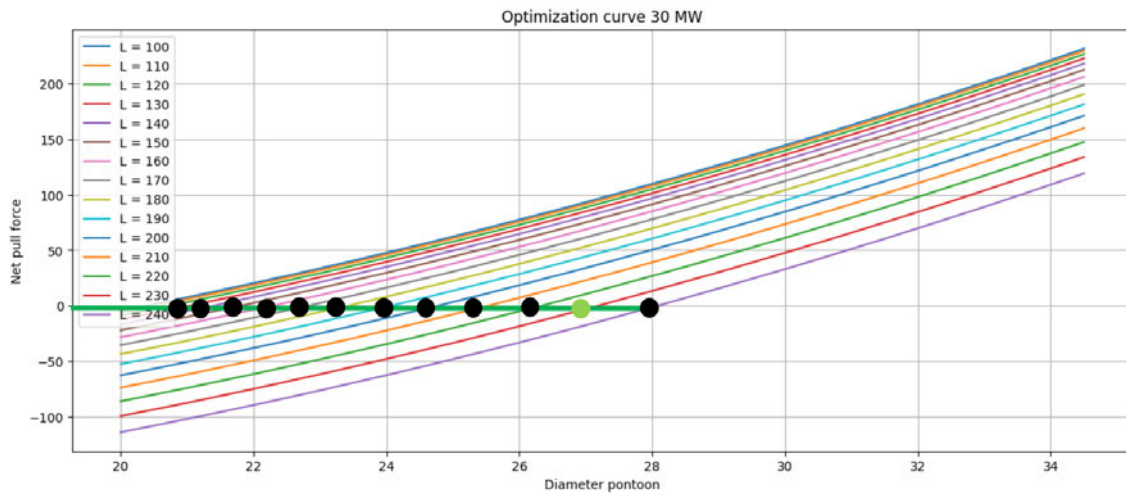


Figure 4.2: Optimization process which ensures no tension in the connector.

After finding the spacing and diameter of the floaters, the dimensions of the connecting elements are found through Euler buckling rules. This gives a cross-section based on the length of the element and forms a preliminary value for the design. After this step, only the height of the pontoons needs to be determined. This height of the pontoon needs to be big enough such that during the maximum thrust force, the needed restoring force in floater B is present. For this, the scenario where floater B is fully submerged is considered. During this full submergence, the restoring buoyancy needs to be bigger than the downward force caused by the maximum thrust. Figure 4.3 shows the equilibrium between this thrust force and the maximum submergence of floater B. It is found that for a floater height of 15.5 m, the restoring force due to buoyancy is larger than the maximum thrust, thus ensuring that maximum submergence of the floater will not occur. In Table 4.2, the dimensions found in the preliminary design tool and used in the rest of the structural analysis are used.

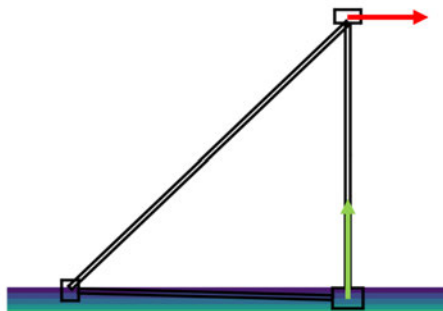


Figure 4.3: Full submergence of pontoon B analysis.

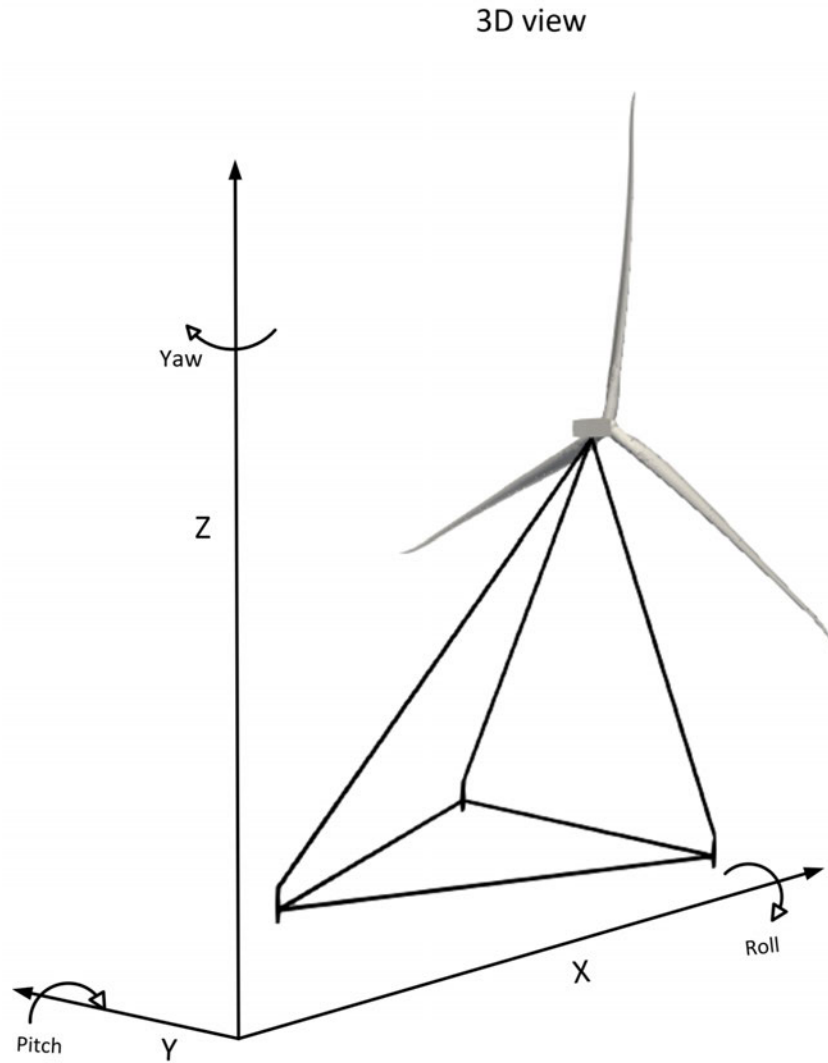


Figure 4.4: 3D representation of 30 MW PivotBuoy design.

Table 4.2: Dimension results from preliminary design.

Element	Diameter [m]	Thickness [m]	Freeboard [m]
Pivot column	19	0.07	10
Nacelle column	27.5	0.07	8
Pontoon	3.69	0.06	-
Nacelle masts	3.47	0.06	-
Pivot mast	5.47	0.09	-
Center to center width of platform [m]		207	-
Draft [m]		8	-

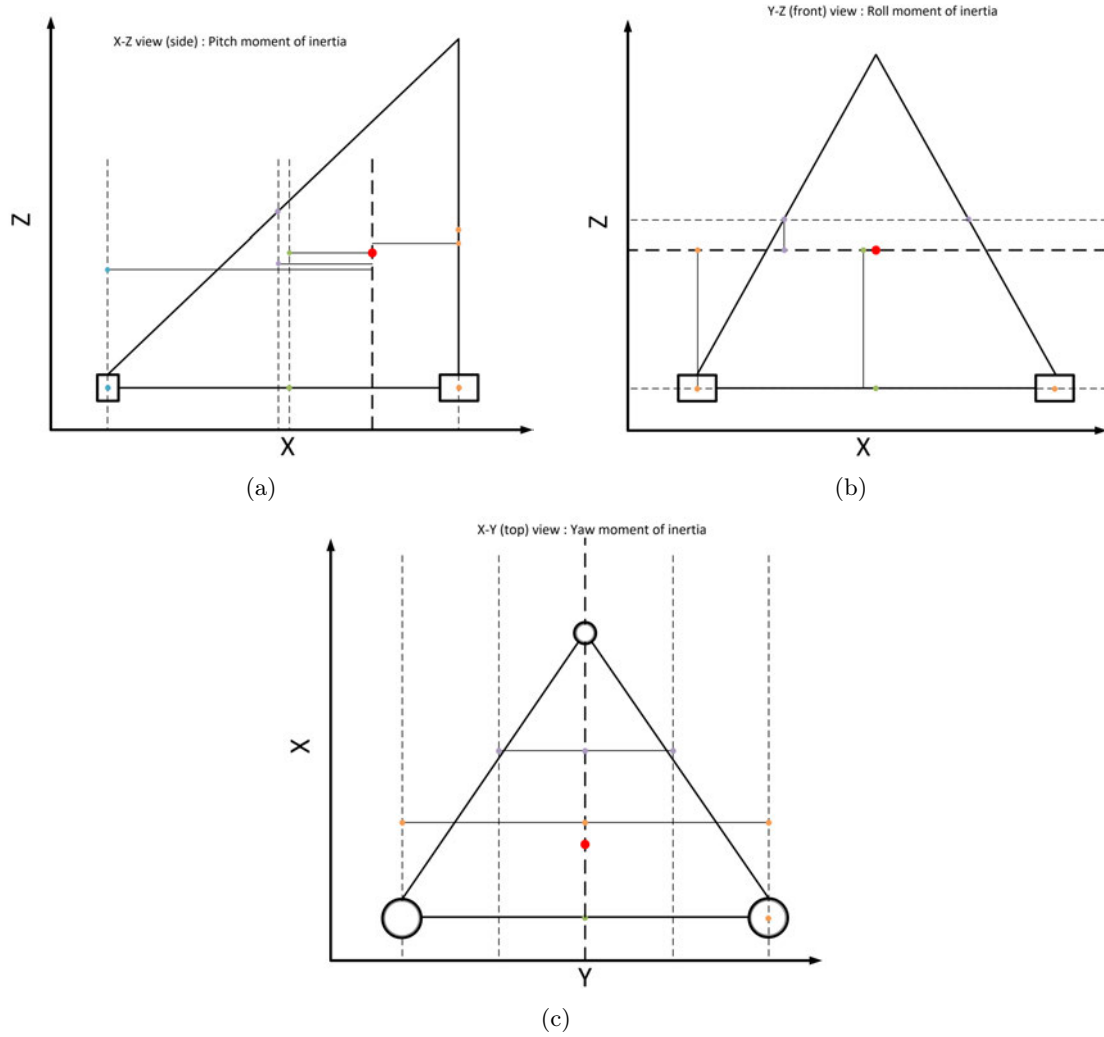


Figure 4.5: Three cross sections of the PivotBuoy necessary for the representative distances to find the pitch, roll, and yaw inertias.

The last part of the preliminary design of the substructure is to determine the mass moment of inertia of the yaw, pitch and roll. Yaw is the movement around the z-axis, pitch is the movement around the y-axis and roll is the movement around the x-axis, as seen in Figure 4.4. The mass moment of inertia is a measure of how much resistance an object has to changes in its rotational motion. To determine these mass moments of inertia, the Parallel axis theorem is used to establish the resistance the entire substructure experiences. The parallel axis theorem (Steiner's rule) is described in Equation 4.6 and is composed of two parts. The first part is the mass moment of inertia of the structural component itself and the second part is composed of the mass and the distance of the normal axis of the structural component towards a parallel axis through the centre of gravity of the structure, as seen in Figure 4.5a - 4.5c. A simplified parallel axis for the diagonal components is adapted.

$$I = \sum_{i=1}^k (I_{cm,i} + m_i d_i^2) \quad (4.6)$$

To find the individual moments of inertia for the different structural components, different equations are used for the different axes possible through our circular hollow sections. If the cross-section

view has a normal axis through the hollow section, the equation of I_z is used, as shown in Figure 4.6. This will only occur in the x-y (top view) for the floaters. In case the cross-section view has a normal axis through the "rectangular" section, equation $I_x = I_y$ is used. This simplifies the diagonal components as well. The final moment of inertias for the pitch, roll, and yaw directions can be found in Table 4.3

Mass moment of inertia about x axis	$I_x = (m/12) * (3*(R_2^2 + R_1^2) + h^2)$
Mass moment of inertia about y axis	$I_y = (m/12) * (3*(R_2^2 + R_1^2) + h^2)$
Mass moment of inertia about z axis	$I_z = (m/2) * (R_1^2 + R_2^2)$

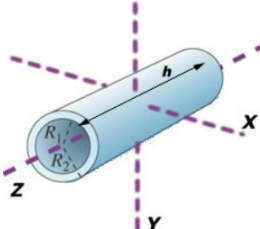


Figure 4.6: Different moments of inertia based on axis for circular hollow sections [17].

Table 4.3: Pitch, roll and yaw moment of inertias.

Rotation direction	Inertia [kg/m ²]
Pitch	14.85E+10
Roll	26.41E+10
Yaw	16.22E+10

4.3 Global stability response

4.3.1 Method

In this study, OpenFAST is used to analyze the global stability of the 30 MW downwind turbine on top of the floating TLP. With global stability, it means that the structure as a whole will stay within certain boundaries in terms of movement (pitch and heave). If the platform is deemed unstable in this analysis, or if it is considered too stable, it is redimensioned. The redimensioning will be performed using the preliminary design tool options, to get realistic values and to evaluate the vertical forces in the pivot column with maximum thrust force. These steps are repeated until the platform has realistic dimensions and the movement of the platform due to wave and wind loading stays within certain movement boundaries. To keep structured, a logbook is kept, which can be provided to the reader upon request.

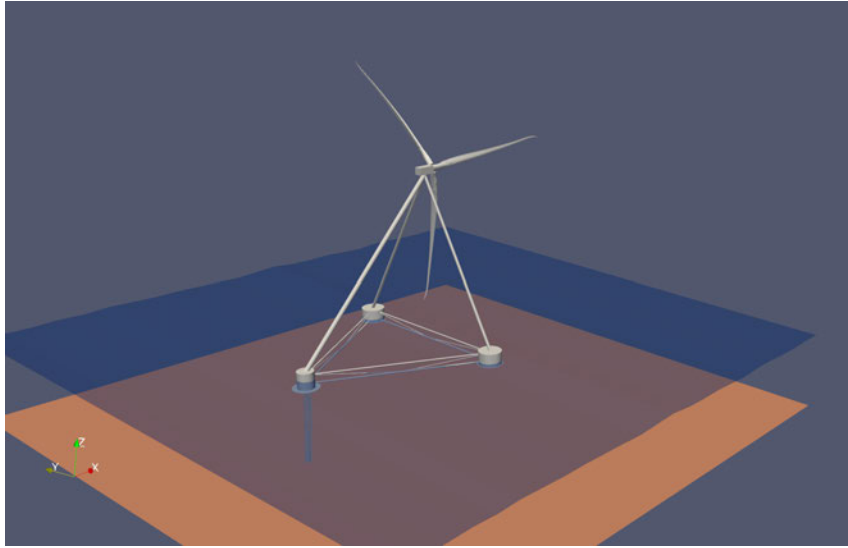


Figure 4.7: Visualization of design of the 30 MW PivotBuoy in ParaView.

4.3.2 Movement boundaries

As stated in subsection 4.3.1, certain boundaries in terms of movement were determined. The most important criterion in this assessment is the pitch because large pitching movements of the platform could reduce aerodynamic performance and increase fatigue and thus increase needed maintenance. The movement boundaries are listed in Table 4.4.

Table 4.4: Movement boundaries of the platform.

Type	Boundary
Pitch motion	-5 deg to +5 deg
Heave motion	+/- 1.5 wave height

4.3.3 Design load cases (DLC)

This study focuses on comparing a 30 MW downwind configuration to a 15 MW upwind and downwind configuration. L. Trezza wrote his master thesis on the comparison between a 15 MW upwind configuration and the 15 MW X1 Wind PivotBuoy design. [15] To be able to compare the 30 MW design to this, the design load cases from L. Trezza's thesis are also applied to the 30 MW design. The three different DLCs are listed below. DLC 1.2 has been adapted compared to the DLC 1.2 in L. Trezza's thesis. Only the 2nd and 8th columns of this DLC are taken into account.

DLC 6.1

This DLC corresponds to the situation where the turbine is parked. This means the turbine is idling, so the blades are pitched, the rotor is rotating very slowly and no power is produced. The wind, wave, and current conditions correspond to an extreme case.

Table 4.5: DLC 6.1 wind and waves input.

Parameter	Value
Wind Speed	42.5 m/s
Wind Direction	0°
IEC Wind Turbulence Type	2EWM-50
Hub Turbulence Intensity	11%
Wave Direction	0°
Wave Hs	10.1 m
Wave Tp	15.7 s

DLC 1.6

For DLC 1.6 the turbine is producing power with max thrust, so for the wind speed for which the blades are just about to start pitching/feathering. In this DLC, the platform is tested under wind, waves, and currents in different directions.

Table 4.6: DLC 1.6 wind, waves and current input.

Parameter	Value
Wind Speed	11.5 m/s
Wind Direction	15°
IEC Wind Turbulence Type	Normal
Hub Turbulence Intensity	10%
Wave Direction	0°
Wave Hs	6.81 m
Wave Tp	13.0 s
Current velocity	0.5 m/s
Current direction	30°

DLC 1.2

DLC 1.2 goes further into the turbine during production circumstances. This DLC tries to mimic normal operating conditions. It consists of 2 cases; both have a different wind speed in combination with a different Hs and Tp. The first case goes into very easy conditions and the second one mimics the most rough conditions in which the turbine is still producing power. The two different cases will be called DLC 1.2.1 and DLC 1.2.2 respectively.

Table 4.7: DLC 1.2 wind, waves and current input.

Parameter	Value
Wind Speed	[6.2, 25] m/s
Wind Direction	0°
IEC Wind Turbulence Type	Normal
Hub Turbulence Intensity	[0.184, 0.122]
Wave Direction	0°
Wave Hs	[1.84, 7.13] m
Wave Tp	[9.36, 13.7] s
Current velocity	0.0 m/s
Current direction	0°

4.3.4 Dimensions from initial design tool

The initial design tool provides initial values for many inputs of OpenFAST. It provides the initial dimensions of the profiles (Table 4.2, the platform inertia for roll, pitch, and yaw (Table 4.3), the

self-weight of the platform, and the location of the centre of mass.

4.3.5 Assumptions and potential model improvements

This section goes into the assumptions that were made for creating the OpenFAST model for the 30 MW PivotBuoy. Also, in this section suggestions for potential further research and model development for this design are stated. For the model, many assumptions were made because of time limitations. Putting more research into the assumptions would make for a more accurate model. Below, the assumptions accompanying improvement suggestions are listed.

1. For regular upwind wind turbines, OpenFAST has a 'tower' input section. This section does not allow the user to input three masts like the 30 MW PivotBuoy design has. The masts are defined in HydroDyn instead. As the masts are now defined in HydroDyn and not in AeroDyn, the aerodynamic forces on the masts are not calculated, leading to inaccuracies. The model has a tower reaching from 199 m to 200 m, as it is required to define a tower in OpenFAST.
2. The substructure is assumed to be stiff. This means that no internal forces and displacements are calculated.
3. The Degree of freedom (DOF) for the yaw motion of the nacelle was turned off as the platform is self-aligning.
4. For the model, the horizontal connectors are assumed to not contribute to the buoyancy nor the hydrodynamic or aerodynamic forcing. This is the case because, in simulations of initial designs, the platform heaved a lot due to the very buoyant horizontal connectors. Also, the horizontal connectors are placed at the height of the top of the buoys because when they are placed lower, OpenFAST crashes since these members will become partially or fully submerged. OpenFAST does not allow members that are defined as emerged to become submerged. To perform a more accurate study, the buoyancy, hydrodynamic, and aerodynamic forces from these members need to be taken into account.
5. The pivot bottom and the floating substructure that is situated on top are modelled as one unit due to limitations in model possibilities. This could lead to inaccuracies in terms of yaw movement because the platform can not rotate as freely around its' pivot as it should be able to in reality.
6. The mooring lines have an unrealistically low stiffness (EA, Elasticity modulus * area) because, for realistic EA values, the OpenFAST simulations will crash. This reduced stiffness of the mooring lines enables the platform to surge and sway more than it should.
7. A rated rpm of 5.5 is picked for the 30 MW wind turbine. This is reasonable because, with this rpm, the tip speed stays within reasonable limits. The distance the tip of one rotor travels is as follows:

$$Dist = 2 * \pi * r_{rotor} = 2 * \pi * 179 = 1124.69m \quad (4.7)$$

With an rpm of 5.5, this means the tip speed is as follows:

$$v_{rotortip} = \frac{5.5}{60} * 1124.69 = 103.097 \left[\frac{m}{s} \right] \quad (4.8)$$

Extrapolating a trend line with rated tip speed to diameter from [18], the tip speed of the rotor of 103.1 m/s seems reasonable.

8. The axial hydrodynamic drag coefficients are assumed to be the same as in a paper found online. However, it is needed to perform CFD (computational fluid dynamics) on members to determine the axial drag coefficients to increase the accuracy of the model.

9. The dimensions of the heave plates are roughly assumed. The diameter of these plates could be optimized to make the model perform better or to meet reality more.
10. In this study, the roughness length k is assumed to be between the value of new, uncoated steel and the lower bound of the value of k for marine growth (see Table 4.8) from [19]. However, a study on the actual surface roughness of the members needs to be performed for a more accurate calculation of the hydrodynamic drag coefficients and with that the hydrodynamic forcing.
11. The dynamic pressure coefficients of the members in HydroDyn are assumed to be 1 for all members. The added mass coefficients are assumed to be zero. These need to be determined for more accuracy. Also, modelling the substructure using WAMIT could lead to more accurate results.

4.3.6 Axial and member hydrodynamic drag coefficients

Figure 4.8 displays how the axial and member drag coefficients are defined. The axial and member hydrodynamic coefficients are defined separately in OpenFAST.

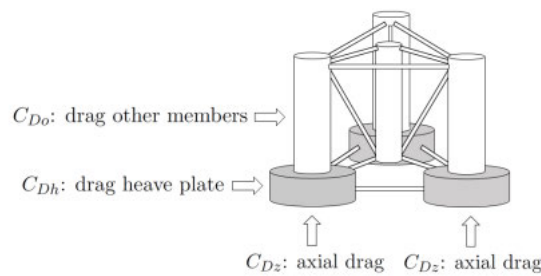


Figure 4.8: Visualization of how drag coefficients are applied [20].

4.3.6.1 Axial drag coefficients

The axial drag coefficients are the coefficients used for calculating the drag on the joints that connect members. To determine the axial drag accurately, for example around heave plates, it is required to either perform physical modelling or CFD. [21] Because this is very time-consuming, this is considered to be outside of the scope of this research. Therefore, a paper on the calibration of hydrodynamic drag coefficients is used as a reference for the axial drag coefficient in this research. [20] This paper uses an axial drag coefficient of $C_{dAx} = 8.2$. This is assumed to be representative for this study.

4.3.6.2 Member drag coefficients

For calculating the member drag coefficient (drag coefficient in Figure 4.8), section 6.7 of the recommended practice report of DNV is used. [19] This section provides standards for calculating the drag coefficients for circular cylinders. For this, high turbulence so a high Reynolds number ($Re > 10^6$) is assumed. DNV provides different surface roughness parameters k , which can be seen in table 4.8. It is assumed that the roughness of the members of the proposed solution lies in between the values for 'Steel, new uncoated' and the lower bound of 'Marine growth.' This makes for $k = (5E^{-5} + 5E^{-3})/2 = 2.5E^{-3} \frac{m}{s}$

Table 4.8: Surface roughness for different materials.

Material	k [m]
Steel, new uncoated	5×10^{-5}
Steel, painted	5×10^{-6}
Steel, highly corroded	3×10^{-3}
Concrete	3×10^{-3}
Marine growth	5×10^{-3} to 5×10^{-2}

First, the drag coefficients C_{DS} for all profiles in the 30 MW substructure are calculated using the formulas defined in Equation 4.9. For this calculation, large values for the Keulegan Carpenter number K_C are assumed.

$$C_{DS}(\Delta) = \begin{cases} 0.65 & ; \Delta < 10^{-4} \text{ (smooth)} \\ (29 + 4 \cdot \log_{10}(\Delta)) / 20 & ; 10^{-4} < \Delta < 10^{-2} \\ 1.05 & ; \Delta > 10^{-2} \text{ (rough)} \end{cases} \quad (4.9)$$

Where $\Delta = k/D$ with D = profile diameter.

As $K_C = \frac{\pi * H}{D}$, where H is the wave height (assumed to be significant wave height H_s), and because there are many non-slender profiles, K_C can not be assumed low. To account for this non-slenderness, the following relation is used:

$$C_D = C_{DS}(\Delta) * \Psi(K_C) \quad (4.10)$$

Where $\Psi(K_C)$ is the wake amplification factor. The following relation is used for calculating the different wave amplification numbers $\Psi(K_C)$:

$$\Psi(K_C) = \begin{cases} C_\pi + 0.10(K_C - 12) & 2 \leq K_C < 12 \\ C_\pi - 1.00 & 0.75 \leq K_C < 2 \\ C_\pi - 1.00 - 2.00(K_C - 0.75) & K_C \leq 0.75 \end{cases} \quad (4.11)$$

where

$$C_\pi = 1.50 - 0.024 \cdot (12/C_{DS} - 10) \quad (4.12)$$

As the drag coefficients are dependent on the significant wave height, the drag coefficients differ for each load case. An overview of the member drag coefficients can be found in table 4.9:

Table 4.9: Hydrodynamic drag coefficients for different members for different load cases.

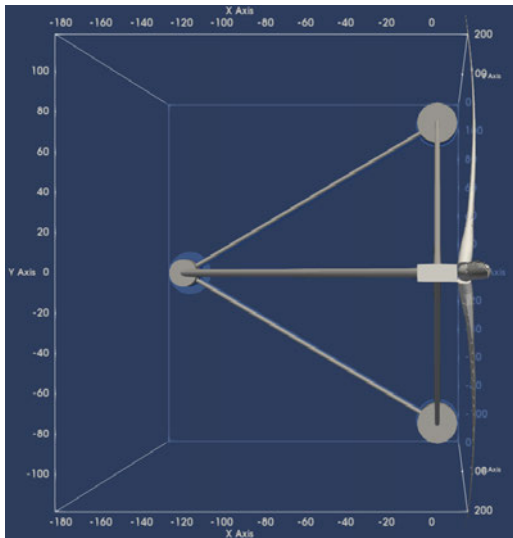
Member diameter [m]	$C_{D,DLC6.1}$	$C_{D,DLC1.6}$	$C_{D,DLC1.2.1}$	$C_{D,DLC1.2.2}$
27.50	0.193	0.193	0.895	0.193
19.00	0.211	0.211	0.811	0.211
3.69	0.855	0.626	0.316	0.648
3.56	0.885	0.647	0.318	0.670
5.23	0.613	0.458	0.294	0.473
30.00	0.193	0.241	0.918	0.197

4.3.7 Heave plates

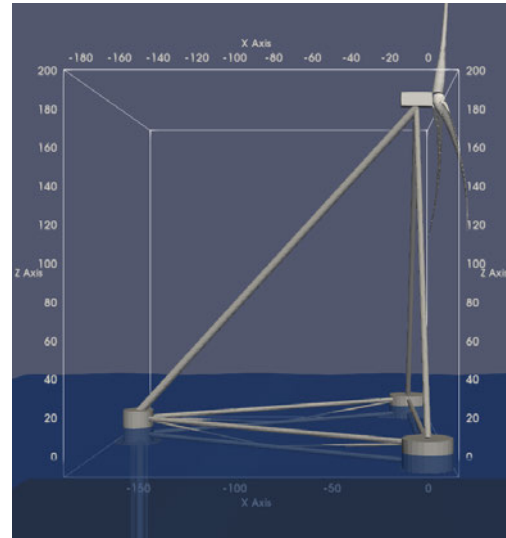
To reduce the vertical movement of the platform due to wave action, heave plates are installed underneath the three columns. The heave plates have a diameter that is larger than the columns themselves to cause more vertical hydrodynamic drag, reducing vertical motion. The diameters of the heave plates are set to D = 30 meters.

4.3.8 Final dimensions

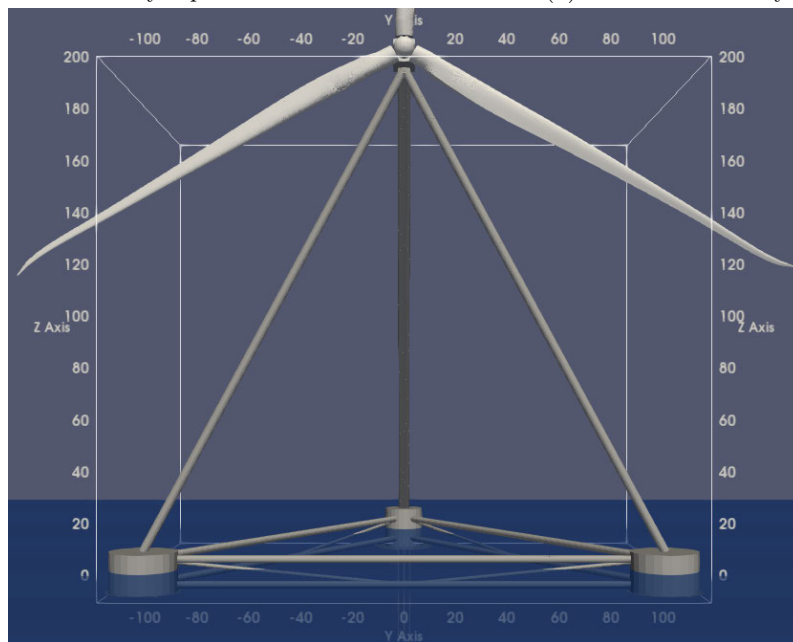
In Table 4.2, the final dimensions of the structure and a broad overview of important model settings are given. For the smooth running of the program, the dimensions of the horizontal connectors are not taken into account. However, the horizontal connectors are visualized in Figure 4.9. The weight of these profiles and their effect on the platform rotational inertia and the centre of mass are however taken into account. The coordinates of all the nodes of the design can be found in Appendix D.



(a) 30 MW PivotBuoy top view.



(b) 30 MW PivotBuoy side view.



(c) 30 MW PivotBuoy front view.

Figure 4.9: Dimensions of the 30 MW PivotBuoy visualized using ParaView.

4.3.9 Final design performance (DLC's applied)

In this section, the performance of the final design of the 30 MW solution is evaluated. As stated in subsection 4.3.2, the movement of the platform has to stay within the boundaries for all DLCs. As stated before, the platform is tested on its Pitch and Heave motion. The other motions are also provided in the table to show the overall performance of the floater on other movements, but these are of less importance.

Results DLC 6.1

The platform performs well in terms of both heave and pitch motion. Especially for pitch, the platform is very stable. The standard deviation for pitch comes down to 0.851 degrees.

Table 4.10: Simulation results from DLC 6.1.

Motion	Max	Min	Mean	Std
Platform Surge (m)	5.913	-3.457	1.580	1.549
Platform Sway (m)	16.810	-20.540	-0.661	5.692
Platform Heave (m)	6.183	-6.472	0.162	2.446
Platform Roll (deg)	0.166	-0.215	-0.002	0.046
Platform Pitch (deg)	2.210	-2.496	-0.025	0.851
Platform Yaw (deg)	5.714	-7.042	-0.221	2.008

Results DLC 1.6

As DLC 1.6 is less extreme than DLC 6.1 (Table 4.6 and Table 4.5, respectively), it is expected that both the heave and the pitch motion for this DLC are lower than for DLC 6.1. However, due to the high thrust force the platform surges and sways a lot. This has to be reduced with stiffer mooring. However, as stated in the 6th assumption in subsection 4.3.5, the mooring is not as stiff as it would be in reality due to modelling limitations, so these values are unrealistic.

Table 4.11: Simulation results from DLC 1.6.

Motion	Max	Min	Mean	Std
Platform Surge (m)	19.570	3.658	10.567	2.816
Platform Sway (m)	-11.720	-60.950	-44.239	10.526
Platform Heave (m)	4.484	-5.263	-0.166	1.838
Platform Roll (deg)	0.566	-0.643	-0.016	0.215
Platform Pitch (deg)	1.554	-2.152	-0.356	0.706
Platform Yaw (deg)	-3.640	-19.070	-13.828	3.438

Results DLC 1.2.1

DLC 1.2.1 is a very low-intensity DLC. The platform heave and pitch movements are small.

Table 4.12: Simulation results DLC 1.2.1.

Motion	Max	Min	Mean	Std
Platform Surge (m)	11.460	-1.036	5.436	2.960
Platform Sway (m)	4.912	-57.340	-35.212	15.549
Platform Heave (m)	1.951	-1.774	0.017	0.676
Platform Roll (deg)	0.353	-0.372	-0.005	0.112
Platform Pitch (deg)	0.547	-0.804	-0.099	0.245
Platform Yaw (deg)	1.525	-18.670	-11.304	5.107

Results DLC 1.2.2

Table 4.13: Simulation results DLC 1.2.2.

Motion	Max	Min	Mean	Std
Platform Surge (m)	3.998	-3.089	0.593	1.163
Platform Sway (m)	16.050	-14.390	-0.375	6.146
Platform Heave (m)	4.905	-5.098	0.174	1.872
Platform Roll (deg)	0.163	-0.139	-0.001	0.031
Platform Pitch (deg)	1.754	-1.617	-0.001	0.633
Platform Yaw (deg)	5.403	-4.745	-0.124	2.072

4.3.10 Comparison to L. Trezza's model

Initially, the idea was to compare the outcomes of the 30 MW PivotBuoy OpenFAST model to the 15 MW X1 Wind PivotBuoy design by L. Trezza [15]. However, judging by the performance of the design, the 15 MW X1 Wind PivotBuoy design from the thesis of L. Trezza requires optimization. Also, due to the many assumptions and inaccuracies, it is hard to compare two models and state if a 15 MW X1 Wind PivotBuoy or a 30 MW downwind design performs better.

4.4 Finite Element Analysis

To assess the dynamic response of the structure to the time-varying wind and wave loads, a FEM analysis is conducted based on the initial design proposed in section 4.3. The goal of this analysis is to perform a natural frequency analysis from which the design can be checked that there are no external loading conditions that induce resonance or dynamic amplification. The main sources of excitation are wind, wave, and rotor motions, these will be investigated later. First, the natural frequencies of the structure itself will be investigated. Besides this, the FEM analysis is also used to find the deflections and finally the stresses in the members. With this, the members can be checked against the steel strength.

To perform the FEM analysis on the structure, a numerical model is set up to find the behaviour of the design. All elements of the structure, floaters, and TLP system are modelled as a 12-DOF Euler-Bernoulli beam. The Anchor of the TLP is considered to be clamped, and various assumptions are implemented to simplify the model in other areas. These simplifications, their consequences, and limitations will be discussed.

4.4.1 Approach

To model the behaviour of the floater solution, the system is simplified to multiple connected rod-beam elements with 12 degrees of freedom each. It is assumed that the structure can be modelled as a frame with structural elements that are subject to axial displacement, bending, and torsion. The more detailed approach including the definition of the Equations of Motion of the system through the Hamiltonian approach can be found in Appendix B.

4.4.2 Assumptions

Seven connected elements

As seen in Figure 4.10, the floating solution comprises six connected beam elements. Besides this, an extra element representing the TLP system is added.

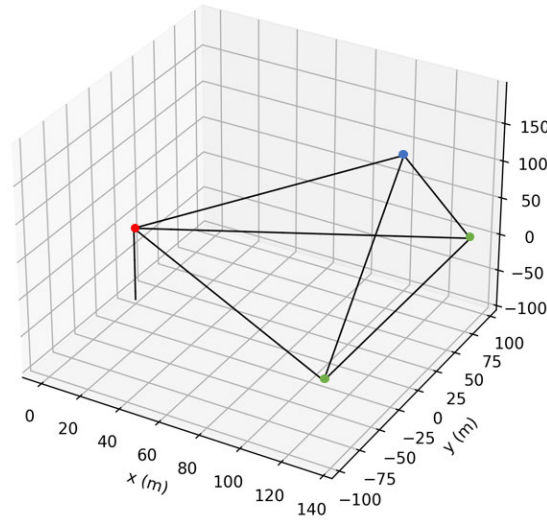


Figure 4.10: The final floating model consisting of 7 elements.

TLP as a clamped beam with low bending stiffness

To resemble the behavior of the TLP it is modelled as a beam with a low bending stiffness. This way, it represents a string. Since the beam still has a high axial stiffness, the Pivot Buoy Column will stay at its vertical position, resulting in a good representation of the TLP system. The TLP-ground connection is designed to be a clamped support. This assumes a rigid connection of the TLP tendon with the foundation system in place. This assumption is made to ensure the stability of the floater support. It simplifies the modelling process by providing a fixed support condition at the seabed.

Point masses

The nacelle and the columns are modelled as point masses by adding their respective calculated mass to the mass matrix at the respective node.

Table 4.14: Point masses present in model.

Element	Weight [kg]
Rotor nacelle assembly	2,234,833
Pivot column	143,000
Right column	257,677
Left column	257,677

Added masses

The columns and pontoons are modelled as nodes and elements in this approach. In reality, these members have large dimensions that displace a significant amount of water. To include this added mass, they are firstly calculated by Equation 4.13.

$$M = c_a * V * \rho_{water} \quad (4.13)$$

with:

c_a : Added mass coefficients (0.5 for circular and 0.68 for rectangular sections. [22]) [-]

V : Volume of displaced water based on diameter and the draft of specific elements

ρ_{water} : density of water [kg/m³]

The respective added masses can be found in Table 4.15. For the columns, these masses are directly added. However, for the pontoons, these masses are first divided by the number of pontoon nodes and then added to each individual pontoon node.

Table 4.15: Added mass present in model.

Element	Weight [kg]
Added mass pivot column	195,313
Added mass right column	632,813
Added mass left column	632,813
Added mass pontoons [kg/m]	110,466

4.4.3 Consequences and Limitations

Representing the floating solution as a multiple rod-beam system captures the overall behaviour of the structure sufficiently for a natural frequency analysis and preliminary stress analysis. The limitations of these assumptions are important to acknowledge. The simplified model will not capture all the intricate details and interactions of the real-world floating solution. The behaviour of the TLP, for example, will be more complex than represented in the model, requiring additional analysis to accurately capture their dynamic response and interaction with the floating solution.

It is important to note that the assumption of the added mass does not fully capture the complex behaviour and interactions between the floating solution and the water. The movement response of the floaters is not captured in this model, assuming the structure has a fixed pivot and is not able to pivot. In the case of this study, this assumption can be used as an accidental load case where the pivot system fails and the structure can not move. Interaction with the surrounding environment requires more detailed and specialized analysis beyond the simplified representation used in the model.

Similarly, the assumption of point masses for the different weights forms a simplification. Modelling the columns and pontoons as an individual element (rigid body) would be a more accurate representation. Neglecting these elements oversimplifies the structural behaviour, and a more detailed analysis would be necessary to understand the effects of this simplification to the full extent.

Furthermore, the assumptions made regarding the material properties, such as the homogeneity and isotropy of the beam elements, may not reflect the actual characteristics of the floating solution. Real-world materials may exhibit nonlinear behaviour, anisotropic properties, and other complexities that are not considered in the simplified model. Incorporating nonlinear material models would provide more accurate representations, but would also increase the complexity and computational requirements of the analysis.

Finally, the uncertainty of the input parameters must be noted, influencing the accuracy of the numerical modal. In further design stages, it is crucial to consider these uncertainties and perform sensitivity analyses to assess the robustness of the results obtained from the numerical model.

Also, the computational limit must be acknowledged. To achieve increasing accuracy with the model, a finer mesh size would be beneficial, but not necessary at this design stage, since it gives a good representation of the magnitude.

4.4.4 Model set-up

The FEM analysis consists of a precise order of steps, which are implemented to obtain the results. The process can be summarized as follows: the spatial domain is discretized into elements and nodes, and the properties of each element are defined. The local matrices are then computed using

shape functions or existing element matrices. These local matrices are assembled to form the global Mass and Stiffness matrix by taking into account the connectivity of the nodes. Finally, boundary conditions are applied by adapting a specific node inside the global matrix and right-hand side to account for the prescribed constraints.

Step 1) Discretize the Domain

The first step creates a mesh which is used to translate the model of the wind turbine to a numerical model. The entire substructure consists of 61 nodes and 63 elements which are connecting these nodes. The elements are assigned to the nodes by a connectivity matrix. In Figure 4.10 the final discretization of the floater solution is shown. The vertical column at the end of the substructure represents the tension leg of the 30 MW solution.

Step 2) Define element properties

The second step includes the determination of the elemental properties of the model. The first assumption is that all the elements are defined as circular hollow sections and are made of steel. Note that the Young's modulus of the tension leg is not similar to the Young's modulus of the other elements of the 30 MW solution. in Equation 4.14 - Equation 4.17 the equation for the properties are listed.

$$A = \pi * \frac{D_{out}^2}{4} - \pi * \frac{D_{in}^2}{4} \quad (4.14)$$

$$I = \pi * \frac{D_{out}^4}{64} - \pi * \frac{D_{in}^4}{64} \quad (4.15)$$

$$J = 2 * I \quad (4.16)$$

$$Im = \frac{\pi}{32} * D_{out}^4 - D_{in}^4 \quad (4.17)$$

On top of that, some material properties are also defined as follows:

$$G_{steel} = \frac{E_{steel}}{(2*(1-\nu_{steel}))}$$

$$\nu_{steel} = 0.2 \text{ [-]}$$

$$\rho_{water} = 1000 \left[\frac{kg}{m^3} \right]$$

$$\rho_{steel} = 7850 \left[\frac{kg}{m^3} \right]$$

$$E_{steel} = 78.5 \text{ E9} \left[\frac{N}{m^2} \right]$$

In table Table 4.17 the material properties of the individual structural components are given

Table 4.16: Diameters of the respective cross-sections.

Element	D _{out} [m]	D _{in} [m]	Thickness [m]	Length [m]
Pivot column	19.0	18.86	0.07	19.5
Right column	27.5	27.36	0.07	15.9
Pontoons	3.69	3.57	0.06	203
Mast	3.47	3.35	0.06	217
Pivot mast	5.47	5.29	0.09	259

Table 4.17: Properties of the elements.

Element	m [kg]	EI [N/m ²]	EA [N]	GJ [N/m ²]	Im [m ²]
Pivot column	3.27E+03	7.83E+13	8.74E+11	6.17E+13	3.73E+02
Right column	4.74E+04	2.38E+14	1.27E+12	1.88E+14	1.13E+03
Pontoon	5.37E+04	4.73E+11	1.44E+11	3.73E+11	2.25E+00
Mast	5.05E+03	3.93E+11	1.35E+11	3.09E+11	1.87E+00
Pivot mast	1.19E+04	2.31E+12	3.19E+11	1.82E+12	1.10E+01

Step 3) Approximate solution

In the next step, the local matrices of every individual element are defined by using two different shape functions. For the axial displacement, the linear shape function is applied. While for the deflection and rotation, the cubic shape function is used. See Equation 4.18.

$$N_i^k = a_i + b_i y \quad \text{and} \quad N_i^k = c_i + d_i y + e_i y^2 + f_i y^3 \quad (4.18)$$

Each individual node has 6 degrees of freedom. An element consists of two nodes, given 12 degrees of freedom for every element.

Every shape function associated with every DOF is one at the location of the location of that specific DOF and zero at the other DOFs. With the shape function as mentioned above, the elemental weak form and the particular local mass matrices and stiffness matrices can be defined.

$$M = \frac{mL}{420} \begin{bmatrix} 140 & 0 & 0 & 0 & 0 & 0 & 70 & 0 & 0 & 0 & 0 & 0 \\ 0 & 156 & 0 & 0 & 0 & 22L & 0 & 54 & 0 & 0 & 0 & -13L \\ 0 & 0 & 156 & 0 & 22L & 0 & 0 & 0 & 54 & 0 & 13L & 0 \\ 0 & 0 & 0 & 140 & 0 & 0 & 0 & 0 & 0 & 70 & 0 & 0 \\ 0 & 0 & 22L & 0 & 4L^2 & 0 & 0 & 0 & -13L & 0 & -3L^2 & 0 \\ 0 & 22L & 0 & 0 & 0 & 4L^2 & 0 & 13L & 0 & 0 & 0 & -3L^2 \\ 70 & 0 & 0 & 0 & 0 & 0 & 140 & 0 & 0 & 0 & 0 & 0 \\ 0 & 54 & 0 & 0 & 0 & 13L & 0 & 156 & 0 & 0 & 0 & -22L \\ 0 & 0 & 54 & 0 & -13L & 0 & 0 & 0 & 156 & 0 & 22L & 0 \\ 0 & 0 & 0 & 70 & 0 & 0 & 0 & 0 & 0 & 140 & 0 & 0 \\ 0 & 0 & 13L & 0 & -3L^2 & 0 & 0 & 0 & 22L & 0 & 4L^2 & 0 \\ 0 & -13L & 0 & 0 & 0 & -3L^2 & 0 & -22L & 0 & 0 & 0 & 4L^2 \end{bmatrix} \quad (4.19)$$

$$K = \begin{bmatrix} \frac{EA}{L} & 0 & 0 & 0 & 0 & 0 & -\frac{EA}{L} & 0 & 0 & 0 & 0 & 0 \\ 0 & \frac{12EI}{L^3} & 0 & 0 & 0 & \frac{6EI}{L^2} & 0 & -\frac{12EI}{L^3} & 0 & 0 & 0 & \frac{6EI}{L^2} \\ 0 & 0 & \frac{12EI}{L^3} & 0 & -\frac{6EI}{L^2} & 0 & 0 & 0 & -\frac{12EI}{L^3} & 0 & -\frac{6EI}{L^2} & 0 \\ 0 & 0 & 0 & \frac{GJ}{L} & 0 & 0 & 0 & 0 & 0 & -\frac{GJ}{L} & 0 & 0 \\ 0 & 0 & -\frac{6EI}{L^2} & 0 & \frac{4EI}{L} & 0 & 0 & 0 & \frac{6EI}{L^2} & 0 & \frac{2EI}{L} & 0 \\ 0 & \frac{6EI}{L^2} & 0 & 0 & 0 & \frac{4EI}{L} & 0 & -\frac{6EI}{L^2} & 0 & 0 & 0 & \frac{2EI}{L} \\ -\frac{EA}{L} & 0 & 0 & 0 & 0 & 0 & \frac{EA}{L} & 0 & 0 & 0 & 0 & 0 \\ 0 & -\frac{12EI}{L^3} & 0 & 0 & 0 & -\frac{6EI}{L^2} & 0 & \frac{12EI}{L^3} & 0 & 0 & 0 & -\frac{6EI}{L^2} \\ 0 & 0 & -\frac{12EI}{L^3} & 0 & \frac{6EI}{L^2} & 0 & 0 & 0 & \frac{12EI}{L^3} & 0 & \frac{6EI}{L^2} & 0 \\ 0 & 0 & 0 & -\frac{GJ}{L} & 0 & 0 & 0 & 0 & 0 & \frac{GJ}{L} & 0 & 0 \\ 0 & 0 & -\frac{6EI}{L^2} & 0 & \frac{2EI}{L} & 0 & 0 & 0 & \frac{6EI}{L^2} & 0 & \frac{4EI}{L} & 0 \\ 0 & \frac{6EI}{L^2} & 0 & 0 & 0 & \frac{2EI}{L} & 0 & -\frac{6EI}{L^2} & 0 & 0 & 0 & \frac{4EI}{L} \end{bmatrix} \quad (4.20)$$

The global matrix can be assembled with these local matrices. For an Euler-Bernoulli beam, the global matrix is diagonally dominant. The equation of the system is derived according to. Note

that M and K are the global matrices instead of the local matrices in this equation. For the boundary condition of this system, the node of the bottom part of the tension leg is identified, and the row correlated to this is deleted.

With these two local matrices, we can assemble the global matrix according to the connectivity matrix. For the Euler-Bernoulli beam, this global matrix will be diagonally dominant. The total equation for this system is derived as Equation 4.21, where M and K are the global matrices.

$$M_{FF} * \ddot{u}_F + K_{FF} * u_F = F_F^{ext} - F_{FP}u_P - M_{FP}\ddot{u}_P \quad (4.21)$$

Step 4) Modal analysis

The last step is to perform the modal analysis. The following steps are executed:

1. Define the equation of motion with free DOFs on the left-hand side and prescribed and forced DOFs on the right-hand side
2. Calculate the eigenshapes and eigenvalues for the free DOFs
3. Calculate the modal matrices and modal forcing
4. Solve each modal equation
5. Combine modal responses

The formula for the Eigenvalue problem is defined as follows:

$$(K_{FF} - \omega_j^2 M_{FF}) * \phi_j = 0 \quad (4.22)$$

The equation gives us the eigenvalues (ω_j) and eigenvectors (ϕ_j) as solutions. These are the natural frequencies and modal shapes of the system, respectively. The number of modes depends on how many natural frequencies we have. One can see the first twelve natural frequencies and their corresponding mode shapes in Figure 4.11 & Figure 4.12

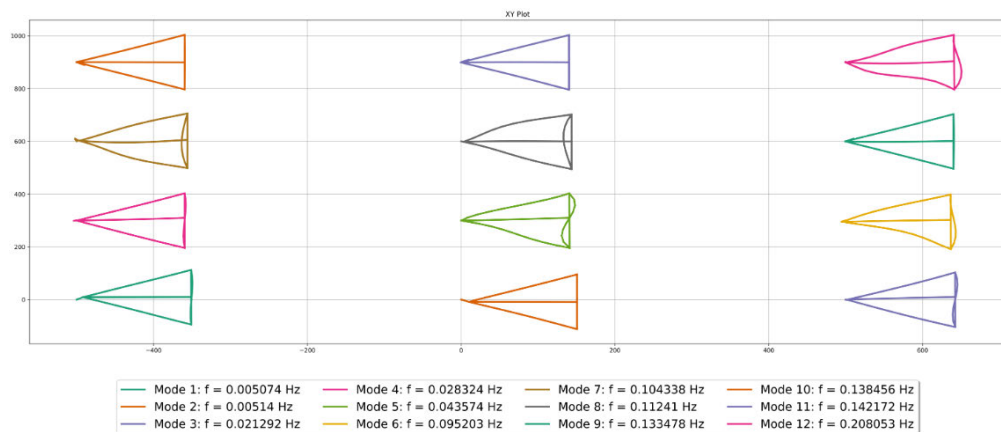


Figure 4.11: x-y plot of the first 12 modes.

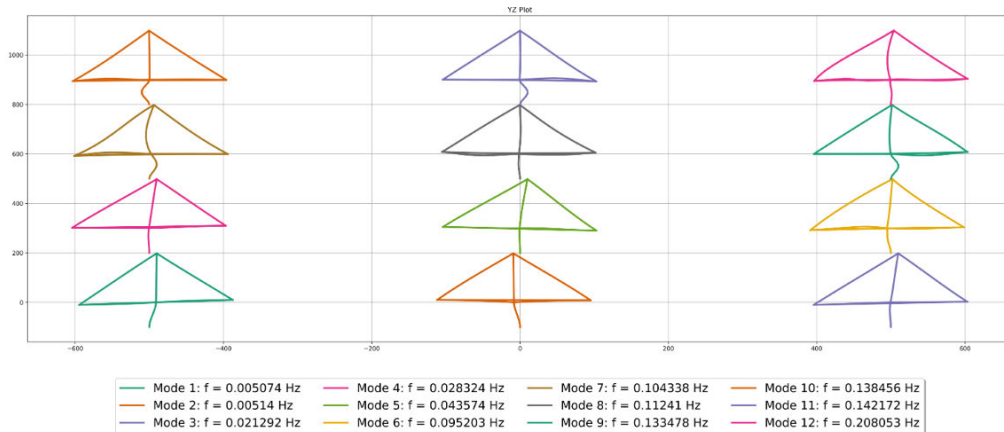


Figure 4.12: y-z plot of the first 12 modes.

Validation

The model's validation, through convergence analysis, is carried out by applying a static force that corresponds to a specific modal shape. When the system is excited with this particular mode shape, only that mode is expected to generate a displacement response with a non-zero amplitude, while all other modes should exhibit zero amplitudes. Due to the static nature of the excitation, the solution is expected to gradually converge to a steady-state response over time.

This validation process assesses the model's ability to accurately capture the dynamic behaviour of the system. By comparing the predicted responses with the actual observations during the steady-state condition, the model's performance can be evaluated and refined as necessary. This validation step plays a crucial role in ensuring the reliability and predictive capability of the model.

4.4.5 Frequency spectrum

After having found the natural frequencies of the relevant modes of the floater solution, a validation is performed to check whether these natural frequencies will not resonate with the wind and wave spectrum or the rotor rotations.

Wind spectrum

For the wind turbulence spectrum, the Kaimal spectrum is adopted. This gives the spectrum for the most prevalent wind frequencies, which has its maximum frequency in the low range of 0.02 Hz.

Wave spectrum

The wave spectrum can be found through a JONSWAP spectrum defined for the local wave conditions. For this, a Matlab file is used [23] in which the significant wave height and zero crossing period ($T_z = T_s/1.4$ [24]) can be defined and the JONSWAP spectrum can be found. This spectrum is shown in Figure 4.13 with $T_z = 13.8s$ and $H_s = 11.94m$ [chapter 3], and from this it can be seen that the wave spectrum ranges from 0.033 to 0.20 Hz.

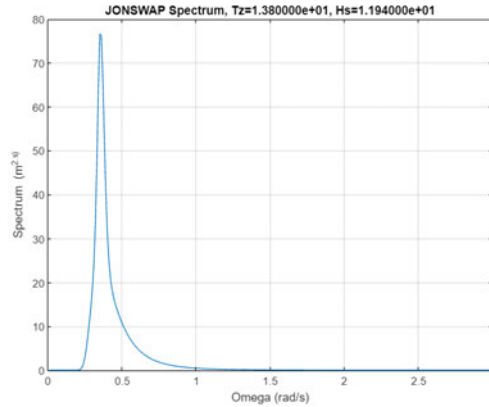


Figure 4.13: JONSWAP spectrum based on wave conditions.

Rotor rotations

In a standard upwind, one mast and three-blade configurations, the 1P (the frequency of all blades passing the one mast) and the 3P (the frequency of one blade passing the one mast) are investigated. Since our design consists of two masts, the 1P/2P (the frequency of all blades passing the two masts), the 3P (1 blade passed 2 masts), and the 6P (Each time a blade passes a mast) are assessed.

1P/2P frequency

As stated in eq. (4.7), the travelled distance is 1124.7 meters. As shown in Figure 4.14, the distance on the path of the tip of a rotor between the 2 masts is 177.8 m. The time it takes for one blade to have passed both masts would be $\frac{Dist_{masts}}{v_{tip}} = \frac{177.8}{103.1} = 1.72s$. The time it takes to complete the rest of the rotation however would be $\frac{1124.7-177.8}{v_{tip}} = \frac{946.9}{103.1} = 9.184s$. This would make for a very irregular frequency pattern and because the masts are quite close, it is assumed that the 1P is equal to the 2P. Making the 1P = 2P:

$$f_{1P/2P} = \frac{103.1}{1124.7} = 0.0917Hz \quad (4.23)$$

3P frequency

The 3P frequency is seen as the frequency at which a blade passes the two masts. This means that for this excitation frequency, the two masts are assumed to be one. The 3P frequency then comes down to:

$$f_{3P} = \frac{103.1}{1124.7} * 3 = 0.275Hz \quad (4.24)$$

It is important to state that the 3P approach is assumed to be accurate for the two-mast design.

6P frequency

The 6P frequency is caused by each time a blade passes a mast. For 1 blade to pass from one mast to the other, it takes $\frac{177.8}{103.1} = 1.72s$. For the next blade to arrive at the first mast once the first blade is located at the second mast, it takes $\frac{1124.7-177.8}{103.1} = 1.913s$. Because these values lie quite close together, the excitation frequency can be assumed quite regular. Therefore, the mean between these frequencies is said to be the 6P frequency:

$$f_{6P} = \frac{1}{\frac{1.913+1.72}{2}} = 0.55Hz \quad (4.25)$$

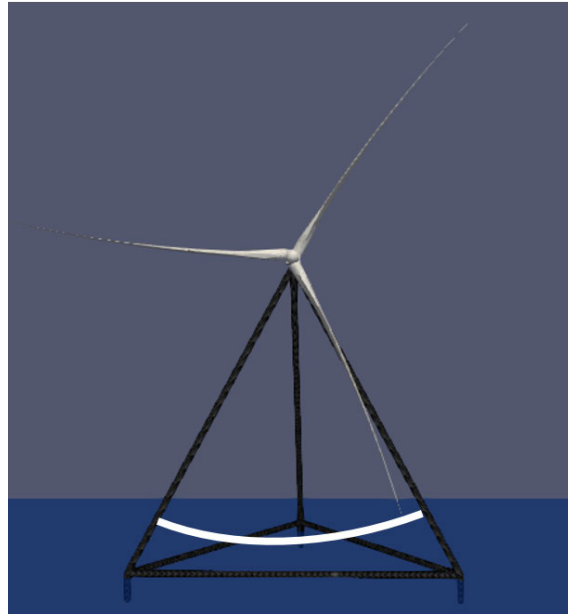


Figure 4.14: Swept distance between the two masts in white (heart to heart) (Dist = 177.8 m).

Full spectrum analysis

Finally, both wind and wave spectra are plotted in combination with the 1P/2P, 3P, and 6P frequencies. These 1P/2P, 3P, and 6P are constructed by looking at a 15% range of their frequencies. With all these frequencies and spectra combined, the natural frequencies from the relevant modal shapes are plotted as well. A modal shape is deemed relevant if it is higher than 50% of the largest modal excitation present. Figure 4.15 shows the full spectrum. From here it can be seen that one natural frequency occurs in the 6P range. This modal shape is checked to make sure there is no excitation present in the masts which would cause issues. Figure 4.16 shows this modal shape. As seen, there is no modal excitation present in the two masts directly in front of the blades. For this reason, it can be deemed acceptable that this modal shape resides in the 6P region. Consequently, the natural frequency analysis at this design stage can be considered to be sufficient.

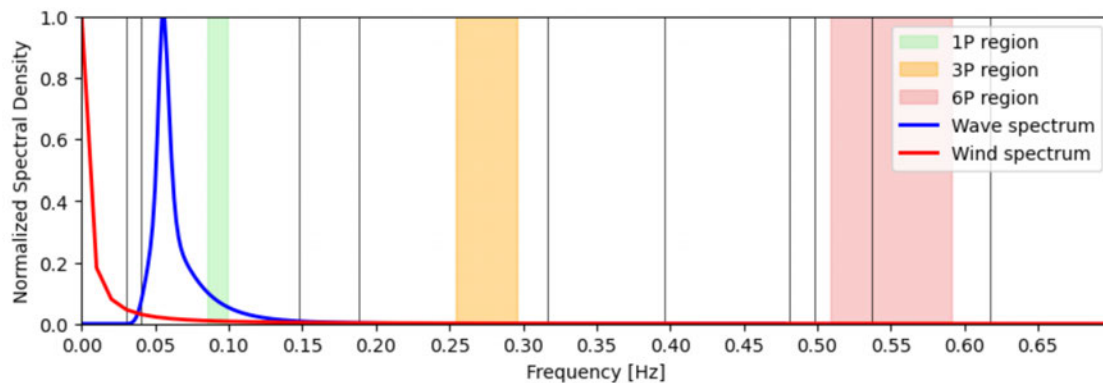


Figure 4.15: Spectrum analysis.

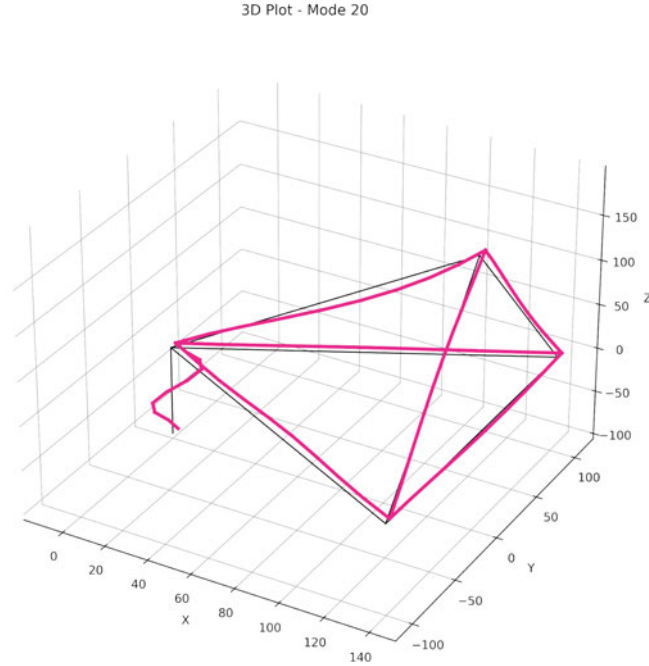


Figure 4.16: Modal excitation of mode 20 which occurs in 6P region.

4.5 Detailed member design

For the detailed member design, the FEM model used to find the natural frequencies is expanded to find the deflections and stresses in the profiles. The first step in this is to load the model with environmental loads. These will cause deflections in the different members. These deflections can then be calculated back towards stresses in the members. These stresses are finally checked with the steel strength.

4.5.1 Environmental loads

To find the environmental loads, this analysis focuses on the Morison force method to find the outcome of the wave loading. This method is performed for all submerged members, however, an example calculation is only given for a pontoon member here.

A force on a submerged body in an oscillatory flow (waves) can be described as in Equation 4.26.

$$F = F_D + F_{FK} + F_{AM} \quad (4.26)$$

where:

F_D : Drag due to viscous effects [N]

F_{FK} : Froude-Krylov force, due to the pressure gradient under the oscillatory flow. [N]

F_{AM} : Hydrodynamic Mass / Added Mass, due to the acceleration of the surrounding fluid. [N]

For a cylindrical body:

$$F_D = \frac{1}{2} C_d \times \rho D u |u| \text{ [N]}$$

$$F_{FK} = \rho A \dot{u} \text{ [N]}$$

$$F_{AM} = C_m \times \rho A \dot{u} \text{ [N]}$$

$$F = \frac{1}{2}C_d \times \rho D u |u| + (1 + C_m)\rho A \dot{u} \text{ [N]}$$

$$C_I = 1 + C_M \text{ [-]}$$

The unknowns in these equations mainly come from wave characteristics such as water velocity and acceleration. To find these characteristics, first, a JONSWAP wave spectrum is created using the WAFO Python module for combined wind and swell wave conditions. This wave spectrum is generated based on the significant wave height and period, as defined in chapter 3. With these characteristics, a time series of 20 minutes is generated. This is long enough to give reliable estimates ($t \geq 15$ minutes) but short enough to ensure stationary wave conditions ($t \leq 30$ minutes), this sea-level elevation time-series is portrayed in Figure 4.17.

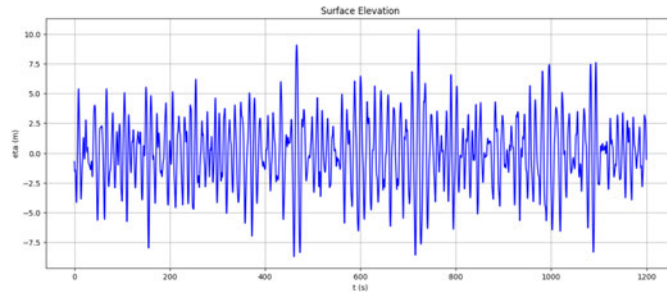


Figure 4.17: JONSWAP sea-level elevation time series for swell waves.

Using this time series, the amplitude spectrum can be constructed using the spectral density function as portrayed in Equation 4.27.

$$\sum_f^{f+\Delta f} \frac{1}{2} a_n^2 = S_n(f) \Delta f \quad (4.27)$$

This amplitude spectrum for swell waves can be seen in Figure 4.18.

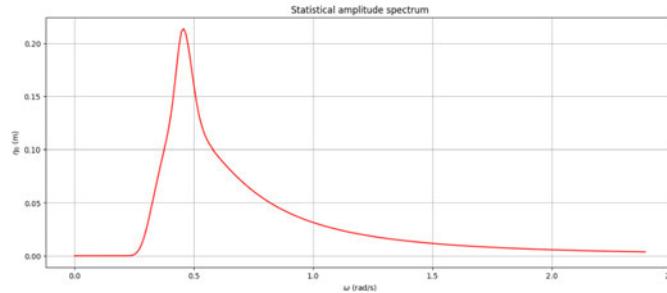


Figure 4.18: the amplitude spectrum for swell waves.

Using the LinearWave package and the amplitudes from the JONSWAP spectrum and random phase; the elevation, velocity, and acceleration time series can be found, with which the wave forces can be calculated.

After this, the velocities and accelerations are calculated from the spectrum by the use of the LinearWave package. This signal that is produced is calculated in a truly random fashion, which gives a high calculation time but also gives a signal that does not repeat itself in the duration of the time frame. An example of these velocities and accelerations that the pontoon element experiences during the 20-minute time-frame are displayed in Figure 4.19 - 4.20. With these velocities, the forces can be calculated through the Morison equation. These forces that occur in the 20-minute

time series are displayed in Figure 4.21 for the pontoon. Taking the maximum forces in these time series gives the design loads for all elements in the combined wind and swell wave conditions. This is portrayed in Table 4.18.

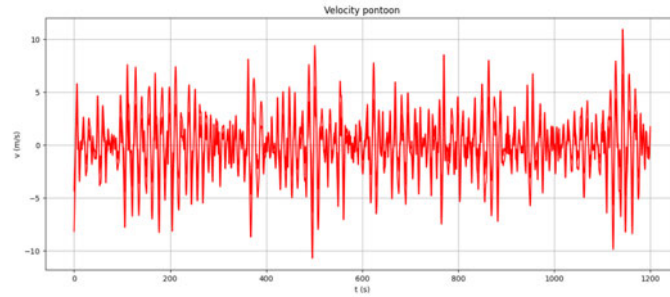


Figure 4.19: Velocities on structural components of variant one.

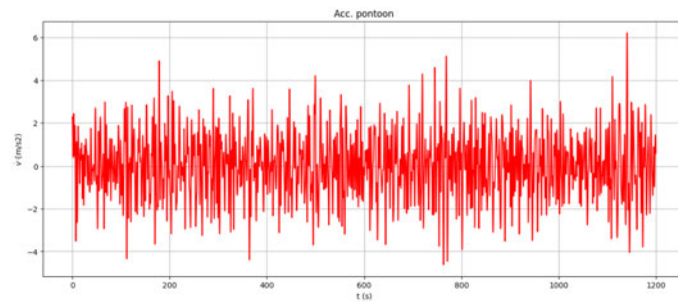


Figure 4.20: Accelerations on structural components of variant one.

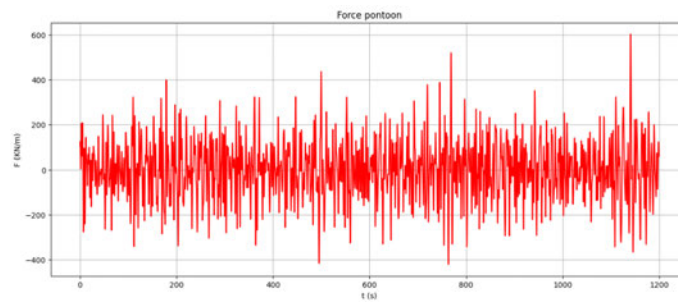


Figure 4.21: Forces on structural components of variant one.

Table 4.18: Maximum forces acting on the structural elements in the combined swell and wind wave conditions.

Element	V _x [kN/m]	V _y [kN/m]	V _z [kN/m]
Horizontal pontoons	602	-	514
Pivot buoy	181	181	170
Nacelle column	699	699	591

4.5.2 Deflections

The deflections of the elements are caused by the external wave forces. To assign certain forces of the time series to the nodes, a force function is created where a linear interpolation is used. With this function, the forces at a certain moment in time can be calculated and assigned to the right node.

With the forces included, the displacement and its corresponding first and second derivative in time can be calculated. this method creates insight into the displacement of every individual node over a time series of 1200 seconds based on the corresponding wave spectrum. The following Figure 4.22 displays the time series at the three distinct corner points of the system in the z direction (heave). Due to the constraints of the model, the PivotBuoy is not moving as the respective node is on top of the TLP that was modelled as an Euler-Bernoulli beam.

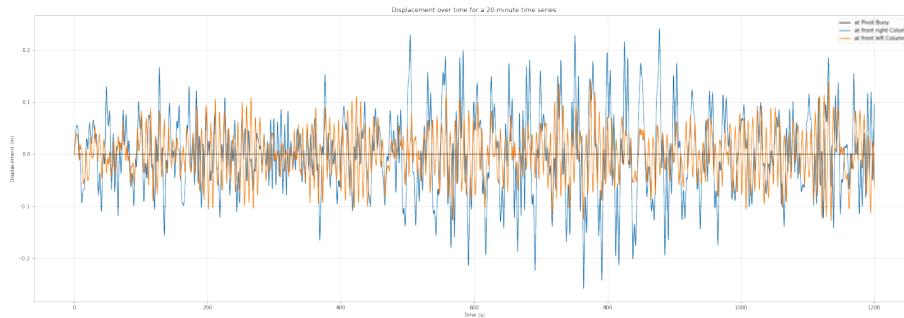


Figure 4.22: Time-series of the displacement at the corner points of the floater.

In Figure 4.23 - Figure 4.25 the displacement of every node of the system is depicted for the three translatory displacements. Note that all structural components are added to a list. For a more detailed display of the displacement per beam refer to Appendix D.

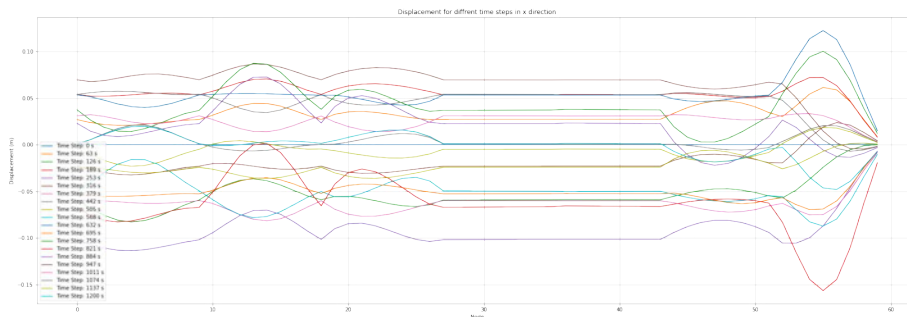


Figure 4.23: Displacement of every single node.

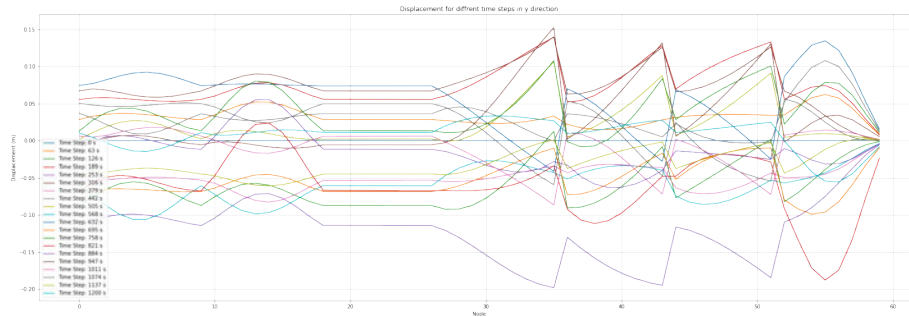


Figure 4.24: Time-series of the displacement of every single node.

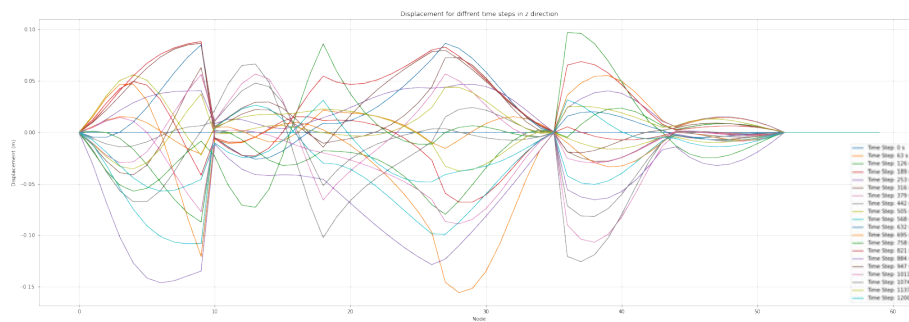


Figure 4.25: Time-series of the displacement of every single node.

4.5.3 Stresses

The stresses in every single element are derived from the displacements. The stresses provided valuable insight into the force distribution in the different beams. The obtained stress should be lower than the provided stress capacity by the quality of the steel beams itself. Therefore, after the stress calculation, the beams are checked for strength to ensure the structural integrity of the structure. This information could lead to possible adaptations of the design. The stresses in the elements can be subdivided into six different types:

- Axial stress in the x-axis
- Shear stress in the y-axis
- Shear stress in the z-axis
- Torsion stress in the x-axis
- Bending stress in the y-axis
- Bending stress in the z-axis

In Equation 4.28 to Equation 4.31 the equations used to calculate the respective stresses are shown. These equations show the stress relation between certain forces and the corresponding surface of an element. Since only the displacements are given, Hooke's law is also applied to represent the relation between the stress ratio, Young's modulus, and elongation.

$$\sigma_{Axial} = \frac{F}{A} \quad (4.28)$$

$$\sigma_{shear} = \frac{F}{A} \quad (4.29)$$

$$\sigma_{moment} = \frac{Mc}{Z} \quad (4.30)$$

$$\sigma_{torsion} = \frac{Tr}{J} \quad (4.31)$$

In the code provided, the rewritten formulas can be found. In Table 4.19 the maximum occurring stresses in the different members are depicted. The computed stresses for all DOF of all components of the substructure can be found in Appendix B.

Table 4.19: Maximum Stresses for different components.

Component	Stress (MPa)	Type
Left/right pontoon	856	moment y
Front pontoon	1486	moment z
Left/right mast	477	moment z
Pivot mast	2556	moment y

4.5.4 Ultimate limit state criteria

To ensure the safety and structural integrity of the structure for the ultimate limit state, resistance checks are performed whether the occurring stress is lower than the stress resistance of the steel element. The steel strength is set to be 355 N/mm² and it is assumed to be the same for every steel member of the structure. The member checks are done according to the regulations of the Eurocode. However, the FEM model already provides the occurring stresses of the entire structure. The benefit of this is the reduction of steps that need to be taken. In this case, the occurring stresses in the beams are multiplied with a safety factor of 1.15. Equation 4.32 is applied for the individual member check, which takes into account the highest occurring force during the time series of the applied wave forcing. Besides this check, a check where the combination of axial and moment stresses occur needs to be done. In Equation 4.33 this equation is shown.

$$\frac{\sigma_{Ed} * SF}{\sigma_{Rd}} < 1 \quad (4.32)$$

$$\frac{\sigma_{NEd} * SF}{\sigma_{NRd}} + \frac{\sigma_{MEd,y} * SF}{\sigma_{MRd,y}} + \frac{\sigma_{MEd,z} * SF}{\sigma_{MRd,z}} < 1 \quad (4.33)$$

Equation 4.33 is considered to be the most important unity check since all the forces can be considered. In Table 4.20, the most important unity checks are given, when the unity check is below 1, it is considered as safe. However, if the unity check is higher than 1, an adaption to the design is necessary since it can not be considered safe. It needs to be noted that this check is in the worst-case scenario. It is assumed that the highest moment in the y and z directions appears at the same time together with the axial force in the x-axis.

Table 4.20: Comparison of unity check for the Combined axial forces and moments between the standard and proposed improvement method models.

Element	UC [-]	UC threshold
Left and right pontoons	5.13	< 1
Front pontoon	6.95	< 1
Left and right masts	2.06	< 1
Pivot mast	12.64	< 1

None of the member checks are deemed sufficient which means that the design should be adapted. Therefore, extra members should be added to shorten the buckling length or the tube members should be replaced, for example, by trusses.

4.5.5 Structural improvements

Since the stresses in subsection 4.5.4 are above the resistance of the profiles, improvements in the structure are briefly investigated to lower the occurring stresses. This is done by adding additional members in the model, as visible in Figure 4.26. The idea behind the configuration of these beams is to divide each of the large triangles in the structure into four smaller ones, as visible in the front and bottom triangles. However, this was not possible with this model for all elements since the translation of members is only possible in one field (e.g. XY, XZ, or YZ translation) and these elements would need to be translated in two fields. The missing beams are shown in red, these are not implemented in the calculation but are expected to reduce the stresses in the beams. By implementing this, the maximum occurring stresses are already significantly lowered as can be seen in Table 4.21. However, the stresses are still not sufficiently lowered to be acceptable. One stress actually increases, which is the front pontoon. A reason for this could be that the weight of the RNA now gets directed onto the front pontoon instead of the nacelle columns. This quick analysis proposes a starting point for a follow-up structural investigation. In the current analysis, the dimensions of the original structural beams are not adapted and thus could be optimized in the next design cycle. A detailed investigation into this proposed structural analysis is not performed because of the given timeframe and limitations of the created model, it purely proves the structure needs further in-depth structural improvements to become a viable solution.

Table 4.21: Comparison of unity check for the Combined axial forces and moments between the standard and proposed improvement method models.

Element	First model U.C. [-]	Proposed improved model U.C.[-]
Left and right pontoons	5.13	2.57
Front pontoon	6.95	11.63
Left and right masts	2.06	1.76
Pivot mast	12.64	4.93

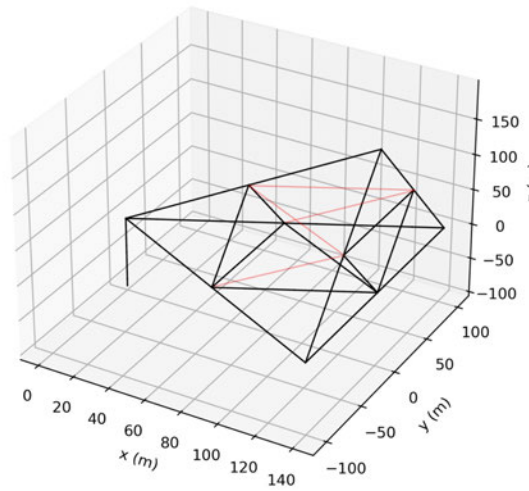


Figure 4.26: Improved structural configuration to resist occurring stresses.

4.6 Weight reduction

Currently, the design is equipped with singular tubular beams to simplify the analysis of the buoyant behaviour for the substructure of the 30 MW solution. However, studies show possibilities of weight reduction in a structure by replacing the single tubular beams with trusses. Therefore, in this paragraph, the method to determine the weight reduction by replacing the beams for trusses is discussed [25].

The following should be performed to determine the amount of weight reduction by replacing the beam with a truss:

1. The first step is to create a 2D model of a truss. In Figure 4.27, the model is provided. The truss consists of two horizontal with diagonal members in between. In this model, only the self-weight is included in the loading to simplify things, since the forces on the structure don't change significantly.

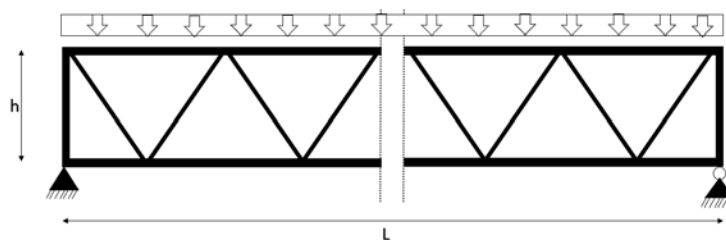


Figure 4.27: Model set-up for truss analysis.

2. Secondly, the reaction forces are determined with the use of force equilibrium. The only force to counteract is the distributed load representing the self-weight of the truss
3. Now the internal forces of every single component in the truss are determined. This is done by using the Method of Sections, (Figure 4.28), this is done for every component in the truss

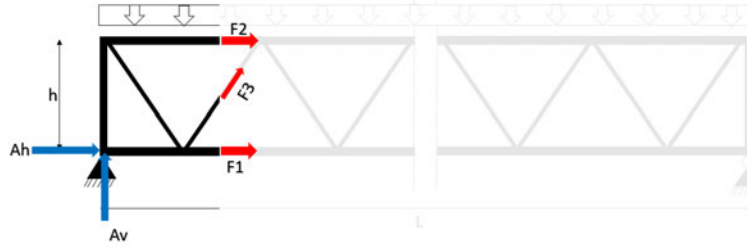


Figure 4.28: Overview method of sections.

4. Finally, the method of virtual work is applied to the truss. First, all the loads are removed from the model. After, a load is applied to the point where the displacement is calculated (in the middle). This is an iterative process, the purpose is to look for a similar deflection and see whether the weight of the truss is less compared to the singular tubular beam.

$$1 * \Delta = \frac{\sum nNL}{EA} \quad (4.34)$$

Where:

- 1 = the applied virtual force
- Δ = Real external deflection
- n = Internal force due to virtual load
- N = Internal force due to real load
- L = Length
- E = Young's Modulus
- A = Area

Because of limitations in the project timeline and resources, this iterative process to calculate an exact percentage of weight reduction could not be performed. This described process forms an opportunity for further research on this topic to increase the feasibility of the 30 MW solution.

4.7 Turret: yaw system with elastic coupling

PivotBuoy proposes a passive yaw system for a downwind turbine. The passive yaw system replaces the need for an active yaw system at the RNA level. PivotBuoy claims the removal of the active yaw system will reduce OPEX. This claim and the technical implications of using a turret system are assessed in the following chapter.

Figure 4.29 shows the setup of the TLP and floater connection using the Quick connect (5) system and a turret system (23) above. This figure is taken from the second patent related to the PivotBuoy system [26]. The Quick Connect System is supposed to allow for fast coupling and decoupling of the floater for maintenance operations. The figure shows the connection of the base structure of the floater (6) and the mooring interface connected to the TLP system (13). Between the two mating parts, elastic coupling elements are implemented to allow for small roll and pitch angles relative to the TLP. The base structure is supposed to be coupled to the floater (2) with the use of a yaw system (37) and bearings (23) coaxial to the longitudinal axis (50) to allow for the alignment of the floater with the direction of the wind. The electrical conductor line is funnelled through the system along the same axis (50).

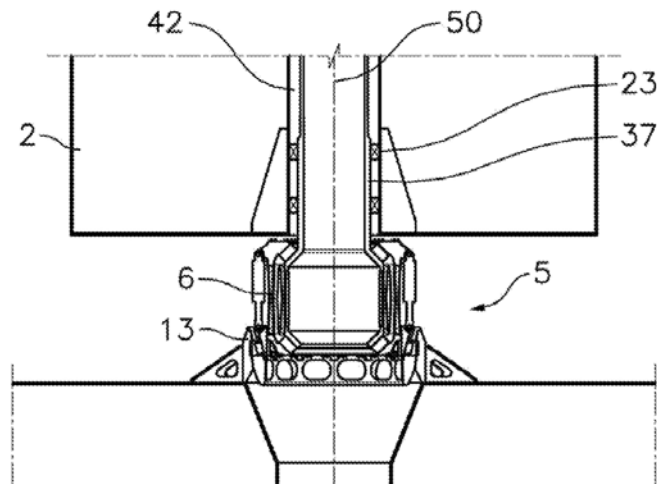


Figure 4.29: Detail of floater to TLP connection, including the quick connector and the turret [26].

The turret system proposed by PivotBuoy is similar to FPSO concepts, but it will have higher stiffness in the system since it is connected to a TLP system instead of catenary mooring lines. The bearing system needs to resist the radial force that is exerted due to the maximum trust force of the turbine. The vertical force on the bearing should be limited to compression forces. Introducing constant load direction changes has a negative impact on the fatigue life of the system. Due to the stiffness of the system and the expected constant pitch of the structure, higher variations in moments are to be expected in the connection between the floater and the turret.

As of yet, there is no design for a turret for a 15 MW or 30 MW DWT. The forces that are exerted on the turret and the bearings are expected to be high, considering the radial thrust force. It is therefore important to choose the right bearings for the turret.

4.7.1 Selection of bearing type

To choose the bearings, an understanding of the forces and movements is required. Depending on the type, bearings can resist or allow one or more of the three loads: radial load, axial load, and moment load. As moments in large turrets are countered by placing two bearings far apart on the same shaft (internal docs), the most important loads, in this case, are the radial and axial loads.

To meet these criteria, two different types are considered: double-row/four-row tapered roller bearings and spherical roller bearings. Both types are designed to withstand large forces in both the axial and radial directions. The double-row/four-row tapered roller bearing is better at resisting axial loads and moment loads, whereas the spherical roller bearing does not resist moment loads and therefore allows for bearing misalignment, meaning that it does not resist pitch movement of the platform, which could reduce stresses in the turret system (if no double bearing system is applied). As this system has to resist high loads at low speeds, ball bearings are not suitable [27].

4.7.2 Design Loads Cases

The loads used in this bearing analysis are based on the loads given from the pre-design model. At maximum thrust, the radial load on the bearings will be highest, and axial loads will be lowest. When there is no wind, this is the other way around. These two load cases are therefore looked at during the bearing dimensioning. A load coefficient $f_w = 2$ is applied to account for vibrations and impact during operation. The applied loads on the system are given in Table 4.22.

Table 4.22: Applied loads for 30 MW WT.

	F Axial	34000	kN
Idle	F Radial	0	kN
	F Axial	16000	kN
Power prod.	F Radial	13200	kN

4.7.3 Bearing calculation - Static analysis following ISO 76

The static equivalent load can be calculated using the following equation.

$$P_0 = X_0 F_r + Y_0 F_a \quad (4.35)$$

The factors X_0 and Y_0 are defined for each bearing [27]. For double-row bearings, X is always 1. Y depends on the angle of the rollers. Based on ISO 76, the required safety factor is defined as $F_s = 2.5$ [28].

4.7.4 Bearing calculation - Fatigue analysis following ISO 281

The dynamic equivalent load can be calculated using the following equation.

$$P = X F_r + Y F_a \quad (4.36)$$

The factors X and Y are defined with the help of Table 4.23.

Table 4.23: Factors for bearing fatigue.

Bearing Type	$\frac{F_a}{F_r} \geq e$		$\frac{F_a}{F_r} > e$		e
	X	Y	X	Y	
Single-row	1	0	0.4	$0.4 \cot(\alpha)$	$1.5 \tan(\alpha)$
Double-row	1	0.45	0.67	$0.67 \cot(\alpha)$	$1.5 \tan(\alpha)$

Based on the dynamic capacity C and the calculated dynamic equivalent load P , the total life of the system L (in revolutions) can be estimated using the following function:

$$L_{10} = \left(\frac{C}{P} \right)^{10/3} \quad (4.37)$$

For simplification, a basic rating life L_{10} with a service life of 90 % reliability is assumed when used under normal usage conditions for bearings of high manufacturing quality. Further research could focus on the modified rating life using different reliability estimates.

The safety coefficient is then calculated by comparing the calculated life L_{10} to the required life (amount of revolutions) L using safety coefficient f_s can be determined. Based on internal documents, the required safety factor for fatigue is defined as $f_f = \blacksquare$ (R&D TotalEnergies internal information, 2023). The required lifetime is 3.75 million revolutions over 25 years, or about 17 per hour, which is similar to lifetime calculations for other SPM solutions (R&D TotalEnergies internal information, 2023).

$$f_s = \frac{C_0}{P_0} \quad (4.38)$$

As the loads applied are larger than the ones for which predesigned bearings are designed, a specialized bearing system will be needed. Based on other bearings, a relation between size and strength is found. This relation can be used to extrapolate the strength of the bearings. From the needed capacity, the diameter can then be determined, as seen in Figure 4.30. The weight is also calculated this way and will be used later in the cost calculations.

Based on the required static and dynamic capacities for the bearing system, a diameter of at least 1.9 m is needed to guarantee safe operations during the lifetime, with a limited probability of failure.

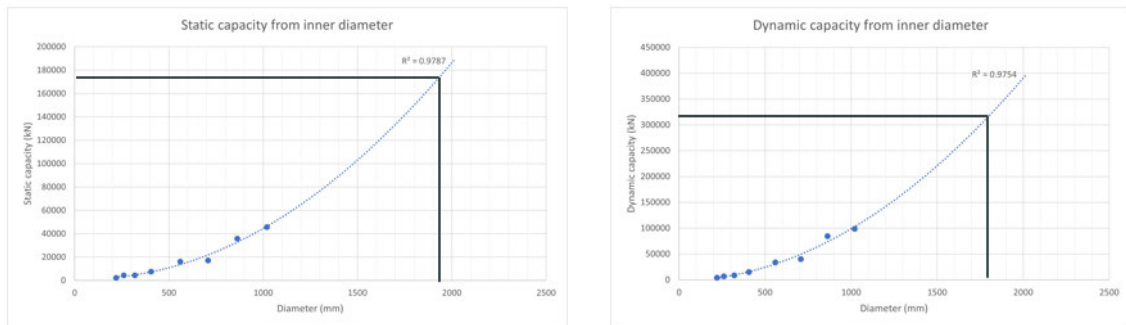


Figure 4.30: Extrapolation of bearing capacity and diameter size.

4.7.5 Failure modes

The failure of the bearing can be considered a critical event for the PivotBuoy system. Numerous potential issues can arise with bearings, both before and during operation. The most important failure modes are named in the table below. The failure of bearings is due to fatigue introduced by the number of revolutions and the magnitude of the load. The damage in bearings occurs at two different stages. Appendix C gives an overview of the relevant failure types.

Fatigue-induced shear stress on the load-bearing surface leads to primary damage types that eventually lead to the development of potentially surface-reaching cracks. If the bearings fail, they are not repairable or replaceable, requiring the change of the entire turret. This not only translates to expensive repairs and significant downtime but also the need to decouple the system. In the case of the PivotBuoy design, this would probably mean a decoupling, tow-to-shore, placing onshore, replacing PivotBuoy, placing in the water, tow-to-site, and coupling. This process could increase OPEX and result in a decrease in AEP. Therefore, efforts should be made to minimize the risk of failure.

Imperfections during assembly and wear throughout the system's lifetime further compound the issue. These combined factors ultimately result in a diminished ability for the system to effectively weathervane. Also, as there are two dominant wind directions, most fatigue is expected to occur on the two opposite sides of the bearing system. To reduce this effect, it is advisable to turn the connection between the turret and the TLP platform after each decoupling, which will be done standard for large maintenance operations.

The preliminary static and dynamic bearing calculations show that it is possible to design a turret system for the given load conditions. Nevertheless, due to constant changes in loading conditions between power production and idle combined with the changing environmental conditions, the bearings will experience high fatigue damage. Based on the initial findings, the turret system should not be considered a pitfall of the system, but instead as a component that requires special attention during its lifetime to guarantee a robust system. Considering the susceptibility of the system and the large efforts needed to replace the system, a reduction in CAPEX when compared

to an active yaw system should not be assumed.

4.8 Conclusion

The goal of the structural analysis was to investigate whether the direct scalability of the X1 Wind PivotBuoy concept is feasible as a 30 MW solution. In Figure 4.31, a short recap of the conclusions can be found.

Proposed 30 MW solution	
Global stability	✓
Stresses CHS	⚠
Natural frequencies	✓
Direct scalability of concept	✗
Proposed turret	
Load transfer	✓
Dimensions	✓

Figure 4.31: Conclusion Structural Analysis.

From the results, it can be concluded that the global stability of the proposed 30 MW solution suffices. However, the stresses in the beams are too high as of now. A method to reduce these stresses is proposed and shows an opportunity to increase the feasibility of this criteria. The natural frequency analysis shows one natural frequency of the structure that overlaps with one of the identified critical regions of the blade dynamics. However, it is noted that this specific eigenfrequency has minor deflections in the masts and therefore will not form a problem for the structural dynamic response. For this reason, the structure is deemed feasible for the natural frequency analysis. It must be noted that this analysis needs to be performed for every new structural adaptation (including the proposed improvement). In the end, it can be concluded that the direct scalability of the X1 Wind PivotBuoy concept as a 30 MW solution is not feasible.

For the proposed turret, it can be concluded that both the load transfer and the dimensions are feasible

Chapter 5

Lifecycle Assessment

In the lifecycle assessment, the feasibility of the proposed 30 MW solution is analyzed on six lifecycle components.

1. Supply chain
2. Construction
3. Transport
4. Installation
5. Operations & Maintenance
6. Decommissioning

This leads to the following research objective:

“Evaluate the feasibility of the supply chain, construction, transport, installation, operations & maintenance, and decommissioning of the proposed 30 MW solution.”

Each of these components will be analyzed separately in a section. For the transport and installation, the weather windows will also be assessed in section 5.7, after which a conclusion will be given on the overall feasibility of the lifecycle in section 5.8.

5.1 Supply chain

The supply chain is considered to be the necessary step before the construction or assembly of the turbine. This includes the fabrication by the original equipment manufacturers (OEM), the transport towards the construction and or maintenance yards, and the storage of the different components. To assess the supply chain, PivotBuoy and Intecsea BV, have made a preliminary industrialization plan based on 15 MW FOWTs in a 500 MW FOWF [29]. The document assesses the industrialization of each component on its fabrication, transportability and storability.

The evaluation method involves assigning a rating ranging from 1 to 5 to each component based on the aforementioned criteria. A score of 5 indicates components that are readily accessible, with conventional methods of transport and storage, an established supply chain, and readily available facilities. Conversely, a score of 1 implies that special measures are required for fabrication, transport, or installation, demanding particular attention. This rating system aids in the identification of bottleneck components within the process. Table 5.1 shows the different components considered in this analysis.

Table 5.1: Components analyzed in industrialization plan.

Sub-Unit	Components
WTG	RNA
Floater	Main Column
	Pontoon
	Damping Plates
	Pivot Mast
	Pivot Top
TLP	Tower Top Adapter
	Pivot Bottom
	Tethers
	Anchors

The industrialization plan by PivotBuoy and Intecsea BV only considers a 15 MW X1 Wind PivotBuoy, this report extends the analysis to the 30 MW (upscaled) solution, by evaluating the design with the same parameters. In the following subsections, an explanation of the ratings will be given per component; first, the ratings as given by the *D3.5: Industrialization plan for serial production of large farms* [29], and then the new ratings for the 30 MW solution. At the end of the section Table 5.2 gives an overview of the ratings.

5.1.1 Wind turbine generator

15 MW X1 Wind PivotBuoy: The Wind turbine generator (WTG) unit, as described by PivotBuoy, is the combination of all elements on top of a standard wind turbine, also known as the RNA. There are only a few manufacturers in Europe that fabricate large-scale RNAs. And these OEMs do not (yet) supply large-scale downwind RNAs. The WTG component fabrication will eventually be done in a centralized location at one (or more) of these OEMs and gets a rating of **3/5**. These large-scale components are not easy to transport, however, there is enough experience in this throughout the sector. The transport gets a rating of **4/5**. Finally, storage is also a well-known process, albeit not necessarily easy, and therefore is rated with **4/5**.

30 MW upscale: As of now, no OEM fabricates 30 MW nacelles, let alone downwind versions. The industry needs to make massive and high-risk investments to create a 30 MW downwind nacelle. As for the blades, the sheer length of the blades could create a bottleneck for the current factories of OEMs are not equipped for moulds of this size. Even though some of the factories themselves would be big enough in theory, the size of the blades could pose difficulties, see Figure 5.1. For the fabrication, the NRA gets a **2/5**.

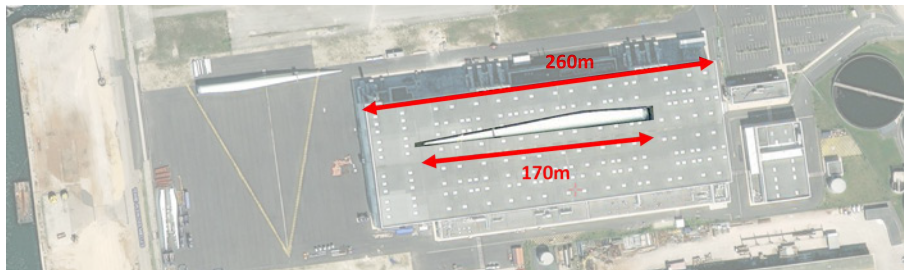


Figure 5.1: 30 MW blade compared to General Electric blade factory, Cherbourg, adapted from Apple Maps [30].

The transportation of the NRA components is also quite difficult. For the nacelle, multiple (very) heavy lifting operations are needed (see section 5.2. For the blades, specialised ships might be needed due to the length of the blades. The transportation of the NRA is given a rating of **3/5**.

Although the components will be bigger than for the 15MW version, there number of components is halved. This means the overall storage space required should be similar **4/5**.

5.1.2 Main columns

15 MW X1 Wind PivotBuoy: The Main columns get a **3/5** for fabrication. This is because they have a simple geometry, but a large diameter, which makes the fabrication process more difficult for larger scales. The fabrication of large cylindrical geometries is considered a specialized industry, with a limited number of yards that have the experience and production capacity. The main columns can be transported by barge, which is a common and cost-effective method for offshore structures. The fabrication yards are typically well connected to open seas, which allows for easy access and transport. For this, the main columns get a **4/5**. The main columns have a small footprint, which means they can be stored efficiently and compactly. The cylindrical geometry also lends itself to a better use of storage area. Thus the main columns are awarded a **5/5**.

30 MW solution: As stated above, with a larger diameter, the fabrication of the main pontoons becomes more difficult and specialized. In internal research of TotalEnergies, a large discrepancy is expected between supply and demand for these kinds of specialized steel structures. The supply chain will need to take significant steps to accommodate this. The fabrication is therefore rated **2/5**. The transportation and storage of these sturdy steel structures should not pose a larger problem than the 15 MW version, since only half of the components are needed, but they are heavier. The ratings thus stay the same at **4/5** and **5/5** respectively.

5.1.3 Pontoons

15 MW X1 Wind PivotBuoy: The pontoons form the structure that connects the three columns. They consist of two beams with diagonal cross bracings between them. This frame is made from universally available tubular sections of existing dimensions. Since the frame consists of long and thin elements, the construction and transportation are delicate processes. The long structures might not be able to support themselves without the connection with the columns or without the buoyant force of the water, resulting in the need for temporary supporting structures. The assembly of the pontoons could either be done at the assembly yard, with the drawback that the yard will need sufficient space to store and assemble the pontoons, but eliminating the need for complex transportation methods. Or be partially assembled at a secondary location. The pontoons receive a rating of **3/5** for the constructability and a **2/5** for both the transportation and storage.

30 MW solution: For the 30 MW solution, the manufacturing problems described above are exacerbated since the elements are even more slender, relatively speaking. This leads to a fabrication score of **2/5**. Transport and storage will not change, hence the scores are both **2/5**.

5.1.4 Damping plates

15 MW X1 Wind PivotBuoy: The damping plates help the platform have less dynamic response to heave. These steel plates are easily constructed, transported and stored. And thus receive a **5/5** for all criteria.

30 MW solution: Since the plates are easily scalable, the ratings do not change for the 30 MW solution, **5/5** for all.

5.1.5 Pivot mast

15 MW X1 Wind PivotBuoy: The masts of the X1 Wind PivotBuoy are constructed using commercially available tubular segments. Using these segments it is possible to use automatic welding, resulting in an uncomplicated fabrication process. Since the masts can be transported in different segments before being bolted together at the assembly yard, transport and storage should

not pose a problem either. The Pivot Masts receive a rating of **5/5** on all criteria. However, installation might pose a problem.

30 MW solution: The upscaled version has larger tubular sections, but the difference in scale should not pose a problem, since the industry is capable of manufacturing these components. Each of the criteria for the 30 MW solution is thus **5/5**.

5.1.6 Pivot top

15 MW X1 Wind PivotBuoy: The pivot top component receives a rating of **2/5** for fabrication due to its novelty and the need for specialized sub-components (connection piece, shaft, turret system, etc.) to be fabricated elsewhere. The pivot top scores **3/5** for transportation as it involves increased complexity and vulnerability compared to the main columns, requiring potential temporary bracing to ensure structural integrity during transit. For storage, the pivot top component is rated **4/5**. This is because it may necessitate additional temporary bracings to mitigate the risk of damage to the connection piece, indicating a relatively higher level of attention required for storage considerations.

30 MW solution: The pivot top is a complex part, it needs to be fabricated precisely. With the larger size, this precision is harder to accomplish. Furthermore, the trust force the pivot top needs to be able to withstand increases significantly. The combination of this precision, size, and strength makes this component very hard to manufacture, for which it receives a **1/5**. The transportation and storage do not change and are awarded a **3/5** and **4/5** respectively.

5.1.7 Tower top adapter

15 MW X1 Wind PivotBuoy: The tower top adapter is designed for convenient manufacturing and assembly. However, as it plays a critical role in connecting various components, precise dimensional control is essential. The component's complex shape, featuring four flanges in different planes, requires careful handling to avoid complications during assembly. Thus, it attains a rating of **3/5** for fabrication. Given its relatively small size, transporting the tower top adapter is not anticipated to present significant difficulties. Consequently, it receives a rating of **4/5** for transport. Due to its compact size, storage is not expected to pose significant challenges for the tower top adapter. As a result, it is rated **4/5** for storage.

30 MW solution: The tower top adapter needs to be fabricated precisely to allow for the long masts to be connected properly. With the larger size, this precision is harder to accomplish. It also needs to withstand the higher weight of the upscaled NRA. The tower top adapter gets a **2/5** for the constructability. The transportation and storage stay the same at **4/5**.

5.1.8 Pivot bottom

15 MW X1 Wind PivotBuoy: The pivot bottom component consists of a main structure with relatively straightforward geometries, allowing for relatively easy fabrication at a wide range of secondary fabrication sites. However, the elastic coupling component requires specialized manufacturing, involving a machined plate installation for flexible coupling. The tight tolerance between the mooring line connection and the flexible coupling further adds complexity to the fabrication process, resulting in a rating of **3/5** for fabrication. Due to its relatively compact size, transportation and storage of the pivot bottom component are not expected to pose significant challenges. The exact fabrication location(s) are not constraining to the overall industrialization plan, allowing for flexibility in logistics. Therefore, it receives a rating of **4/5** for transport. Similarly, the relatively compact size of the pivot bottom component implies that storage considerations will not be a limiting factor. It receives a rating of **4/5** for storage.

30 MW solution: The difficulties in fabrication, transportation and storage for the pivot bottom component will not change significantly when upscaled. Thus the ratings do not change and are **3/5**, **4/5**, and **4/5** respectively.

5.1.9 Tethers

15 MW X1 Wind PivotBuoy: The mooring system, employing vertically tensioned tendons or tethers, is a well-established and industrialized technique in the offshore industry, commonly utilized in oil and gas projects. Each mooring tendon for a full-scale system is likely to be supplied on its own spool of significant dimensions. Given the extensive experience of various manufacturers in this field, the fabrication process is expected to proceed smoothly. Therefore, the mooring system receives a rating of **5/5** for fabrication. The transportation of the mooring system, including the tethers on spools, is a straightforward process. The logistics can be organized directly from the manufacturer's location in preparation for the installation phase. Consequently, the mooring system attains a rating of **5/5** for transport. The storage of the mooring system components, which includes multiple spools, is anticipated to be manageable and is not expected to present significant challenges. Hence, the mooring system is rated **5/5** for storage.

30 MW solution: Tether systems have been developed for large-scale offshore objects before, the industry should be equipped to handle the upscaled turbine. The tethers receive a **5/5** for all criteria.

5.1.10 Anchors

15 MW X1 Wind PivotBuoy: The proposed anchoring system for the PivotBuoy, which involves three concrete blocks with pad eyes and an internal steel structure, is considered highly feasible for fabrication. The steel frames for the gravity bases are easily manufactured by local secondary fabrication sites. This process is efficient and does not pose significant challenges, resulting in a rating of **5/5** for fabrication. The logistics for the transportation of the foundation components are well-established. The steel frames are transported to the quayside, where vessels for anchor placement will embark. The use of concrete, which is readily available from numerous suppliers, allows for efficient mobilization to the offshore installation site. This, combined with the preference for local suppliers to minimize costs, leads to a rating of **5/5** for transport. Due to the widespread availability and cost-effectiveness of concrete, it is possible to select convenient locations for pick-up and mobilization, ensuring optimal storage conditions. This makes storage considerations for the foundation sub-unit manageable and not a limiting factor, resulting in a rating of **5/5** for storage.

30 MW solution: Anchors for large offshore objects have been made before, creating a larger concrete block as an anchoring solution for the 30 MW turbine, should not pose a problem in fabrication, transport, and storage. The ratings do not change in regards to the 15 MW turbine, **5/5** for all criteria.

5.1.11 Summary

Of the 10 components analysed for the supply chain, special emphasis should be given to the RNA, main columns and pivot top. These score the lowest overall for both the 15 MW X1 Wind PivotBuoy and the 30 MW solution. The supply chain of these three components could become a bottleneck for both designs. Furthermore, the pontoons and tower top adapter could potentially be a pitfall for the 30 MW solution. Table 5.2 shows the ratings given to the 15 MW X1 Wind PivotBuoy as given by *D3.5: Industrialization plan for serial production of large farms* [29], compared to the 30 MW solution ratings from this report. The ratings that have changed between the two designs are highlighted in red. The scale up to 30 MW increases R&D, fabrication, transportation, and storage to a level that could reach the limits of the industry. For the 30 MW

solution to be economically viable the supply chain needs to make major commitments. The rapid wind turbine growth comes with an increasing risk for OEMs who have difficulties with their products being outgrown quickly thus leaving limited investment return [31].

Table 5.2: Component rating comparison for 15 MW X1 Wind PivotBuoy [29] and 30 MW solution.

Sub -Unit	Components	Fabrication		Transportation		Storage		Overall	
		15MW	30MW	15MW	30MW	15MW	30MW	15MW	30MW
WTG	RNA	3	2	4	3	4	4	3.7	3.0
	Main Column	3	2	4	4	5	5	4.0	3.7
Floater	Pontoon	3	2	2	2	2	2	2.3	2.0
	Damping plates	5	5	5	5	5	5	5.0	5.0
	Pivot Mast	5	5	5	5	5	5	5.0	5.0
	Pivot Top	2	1	3	3	4	4	3.0	2.7
	Tower Top Adapter	3	2	4	4	4	4	3.7	3.3
	Pivot Bottom	3	3	4	4	4	4	3.7	3.7
TLP	Tethers	5	5	5	5	5	5	5.0	5.0
	Anchors	5	5	5	5	5	5	5.0	5.0

5.2 Construction

5.2.1 Construction steps

To construct the turbine, first, the three main columns will be placed and outlined on a flat surface. After this, the pontoons are placed in between and welded together. For this, cylindrical profiles and ready-made k-joints can be provided by suppliers. Because of the long distance between the main columns, temporary support might be needed [29]. As for the masts, they will also likely have to be supported during assembly. Therefore, a temporary support structure must be made, or multiple cranes have to lift it and keep it in place until it is connected to the rest of the structure. For this action, first, the underlying truss structure will be placed. Then, the two front masts are connected to the substructure and welded together, after which the pivot mast will be placed. As this is the longest and heaviest part of the structure, this requires the most effort. It will be a challenging operation and require multiple cranes.

After the substructure is completed, the RNA can be placed. This is done by first lifting up the nacelle, then installing the hub, after which the blades are installed as well. These parts can be installed on the yard, but that does make it slightly harder to get the construction in the water and the parts will have to be lifted higher. It is also possible to place the substructure in the water first and then lift up the RNA. With this method, the lifting height decreases, but the quay walls need to be strong enough to accommodate the cranes. The nacelle will weigh at least 1000 tons and be placed at a height of about 210 meters. As of now, no crane in the world can lift that much weight that high. Therefore, this is considered to be one of the biggest bottlenecks for the 30 MW design. To make it possible to lift the nacelle up, higher (gantry) cranes are needed, or modular nacelles that can easily be put together at the top of the structure. This is both dependent on the suppliers and therefore not in the hands of the producer of the turbine. As long as these solutions are not provided, the 30 MW concept will therefore be deemed unfeasible.

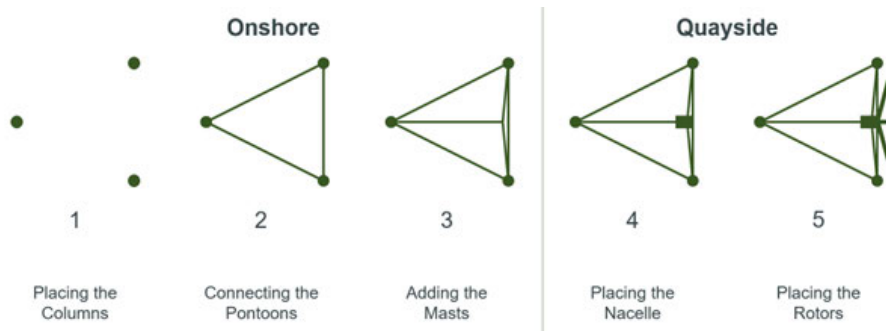


Figure 5.2: Steps of construction.

5.2.2 Construction yards

A construction yard is needed to assemble the separate components that have been delivered by the supply chain. In their quest to make Bretagne a front-runner in marine renewable energies (MRE), Bretagne Ocean Power has designated two ports for the construction and maintenance of FOWTs [8]. The two ports considered are Brest and Lorient. A map of the plans of Bretagne is shown in Figure 5.3. In this subsection, first, the requirements for the construction yards will be listed, after which both yards will be assessed on their suitability to construct the 15 MW X1 Wind PivotBuoy and its 30 MW upscaled version.



Figure 5.3: Map of Bretagne with proposed MRE ports Brest and Lorient [32].

5.2.2.1 Yard requirements

To construct the turbines, a yard has to comply with multiple requirements. There needs to be ample space for all separate parts to be stored before assembly. Wet storage can be used for parts of the substructure and the blades, while generators, transmission and electrical parts require dry

storage. There needs to be a good connection to the hinterland for incoming supplies and workers. Also, there is a need for parking spaces for workers and canteens and offices. The connection to the sea should be deep and wide enough to accommodate the turbines. Depending on the need for lifting operations on the quay wall, it should have a high enough loading capacity. There should be enough cranes with the right lifting capacity and height. Trucks or other vehicles are needed to transport parts across the yard. Lastly, the connection to the sea should be deep and wide enough to accommodate the tow out of the turbines.

5.2.2.2 Lorient

The first construction yard considered is in the port of Lorient. This port is designated as a logistics hub for installation and maintenance [33]. It is, inter alia, meant for the final installation steps before towing the FOWTs towards their intended locations. However, due to the considerable dimensions of the X1 Wind floater solution, the access channel of Lorient is not wide enough to support a tow to and from shore strategy (to Lorient). This is illustrated in Figure 5.4. The figure shows a map of the access channel of the port of Lorient on the left. On the right side, two zoomed-in maps are given; the top shows the area designated for the installation of FOWTs and the bottom shows the most critical point of the access channel. The green on the map shows a depth of less than four meters. The floaters of the 30 MW solution are ± 200 meters apart and have a draft of ± 10 meters. In its current form, the channel does not support such large structures. The access channel has a depth of approximately 8-10 meters for 7 km, making a dredging operation expensive. And, even if the access channel would be dredged, the width of the channel between the Citadelle de Port-Louis and the small islet of La Jument is only around 200 meters. These factors lead to the conclusion that Lorient is not suitable for a tow-to-port strategy. However, the port of Lorient could be used as a base of operations for inspections and minor repairs at sea, as it is in close proximity to Sud de la Bretagne I. Using Lorient as such could lower O&M costs, when compared to Brest.

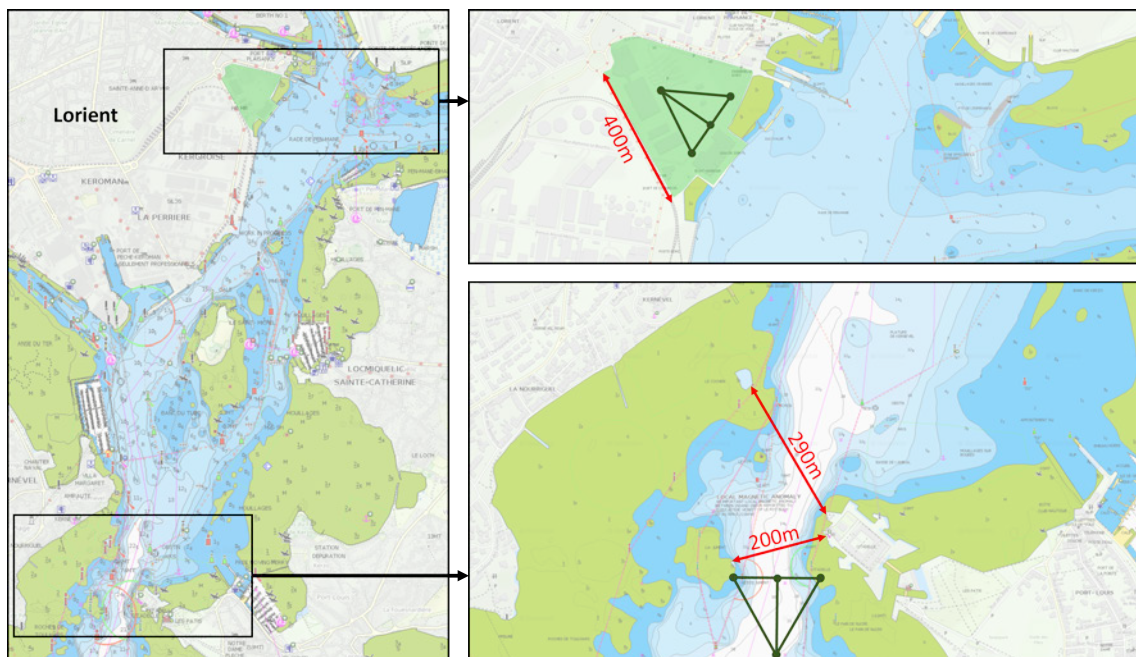


Figure 5.4: Map of Lorient (left) with the proposed yard (top right) and access channel width (bottom right), adapted from Navionics [34].

5.2.2.3 Brest

The Port of Brest is the other port considered for the construction yard. The yard is designated as a terminal dedicated to large MRE projects [35]. Unlike Lorient, the access channel for Brest is wide enough, illustrated by Figure 5.5. The most narrow part of the bay is approximately 750 meters wide. Near the yard, an access channel needs to be dredged to accommodate the draft of the FOWTs. Some of the key information about the yard in Brest is given in Table 5.3.

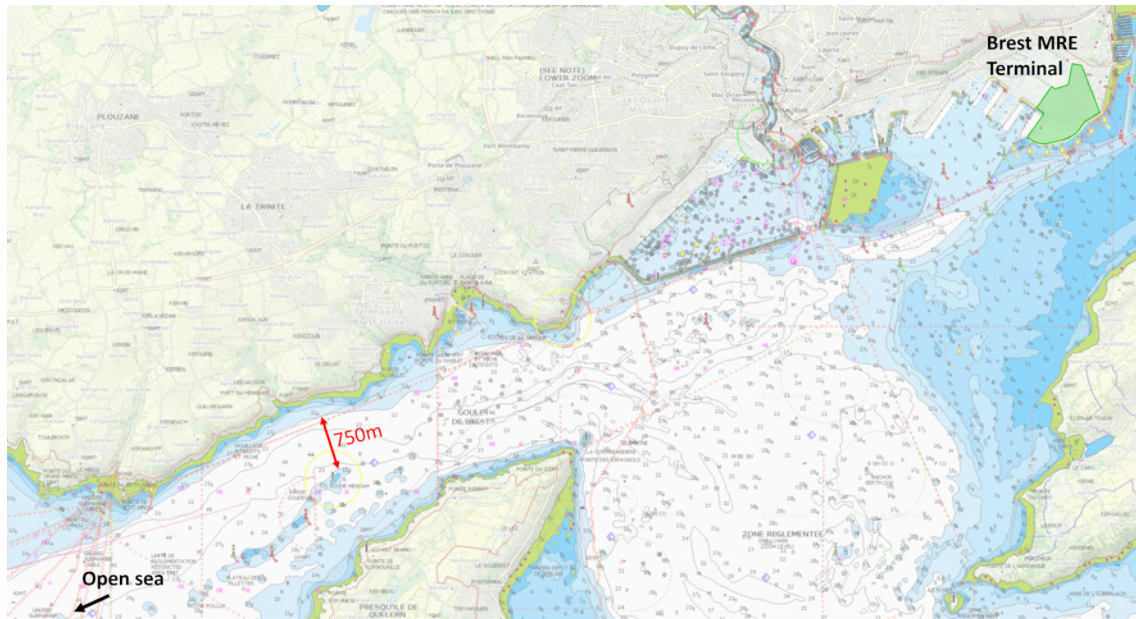


Figure 5.5: Map of Bay of Brest with proposed yard in green in the top right, adapted from Navionics [36].

Table 5.3: Port of Brest information [35].

Parameter	Value
Area	40 ha
Dock width	380 LM
Berth depth access	12 m
Quay load bearing capacity	64 t/m ²

To give an indication and feel of how the terminal in Brest could be used as a construction yard for the 15 and 30 MW X1 Wind PivotBuoy, a possible preliminary assembly layout is given for both turbine sizes in Figure 5.6.

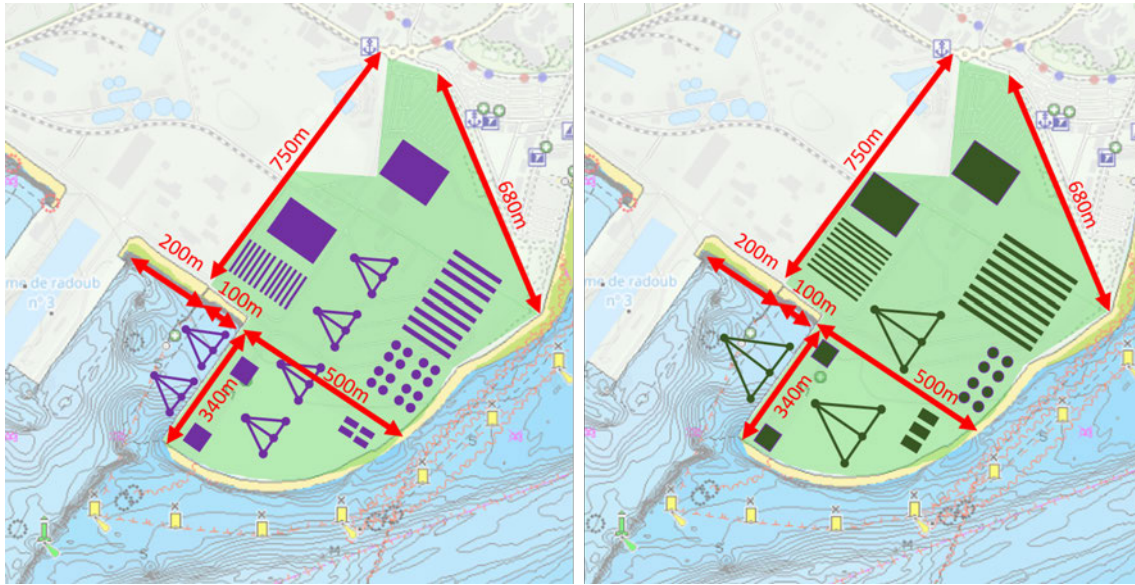


Figure 5.6: Map of Brest construction yard with preliminary layout for 15 and 30 MW X1 Wind PivotBuoy, adapted from Navionics [36].

5.3 Transport

With bottom-founded offshore wind turbines, construction, installation and maintenance of major components of the turbines happens often with heavy lifting operations using jack-up vessels. These operations can be very costly and require the availability of said vessels. However, FOWTs can be towed from and to ports for construction, installation and maintenance. This operation, which can be done by relatively simple tugboats, is a major advantage for FOWTs. As tugs are already used to move 200,000-ton cargo ships in ports, it is assumed they can also transport the 11,000-ton 30MW turbine, given that enough tugs are used [37]. The construction, installation and maintenance can be done in sheltered waters, with equipment on the quayside. For the deployment of the FOWTs at Sud de la Bretagne there are multiple temporary storage locations. Marshalling anchorages, described in subsection 5.3.1 are used to temporarily store turbines in between construction steps, or before towing them towards the site or harbour. The emergency anchorages described in subsection 5.3.2 can be used to temporarily store turbines in case of adverse weather conditions, before connection or after disconnection at the site. After the anchorages, the speeds and costs of the different vessels used are explained in subsection 5.3.3. And finally, the distances between all locations are shown in subsection 5.3.4.

5.3.1 Marshalling anchorages

The Marshalling anchorages can be used in multiple scenarios. They can store the turbines in between construction steps, for example, the floater and substructure can be stored before adding the nacelle and rotor to the structure. They can also store multiple turbines after construction has finished, to wait for a weather window long enough to tow the turbines to the site. Another option is to store turbines that are poised for maintenance when the construction harbour is unavailable. Two locations have been identified to be suitable as marshalling anchorages for the Sud de la Bretagne 1 site, assuming Brest will be used as the port for construction and (major) maintenance. The anchorages have been selected on the following criteria:

1. Draft between 12 and 25 meters;
2. Location near Brest; and

3. Designated for anchoring (large) vessels.

To check locations on these criteria, the Navionics naval charts near Brest [36] and the West coast of Europe sailing directives [38] have been used. The two possible marshalling anchorages are in the Rade de Brest and the Baie de Douarnenez, and are shown in Figure 5.7.

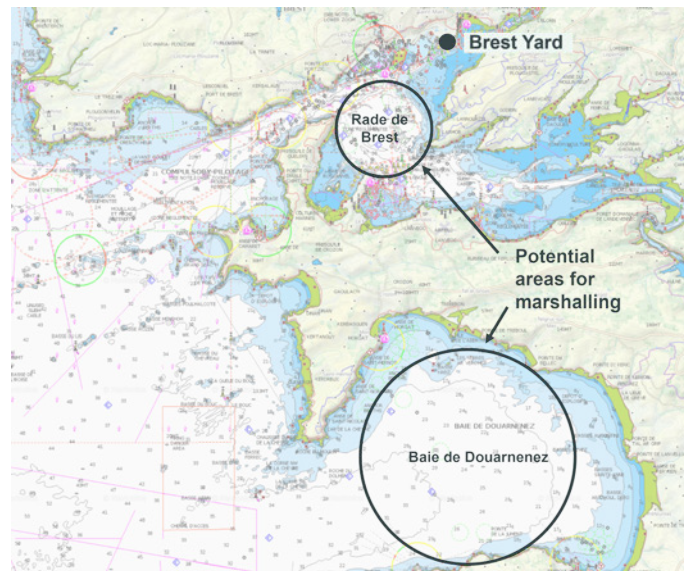


Figure 5.7: Map of possible marshalling anchorages near Brest, adapted from Navionics [36].

5.3.2 Emergency anchorages

The emergency anchorages are meant as a contingency measure and can be used when the weather suddenly changes and becomes too harsh for the towing or installing of the FOWTs. The marshalling anchorages described in subsection 5.3.1 can potentially also be used as emergency anchorages. The emergency anchorages are situated either en route between Brest and the site or near the site. The criteria used to select the emergency anchorages are:

1. Draft between 12 and 25 meters;
2. Location between Brest and the site or near the site; and
3. Designated for adverse weather anchoring.

Three emergency anchorages are identified using the Navionics naval charts near Lorient [34] and the West coast of Europe sailing directives [38]: The Baie d’Audierne, a bay on route between Brest and the site; the Coureau de Croix, a sheltered area between the island of Croix and the mainland near Lorient; and the Rade de Palais, a sheltered roadstead near Belle-île-de-Mer. All these locations are designated as anchorage areas for vessels in case of special weather conditions, and thus can not be used as a marshalling anchorage, but are suitable for emergencies. A map showing these three emergency anchorages in relation to the site is shown in Figure 5.8.

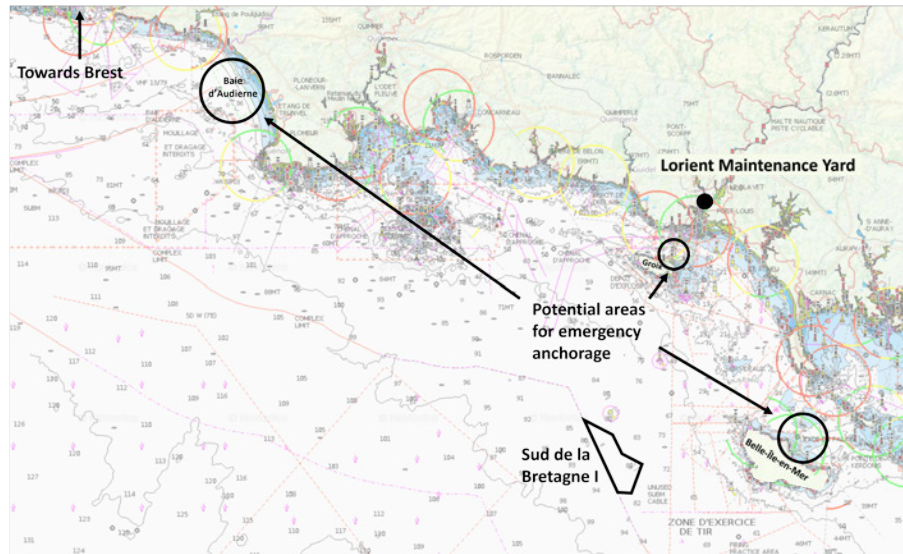


Figure 5.8: Map of possible emergency anchorages near site, adapted from Navionics [34].

5.3.3 Transportation vessels

The FOWT will be towed to and from the site, for installation, maintenance, and eventually decommissioning. With the design of the X1 Wind PivotBuoy platform, comes the benefit that it is possible to execute the towing operations with relatively standard tugboats. These tugboats have a transit speed of approximately 15-17 knots [39, 40], and cost around €50,000 per day [41]. The speed for wet tow operations is usually between 3 and 5 knots [42, 43]. Since the X1 Wind PivotBuoy platform is a stable platform [44], it is assumed that a speed of 5 knots is possible to achieve. For installing the anchors, anchor handling vessels (AHV) are needed, they cost around €50,000 per day each [41], and have a service speed of approximately 12 knots [45, 46]. For the final commissioning on site and smaller operations and maintenance activities, crew transfer vessels (CTV) can be used. Most have a speed of around 20-30 knots [47, 48], for this research 25 knots is used as the CTV transport speed. The costs of a CTV are approximately €2,500 per day per boat [41].

Table 5.4: Speeds of vessels in knots.

Activity	Speed [kn]	Cost [€/day]
Tug boat transit	15	50,000
Wet tug	5	50,000
AHV vessel	12	50,000
CTV vessel	25	2,500

5.3.4 Distances

To log the distances between the construction and maintenance yards, the marshalling and emergency anchorages, and the site, a distance table (Table 5.5) has been made.

Table 5.5: Distances between locations in km [34, 36].

	Brest	Lorient	Site	Rade de Brest	Baie de Douarnenez	Baie d’Audierne	Groix	Belle-île-en-Mer
Brest	x	180	170	5	50	80	170	200
Lorient		x	40	175	165	110	10	50
Site			x	165	150	95	35	30
Rade de Brest				x	45	75	165	195
Baie de Douarnenez					x	55	145	175
Baie d’Audierne						x	90	120
Groix							x	40
Belle-île-en-Mer								x

With the distances from Table 5.5 and the speeds described in Table 5.4, the travel time between the marshalling yards and the site, with some contingency, is estimated to be approximately 23 hours.

5.4 Installation

The installation procedure proposed by X1 Wind includes three steps. The following sequence applies as pictured in Figure 5.9. First, the foundation is installed at the seabed. Second, the tendons of the TLP systems and the Pivot Bottom (the floater) are installed. Last, the floater is connected in a separate step to the TLP system using the previously described Quick Connect system. This installation procedure gives high flexibility since all steps can be done independently. This is beneficial in the installation phase as the construction plan can be adapted flexibly depending on the given weather windows (more in section 5.7).

Steps 1 and 2 are industry standard and will not pose any more difficulties than conventional systems. Especially when using gravity-based anchors, the first step will have considerable time advantages over other types of anchors (rag-embedded anchors, suction anchors) or bottom founded solutions (drill, hammering, or vibration systems) [49].

The installation of the systems can become a cost driver, depending on the depth of the site and the anchor type. At large depths, maintainability can become difficult and thus be another cost driver for projects.

Step 3 can pose difficulties regarding the mating process. The suggested Quick Connect system proposed by X1 Wind [26] uses a male and female member supporting the mating operation. It is supposed to help position and connect the floater and TLP with a self-centring effect. The precise control of the relative motion at sea is a difficult operation. The mating is sensitive to significant wave height, period, wind, and current, thus critical monitoring and positioning are required. For conventional float-over systems, these problems are well-known in the industry and the mating process is well established. Considering the new system with the PivotBuoy the multi-body system’s dynamic reactions when subjected to combined wind, current, and wave forces need to be assessed in further research. With further extensive research, the installation can be considered feasible in the future. If considered feasible, this step would take approximately 4 hours according to PivotBuoy and WavEC [43].

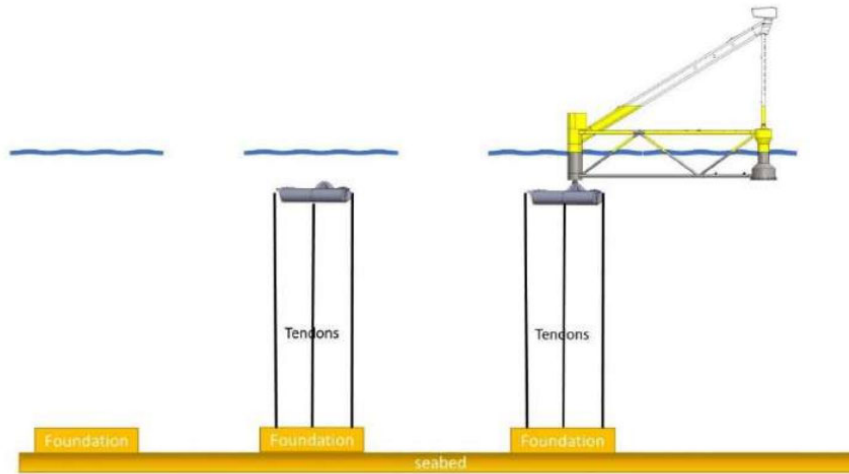


Figure 5.9: Installation sequence: 1) Foundation, 2) Tendons & Pivot Base, 3) Floater [29].

5.5 Operation & Maintenance

5.5.1 Maintenance strategies

There are three main categories for strategies in maintenance: proactive, corrective and a no maintenance or 'run to failure' strategy [50]. Although the latter strategy is not used as a strategy for the maintenance of wind turbines [51]. Corrective maintenance is done after a component has failed. It can either be done as emergency or deferred maintenance. Where emergency maintenance is an action that needs to happen as soon as possible as a response to an urgent situation, and deferred maintenance is work that can be postponed to a more convenient time, like a good weather window. If possible, one would want to avoid corrective maintenance as component failure can have drastic impacts on other parts of the wind turbines or even the wind farm. It can also lead to large losses in revenue if the component failure leads to turbine shutdown, as it can take a long time to mobilize vessels and resources, together with needing a viable weather window [43]. To minimise the risk of component failure proactive maintenance is used. Proactive maintenance entails the maintenance that is performed before it is necessary and can be done in a preventive or predictive manner. Preventive maintenance is time-based, and can either be done in a periodic sequence or after a certain amount of operation time, number of rotations of the turbine or PivotBuoy for example [52, 53]. Predictive maintenance is maintenance executed on either a diagnostic or prognostic basis. Diagnostic-based maintenance is done by monitoring and inspecting with sensors to identify the integrity of components. Prognostic maintenance is predicting the time of failure with data analysis, and modelling or is knowledge-based [54]. Using a combination of the different proactive maintenance strategies is key in minimizing (unplanned) downtime and or failures, however, these measures have costs associated with them, and thus a balance needs to be struck. Figure 5.10 shows the different maintenance strategies.

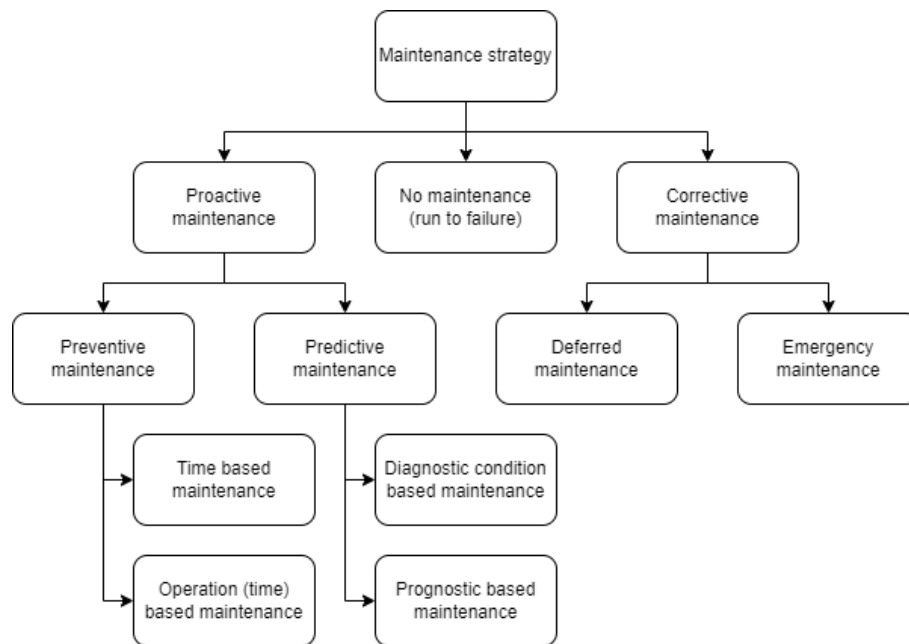


Figure 5.10: Maintenance strategies.

Besides the strategies displayed in Figure 5.10, there are three ways to execute these strategies. The maintenance can be executed by bringing maintenance personnel on-site, using remote monitoring, or by towing the turbine to shore. Most maintenance can be done by the first two options. But for major replacements, the tow-to-shore strategy can be beneficial. Performing major replacements often requires heavy lifting operations, which, in deep waters, are very complex operations due to the fact that both the crane and the turbine are separate floating structures. This, in combination with the scarce availability of heavy-lifting vessels, makes a tow-to-shore strategy viable. Using relatively widely available towing vessels to tow the turbine to shore, and repairing quayside, can eliminate the high costs associated with and the possible delays caused by the heavy lifting vessels.

5.5.2 Failure rates

To find out how often the wind turbines have to be towed to shore, first, the failure rates of components need to be identified. Knowing which components fail, and (on average) how often, can be a good indicator of how often the turbines have to be towed to shore due to failures. Carroll et al. looked at the failures of wind turbines and identified how often different components failed per turbine per year [55]. They categorize failures in three different severities, major replacements, major repairs and minor repairs. It is assumed that only major replacements must necessarily be done at port, while repairs can be done on-site. The most critical components are the generator and the gearbox. However, since the design considered is a direct drive wind turbine, it is fitted without a gearbox, thus mitigating these failures. On the other hand, Perez et al. found that direct drive turbines have up to twice the amount of generator and electric failures [56].

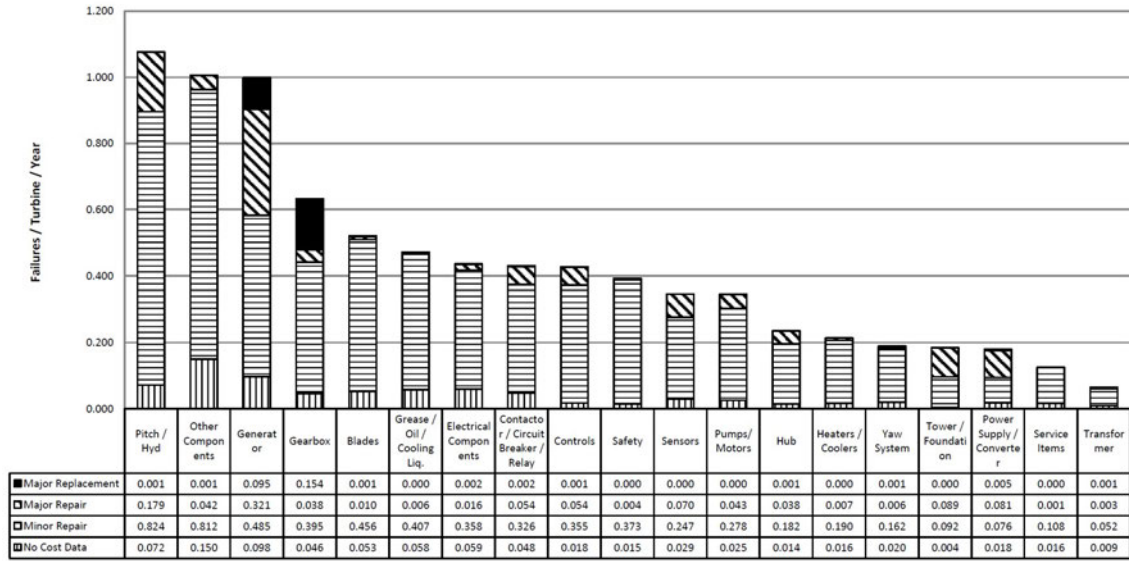


Figure 5.11: Failure rates of components identified by Carroll et al. [55].

Table 5.6 shows the major replacement rates for the different components when combining both papers. The major replacements of the gearbox have been removed, and all electrical components have been doubled. Since this table only focuses on the major replacements, the table does not show the components that have no major replacements. Note that the design does not include a (active) yaw system, and this category has thus been removed. On average each turbine has to be towed to port due to component failure approximately every five years.

Table 5.6: Major replacements per component per turbine per year, adapted from [55, 56].

Component	Rate
Generator	0.190
Power supply / converter	0.010
Electrical components	0.004
Contacto r / circuit breaker / relay	0.004
Transformer	0.002
Pitch / hyd	0.001
Blades	0.001
Controls	0.001
Hub	0.001
Other components	0.001

5.5.3 Applied maintenance strategy

With the possible maintenance strategies and the expected failure rates, the applied maintenance strategy can be formalized. The maintenance should be done mostly in a proactive manner, with both preventive and predictive measures. The preventive maintenance would be inspections on site, where the frequency depends on the parts that are monitored and maintained. For the turret, this would be at least two times a year to check and replace the lubricants. Doing small repairs on site if necessary, and, if conditions of certain critical components such as the generator or turret are indicating impending failure, call for a tow to shore to do large replacement or maintenance activities. At the same time, the most critical components should be monitored frequently using both sensors and data on e.g. energy production. If for example data shows that a turbine does not align as well with the wind as expected, an inspection of the turret can be done, and if needed,

it can be replaced at shore. For costly replacements as such, the cost of replacement should be weighed against the potential loss in revenue (or safety) during the remaining lifetime of the turbine. When a turbine is towed to shore for large maintenance activities, all other components should be inspected as well, potentially forestalling an expensive second trip towards shore. Applying these strategies should aim to minimize unexpected and possibly dangerous failures.

Lorient can be used as an operations & maintenance base. It could be used for the offices for monitoring the site, and house CTVs to transport crew and equipment to the site for inspections and smaller maintenance activities. For large maintenance, where the turbines have to be towed to shore, Brest can be used. These yards, Lorient and Brest, could potentially be used to cater to several wind farms in the Bretagne region, spreading operational costs over multiple projects, and thus reducing the per project OPEX.

A showstopper for the 30 MW turbine in maintenance could be the replacement of the nacelle. As stated in section 5.2, lifting the nacelle is currently a nigh impossible operation. To replace the nacelle, this operation has to be done twice; bringing the old nacelle down, and replacing it with a new one. To combat this bottleneck, it could be possible to replace only parts of the nacelle by making it (semi-)modular.

5.6 Decommissioning

Between the 15 MW semi-sub and the X1 Wind PivotBuoy concept, there are only small differences in decommissioning. Both turbines can be detached and towed to shore, where they can then be taken apart in a deconstruction yard. For the 30MW turbine, the main challenge will be, again, in lifting. Assuming the structure will be decommissioned in a controlled manner, it can be hard to lift the parts of the RNA from the top of the turbine. Another possibility is lifting off the blades, as they are made of a different material (glass fibre) and then using explosives to topple the steel construction, after which parts can be taken from the ground.

Whereas the IEA uses more traditional catenary mooring lines with a drag-embedded anchor, the X1 Wind PivotBuoy concept uses a TLP with a gravity anchor. Drag-embedded anchors are the simplest to remove, as they are based on traditional anchors from ships. For a gravity anchor, if it needs to be removed, it must be lifted out of the sea, which can be hard as it is much heavier. If a new wind farm will be created, the gravity anchors can be left and reused [57]. For the 30MW solution, this gravity anchor also gets more than 3 times as heavy as the one for the 15MW design, so lifting it will be even harder. However, the industry also has at least 30 years to grow with the task of decommissioning larger and larger structures.

5.7 Weather window

Installation of offshore wind turbines normally only happens for a few months each year. This can be a limiting factor for the duration of the process. Therefore, it is advisable to look into the amount of available weather windows that allow for safe installation per year. By doing this, a good estimate can be made of the time it takes to install the wind farm and how to plan this.

To get this estimate of available weather windows, 20 years of ERA5 climate data is used from Copernicus, including wind speed and significant wave heights. In this data, all cases can be found in which wind and wave conditions are below the operational threshold for a certain amount of hours that is needed to install a turbine.

To install a turbine, there are two main operations: towing out to the location and mooring. For the PivotBuoy concept, the anchors and TLP can be installed beforehand, so mooring only consists

of placing the PivotBuoy on the TLP. They state that this operation plan takes about 4 hours [43]. As for the towing, this is estimated to take approximately 23 hours, based on a distance of 170 km and a tow speed of between 3 and 5 knots [42, 43]. To be safe, an extra 3 hours will be taken into account for time loss. In that case, at least 27 hours of good conditions are needed to install. To be safe, an extra 3 hours is taken into account to make sure operations can be done safely.

For the wind conditions, it is assumed that the threshold will be similar to that of vessel crane limits, so 12-15 m/s. The maximum allowed wave height is 1.5 m [43]. For extra safety, a safety factor is applied to the conditions, the so-called alpha factor. For wind, as well as wave conditions, this is 0.78 for significant wave height and 0.8 for the wind speed. These factors are incorporated to account for prediction uncertainty, which means that operations will only happen if a weather window is predicted with 78% or 80% of the threshold value. As an example, the available calculated weather windows in 2003 are shown in Figure 5.12.

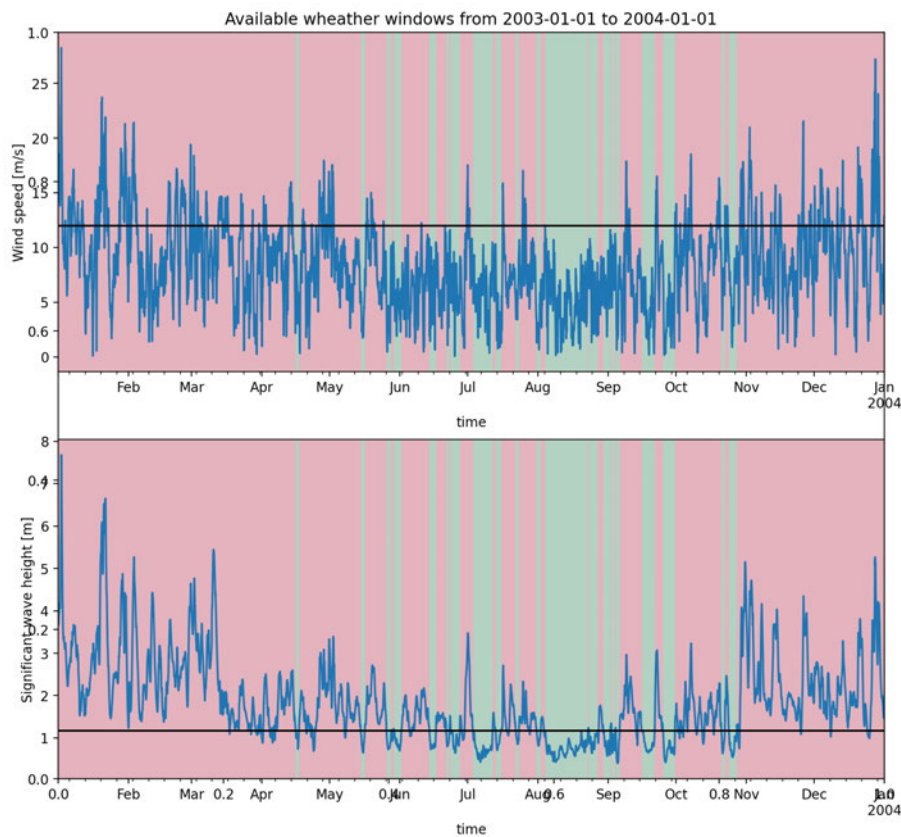


Figure 5.12: Weather window available for installation.

Seasonality is clearly visible here, and it shows why the installation of offshore wind farms is nearly exclusively done during the summer. In Table 5.7, the average windows per month and the hours within these windows are shown. In January, there would in theory be enough time on average to install one turbine. However, not every year has an available window in January, so it would not be advisable to plan maintenance or installation in this month.

From this table, it can be concluded that there is ample time to install turbines from April to September. In these months there are on average about 18 windows available, ranging from 61 to 86 hours of duration on average. This should, in theory, be enough to install fifteen 30MW. The reason this is possible is mainly due to the low installation time at sea. Previous installation time was '6.25 days in 2015 for medium machines (3 to 4 MW) on monopiles' [58]. The minimum

Table 5.7: Weather windows with alpha 0.78 for waves and 0.8 for wind.

Month	Windows (average)	Hours per month (average)	Hours per window (average)
January	0.45	25	56
February	0.6	34	57
March	0.75	46	61
April	2.25	142	63
May	3	214	71
June	3.45	281	81
July	4.1	329	80
August	3.75	321	86
September	2.4	198	82
October	1.4	84	60
November	1	54	54
December	0.45	33	74

construction time for the farm will likely not be limited by the weather windows, but more likely by supply chain or assembly durations. It also depends on the availability of marshalling anchorages. If these are available in winter, assembly could start sooner and - theoretically - the farm could be constructed within one year. However, for this, the electrical infrastructure and anchors should already be installed or be installed in parallel.

5.8 Conclusion

The goal of the lifecycle analysis was to assess the feasibility of the 30MW upscale in six aspects outside of structural and economic feasibility. These categories are shown below, in figure Figure 5.13.

Feasibility	
Supply chain	⚠️
Construction	❌
Installation	✅
Transport	✅
Operation and maintenance	⚠️
Decommissioning	✅

Figure 5.13: Results of life cycle analysis.

For the supply chain, big commitments are required from the industry. Mainly for the RNA, pivot top and main columns this is needed. The RNA is, as of yet, not available for 30MW turbines. To make this possible, they have to be developed first and this has made it hard for manufacturers to make a profit in the past, as 15MW turbines are not even produced on a large scale yet. They have however already invested money in this, so it is unlikely they will upscale before they can earn back their development costs. The same counts for the blades. Also, blade factories need to be expanded, as the blades are made from a single mould, housed in the building.

When looking at construction, the main bottleneck is the lifting of the nacelle. This part can weigh 1400 tons and has to be lifted to a height of 210 meters. Even if this can be lifted in parts, which could lead to dangerous situations, the cast iron hub itself weighs 405 tons and can not be lifted in pieces. With equipment currently available on the market this is impossible. Therefore,

larger cranes have to be designed or new lifting techniques should be investigated to make the construction of the 30 MW solution feasible.

Installation is not likely to pose large new problems. The installation of TLP's has been done before and on an even larger scale. For the coupling, this is considered a regular float-over operation. However, it could be interesting to look at the dynamic behaviour during coupling to find the limits for sea conditions. Right now conditions of 15 m/s wind and 1.5 m significant wave height have been assumed as operationally safe, which is in line with offshore lifting and installation operations. As for the weather windows, it was shown that there is ample time within a year to place the turbines.

Transport is, in this case, the tow-out to the farm location. Tugs can be used to tow and move 200,000-ton cargo ships, so it is assumed the same can be done with the 11,000-ton 30MW turbine. No problems are expected with this operation.

The biggest potential problem for operations and maintenance lies in the large maintenance, where the heavy and high lifting operation might cause inconveniences. One opportunity in this part is the use of the ports of Lorient and Brest for multiple wind farms in Bretagne, to alleviate O&M costs.

As for the decommissioning, no big problems are foreseen. The operations themselves are all well-known, with a tow-to-shore operation and decommissioning happening on land. Calculating in the construction time and lifetime, the industry would also have 30 years to grow with the larger turbines until decommissioning needs to happen.

Chapter 6

Economic Evaluation

The goal of the economic evaluation is to investigate whether the 15 MW and 30 MW downwind solutions are economically feasible when compared to the 15 MW IEA. To achieve this, the three wind farm designs will be analyzed and finally compared based on their LCOE. This LCOE is found through Equation 6.1. From this equation, it can be seen that the AEP, the CAPEX, and OPEX first need to be investigated and found. This chapter will look at all three wind farm designs. firstly, calculating the AEPs. After this, the CAPEX, OPEX, and ABEX are investigated and calculated. Then, the uncertainties together with the CAPEX and OPEX are explored and quantified. Finally, the three LCOEs are calculated with the uncertainties taken into account, and a comparison is performed between these three LCOEs. With this, an answer can be formed on whether the 15 MW and 30 MW downwind solutions are economically feasible when compared to the 15 MW IEA.

$$LCOE = \frac{(CAPEX * FCR) + OPEX}{AEP} \quad (6.1)$$

6.1 AEP

To compare the production performance of the different wind turbine designs on a farm level, the AEP is calculated. This is done for the upwind 15 MW IEA wind farm and the two downwind farms. The major difference is in the yaw misalignment between these two wind turbine designs. This difference is investigated in this paragraph.

6.1.1 Price of Energy

To calculate the AEP, the price level at which the energy is sold is needed. To come to a valid energy price, multiple sources are used. these are the monthly weighted average of the European power exchange (EPEX) continuous energy market in September [59], the French market analysis by Haya Energy Solutions [60], France Electricity Price September by Trading Economics [61], Reuters based on Refinitiv Eikon [62], and Statistica Research Department August average [63]. The values for the price of energy from each of these sources are given in Table 6.1. The average of these energy prices is approximately **0.11 €/kWh**, which is used in the rest of this report as the price of energy.

Table 6.1: Prices of Energy.

Source	€/MWh
EPEX spot market monthly average	104.45
Haya Energy Solutions average Aug	86.16
Haya Energy Solutions futures Oct	99.36
Trading Economics	134.05
Refinitiv Eikon Year Ahead	141.00
Refinitiv Eikon 2030 forecast	80.20
Statica average Aug	90.96
Average	105.17

6.1.2 Wind farm optimization

6.1.2.1 15 MW

The optimization of the wind farm layout is based on the predefined site conditions and layout constraints described in section 1.4, chapter 3, and section A.1. With a predefined turbine power of 15 MW, the site is optimized for 30 turbines resulting in a total capacity of 450 MW. The model takes into account the following parameters, as summarized in Table 6.2:

Table 6.2: Parameters for optimization of 15 MW turbine.

Parameter	Value	Unit
Number of turbines	30	-
Power rating	15	MW
Min. turbine distance	1440 (6 x Rotor diameter)	m
Distance from Shore	60	km
Energy Price	0.11	€/kWh
Project Duration	25	years
Rated RPM Array	12 (* n_{wt})	rpm
Water Depth Array	100 (* n_{wt})	m
Discount Rate	7	%

Note, that the energy price is subject to frequent fluctuations. In this report, a fixed value of 0.11 €/kWh has been used, as described in subsection 6.1.1. This value can be adjusted within the model, and its sensitivity will be explored later in this report.

The main driver of the optimization of the IRR (Internal Rate of Return) is the AEP. Therefore, this optimization of \blacksquare % resembles the optimized layout based on maximizing the AEP. Figure 6.1 displays the initial and optimized turbine layout. The IRR of the 15 MW IEA is \blacksquare % and in the case of the 15 MW X1 Wind (not displayed here) the IRR after optimization is \blacksquare %.

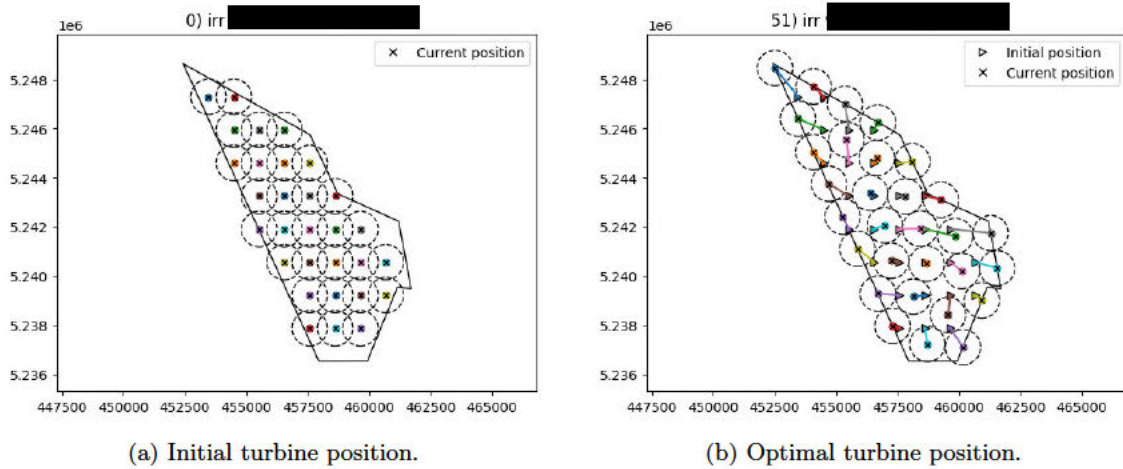


Figure 6.1: Comparison of 15 MW IEA Wind Turbine Positions.

6.1.2.2 30 MW

The optimization of the 30 MW wind farm is done similarly to the 15 MW layout. With a predefined turbine power of 30 MW, the site is optimized for 15 turbines resulting in a total capacity of 450 MW. The model takes into account the following parameters, as summarized in Table 6.3:

Table 6.3: Parameters for optimization of 30 MW turbine.

Parameter	Value	Unit
Number of turbines	15	-
Power rating	30	MW
Min. turbine distance	2040 (6 x Rotor diameter)	m
Distance from Shore	60	km
Energy Price	0.11	€/kWh
Project Duration	25	years
Rated RPM Array	5.5 (* n_{wt})	rpm
Water Depth Array	100 (* n_{wt})	m
Discount Rate	7	%

Figure 6.2 displays the initial and optimized turbine layout. The IRR for the 30 MW wind turbine is [REDACTED]

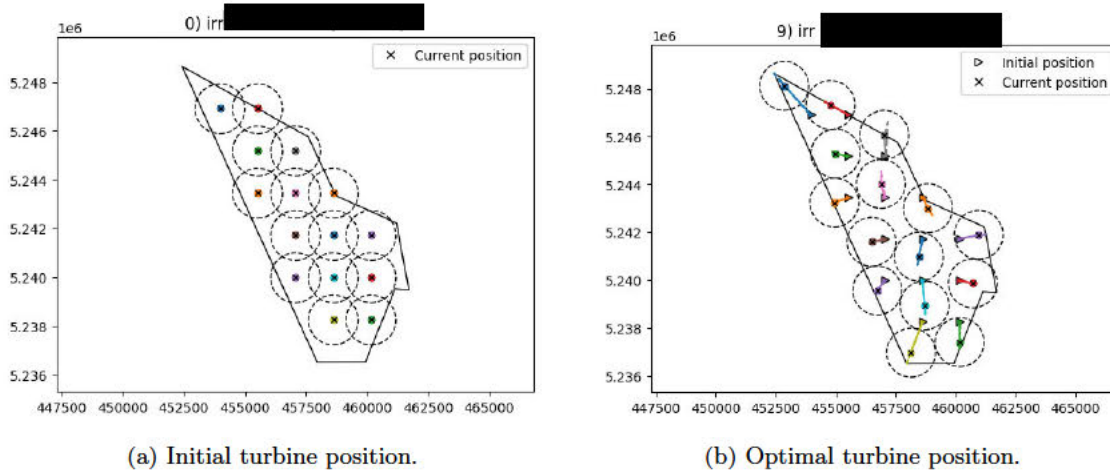


Figure 6.2: Comparison of Wind Turbine Positions.

6.1.3 Yaw Misalignment

Misalignment plays an essential role in the AEP estimation of a wind farm. Since `PyWake` has no integration for a DWT, a clear difference needs to be made in order to calculate the AEP when compared to a UWT. A UWT needs an active yaw system to turn the turbine rotor and face it in the wind direction. A DWT on the other hand, does not need an active yaw system because it naturally turns and faces into the wind as the wind flows past it. More on that in section 2.2.

6.1.3.1 Active Yaw system

Conventional active yaw systems operate on a measured 10 minute mean wind speed and usually respond to mean yaw errors above 10° . The AEP decreases significantly when the misalignment angle exceeds 10° . For active systems, a mean misalignment of approximately 5° can be achieved. Thus, the `PyWake` model is set up using a constant mean yaw of 5° to resemble the mean loss due to the yaw misalignment. Table 6.4 highlights the variations in energy production for different mean yaw angles.

Table 6.4: Influence of mean yaw misalignment on AEP for the IEA 15 MW wind farm.

Yaw (degrees)	AEP (GWh)
0	
5	
10	
20	
45	

6.1.3.2 Passive Weathervaning Yaw system

With passive weathervaning yaw systems, the turbine yaws towards the direction of the wind due to an aerodynamic shape. In theory, the turbine should thus always be aligned with the wind. However, due to differences between wind and current direction, the turbine will have some misalignment. Little research has been conducted so far on the influence of yaw misalignment of DWT. Netzband et al. [64] gave insight into the impact of wind and current offset on the yaw misalignment and power loss for a 6 MW DWT with a ‘SelfAligner FOWT’ [65]. The difference in turbine size is significant compared to the 15 MW X1 Wind PivotBuoy and a possible 30 MW scale-up, but the research gives clear trends on the behaviour of DWTs that can serve as guidance for a first AEP estimation. The following trends are observed:

1. Yaw misalignment increases with increasing wind-current offset.
2. Yaw misalignment increases with increasing current velocity.
3. Yaw misalignment decreases with increasing wind velocity.
4. At a wind velocity of around 11 m/s an increased misalignment is noticeable. Note, that the study assumes the worst-case scenario where the wave energy in the seaway amplifies with higher wind speeds, and the direction of wave propagation aligns with the current flow.

For this study interpolation of the given data from Netzband et al. [64] is performed to estimate the AEP of the 15 MW X1 Wind PivotBuoy DWT and the 30 MW scale-up. Besides the above-introduced observation, we define the following assumptions:

5. Yaw misalignment below a current velocity of 0.2 m/s is interpolated linearly between 0 m/s and 0.2 m/s.
6. Yaw misalignment for wind speeds exceeding 11 m/s is assumed to be equivalent to that at 11 m/s. Note, this way the prior mentioned assumption from the study by Netzband et al. is not overestimating the influence of the wave propagation aligning with the current flow.

The following Table 6.5 displays the misalignment for wind-current offsets ranging from 15° to 90°. When cross-current is low, the yaw misalignment up to 10° is comparable to conventional turbine design with an active yaw system. A misalignment between the turbine and the wind of 15 degrees can already give a 6 per cent decrease in energy production. [64].

15° Offset						30° Offset					
	0.1	0.2	0.3	0.4	0.5	0.1	0.2	0.3	0.4	0.5	
3	2.3	4.6	6.3	8.6	10.8	4.6	9.2	12.6	17.2	21.5	
4	1.6	3.2	5.2	7.3	9.2	3.3	6.5	10.4	14.6	18.5	
5	1.1	2.1	4.1	6.0	7.8	2.1	4.2	8.2	12.1	15.6	
6	0.6	1.2	3.1	4.9	6.4	1.2	2.4	6.2	9.7	12.9	
7	0.3	0.5	2.2	3.8	5.3	0.6	1.1	4.5	7.6	10.5	
8	0.1	0.2	1.6	3.0	4.3	0.2	0.4	3.2	6.0	8.6	
9	0.2	0.1	1.2	2.4	3.7	0.1	0.2	2.5	4.9	7.3	
10	0.5	0.3	1.2	2.2	3.3	0.3	0.6	2.4	4.5	6.6	
11	0.5	0.9	1.6	2.5	3.4	0.9	1.7	3.2	4.9	6.8	

45° Offset						60° Offset					
	0.1	0.2	0.3	0.4	0.5	0.1	0.2	0.3	0.4	0.5	
3	6.9	13.8	18.9	25.8	32.3	7.0	13.9	24.2	44.0	58.6	
4	4.5	9.7	15.6	22.0	27.7	5.5	11.0	19.6	34.0	46.1	
5	3.2	6.3	12.3	18.1	23.3	4.2	8.4	15.5	25.9	35.8	
6	1.8	3.6	9.3	14.6	19.3	3.2	6.4	12.2	19.6	27.6	
7	0.8	1.6	6.7	11.4	15.8	2.5	4.9	9.6	15.0	21.4	
8	0.3	0.5	4.8	8.9	13.0	2.0	4.0	7.8	11.9	17.0	
9	0.2	0.3	3.7	7.3	11.0	1.9	3.8	6.9	10.2	14.4	
10	0.5	1.0	3.6	6.7	10.0	2.2	4.3	6.9	9.8	13.3	
11	1.3	2.6	4.8	7.4	10.1	2.8	5.5	8	10.7	13.7	

75° Offset						90° Offset					
	0.1	0.2	0.3	0.4	0.5	0.1	0.2	0.3	0.4	0.5	
3	11.6	23.1	31.6	43.1	53.8	9.4	18.7	51.7	65.7	86.3	
4	8.1	16.2	26.0	36.6	46.2	7.1	14.2	38.0	52.3	72.4	
5	5.3	10.5	20.6	30.2	38.9	5.3	10.5	27.2	40.8	59.4	
6	3.0	6.0	15.5	24.3	32.2	3.9	7.7	19.2	31.3	47.8	
7	1.4	2.7	11.2	19.0	26.3	2.9	5.8	13.6	23.2	37.9	
8	0.5	0.9	8.0	14.9	21.6	2.4	4.7	10.1	18.5	30.0	
9	0.3	0.5	6.2	12.2	18.3	2.3	4.6	8.7	15.2	24.4	
10	0.8	1.6	6.1	11.2	16.6	2.7	5.3	8.9	14.1	21.7	
11	2.2	4.3	8.0	12.4	16.9	3.5	6.9	10.5	15.0	21.4	

Table 6.5: Misalignment [°] under wind [m/s] - current [m/s] offset.

Combinations of wind and current conditions are generated using stratified sampling. This means that the conditions are divided into subgroups known as strata. These strata contain the possibilities of each current/wind speed given a certain direction. To sample, first a direction is generated, using the probability of each direction occurring as the input, as given in the SEM-REV. Next, after fitting a Weibull distribution to the data, inverse transform sampling generates a speed. By doing this separately for wind and current a million times, just as many combinations of speed and direction of both are generated and stored in a Data Frame. The offset between current and wind direction is also stored in a separate column. A very important assumption to mention in this is that the current and wind are assumed to be two completely independent variables. Finally, a joint probability matrix is made, that stores the frequency of all combinations of conditions. The result is visualized in Figure 6.3 and represents the 2D Histogram for the misalignment and the wind speed.

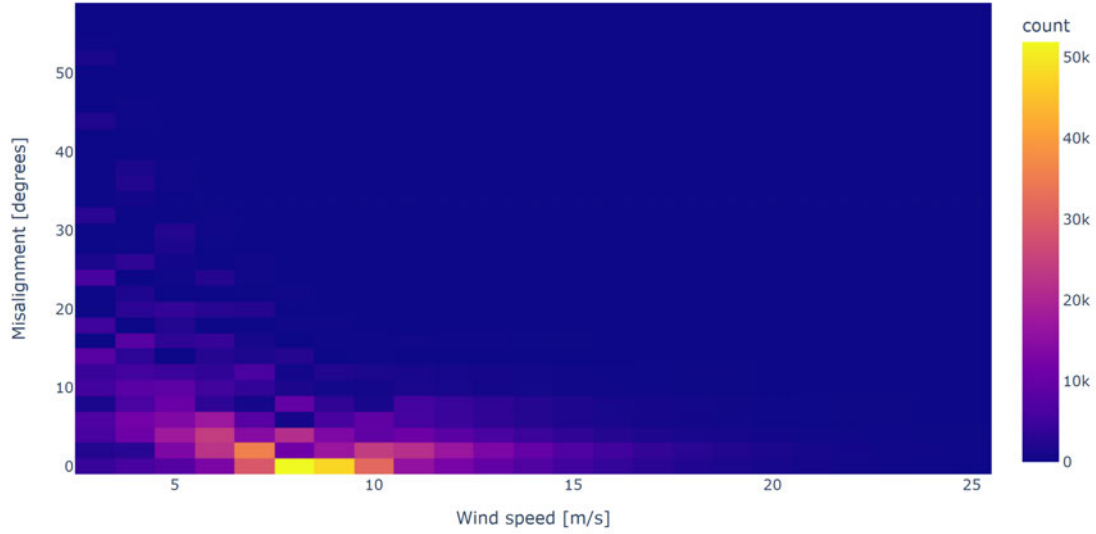


Figure 6.3: Histogram alignment for misalignment [°] and wind speed [m/s].

6.1.4 Results

Based on the above-mentioned layout optimization and the assumption regarding the yaw misalignment, the AEP of the wind farms can be computed.

Table 6.6: AEP estimation.

Turbine type	Number of turbines	Yaw misalignment [°]	Tilt misalignment [°]	AEP [GWh]
15 MW IEA	30	5 mean misalignment	not included	
15 MW X1 Wind	30	misalignment sampling	not included	
30 MW up-scale	15	misalignment sampling	not included	

As stated before, the AEP of the 15 MW IEA is calculated with a constant 5° yaw misalignment. For the DWT the prior described sampling method was used. For each combination in the joint probability matrix, the AEP is calculated as if these conditions would occur for one year on end. Next, it is multiplied by its frequency of occurrence. Thus resulting in an AEP with the included effect of passive yaw misalignment.

The AEP of the 15 MW X1 Wind is around 5 % lower compared to the 15 MW IEA UWT. As expected, this indicates that the mean misalignment of DWT is slightly higher than for UWT. In the case of the sampling method, it relates to a mean yaw misalignment of 17°. This first estimate of the mean misalignment for DWT must be used with caution since the method is likely to overestimate the influence of the current.

It is important to note that a 0° tilt misalignment is assumed. This influences the semi-sub 15MW IEA AEP positively since this floater solution is more susceptible to tilt misalignment and therefore a lower AEP.

The AEP per individual turbine is represented in Figure 6.4. It gives insight into the AEP of every wind turbine in the wind farm, showing clear differences based on the turbine position. The visualization highlights an essential aspect: not all wind turbines generate the same amount of energy due to factors like wake effects, wind direction, and local wind speeds. This is why optimizing the spacing of turbines is critical. The primary challenge in wind farms is wake interference.

Consequently, wind turbines located at the perimeter of the wind farm tend to have a higher AEP per turbine.

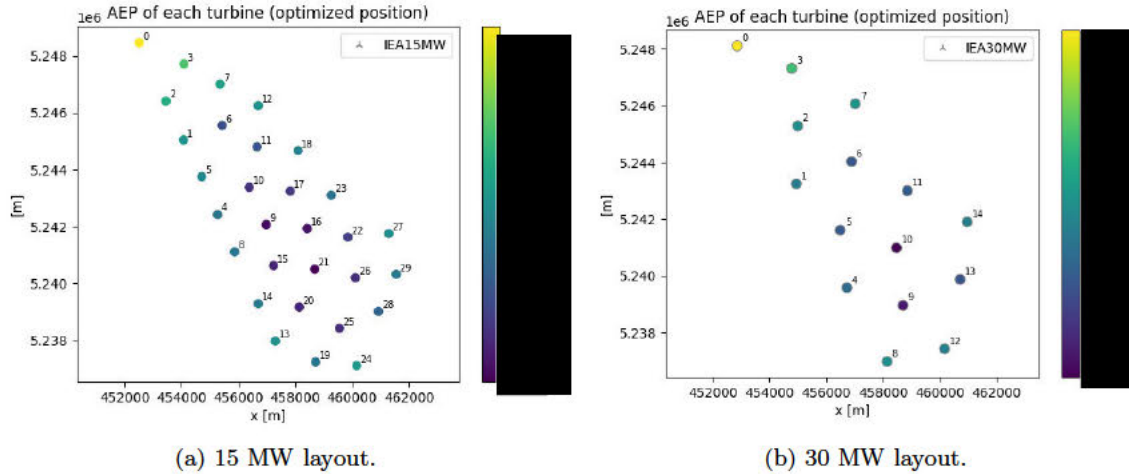


Figure 6.4: AEP of individual wind turbine.

The following Figure 6.5 presented below, illustrates the relationship between the AEP and wind speed, as well as the AEP and wind direction. These visualizations provide insights into the wind speeds and directions at which the wind farm generates the most energy.

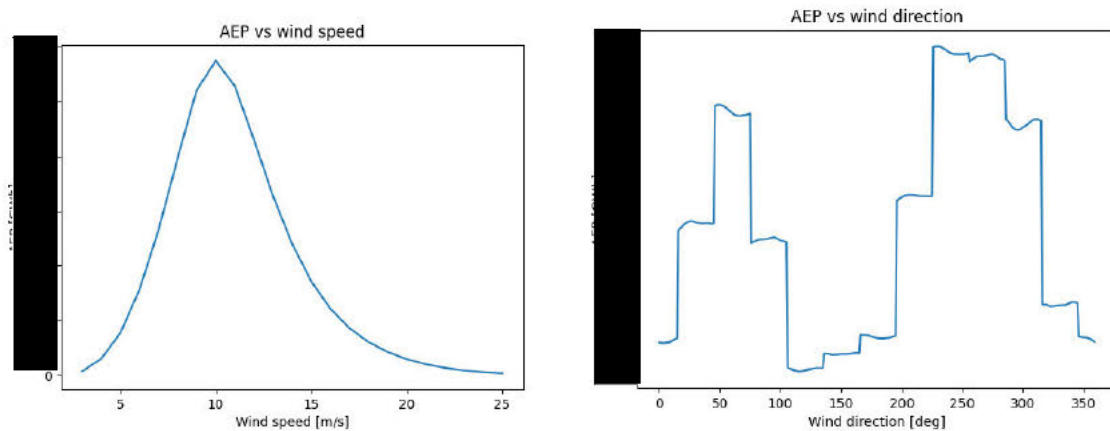


Figure 6.5: AEP distribution based on wind speeds and directions.

6.2 CAPEX

CAPEX are funds used by an entity to acquire, build or upgrade physical assets [66]. In the case of a floating offshore wind farm, the CAPEX consists of the costs of the development & project management, the wind turbines, the foundations, the Balance of Plant (BoP) and the Installation and Commissioning (I&C). These categories are based on the 'Guide to a Floating Offshore Wind Farm' by BVG Associates [41]. The CAPEX is the sum of these parts. The CAPEX analysis is performed in Excel, which is added in the accompanying files. After this, the output of the Excel is translated into the Python-based cost model for the PyWake analysis.

The four components comprised in the CAPEX will be further elaborated in the following subsections.

Turbines

The turbine is the first cost category of the CAPEX for a floating offshore wind farm. The turbine transforms kinetic energy from the wind into electrical energy. In this category five major cost components are identified; The rotor, nacelle, tower, floating substructure, and PivotBuoy. The CAPEX for the turbine is the sum of these elements.

Foundations

Floating offshore wind farms have less foundational CAPEX costs when compared to non-floating solutions such as monopiles. The only cost associated with the foundation of a floating offshore wind farm is the mooring system. This system consists of anchoring systems, mooring lines, jewelry (all elements attached to the mooring lines), topside connection (the connection between the mooring lines and the floating substructure), and installation aids.

Balance of Plant

The BoP of a floating offshore wind farm consist of all the physical elements that are not part of the turbine or foundation; the array cables, export cables, cable accessories, offshore substation, and onshore substation. Like the foundation CAPEX, the categories in the formula for the BoP CAPEX are based on [41].

Installation and Commissioning

The previous three categories consist of physical elements within a floating offshore wind farm, this category comprises the costs to install and commission those elements. This consists of inbound transport, export cable installation, array cable installation, mooring & anchoring pre-installation, floating substructure assembly, floating substructure installation, offshore substation installation, onshore export cable installation, and offshore logistics [41].

6.2.1 CAPEX 15 MW IEA

The cost model for the IEA 15 MW reference wind turbine is based on the 2023 guide to a floating wind farm by BVG-associates [41]. This guide takes a reference 15 MW wind turbine and describes the costs for a hypothetical wind farm of 450 MW. Using this guide as a source for the cost model for the IEA 15 MW turbine gives a good baseline to compare the other designs with. The cost model based on the report of BVG is given in £per rated power. This has to be converted to €and multiplied by the rated power of the total wind farm, i.e. 450 MW.

6.2.1.1 CAPEX 15 MW IEA Turbine

The CAPEX of the turbine is ██████████ ██████████ as shown in Table 6.7. With a £/€ exchange rate of 1.16 as of September 18 2023 [67], this leads to a CAPEX of ██████████. For a wind farm of 450 MW, the total CAPEX of the turbines is ██████████

Table 6.7: 15 MW IEA Turbine CAPEX.

Category	£/MW
Nacelle	██████████
Rotor	██████████
Tower	██████████
Floating substructure	██████████
Total	██████████

6.2.1.2 CAPEX 15 MW IEA Foundation

The CAPEX of the foundation is ██████████ ██████████ as shown in Table 6.8. With a £/€ exchange rate of 1.16 as of September 18 2023 [67], this leads to a CAPEX of ██████████. For a wind farm of 450 MW, the total CAPEX of the foundation is ██████████.

Table 6.8: 15 MW IEA Foundation CAPEX.

Category	██████████
Anchor systems	██████████
Mooring lines	██████████
Jewellery	██████████
Topside connection	██████████
Installation aids	██████████
Total	██████████

6.2.1.3 CAPEX 15 MW IEA BoP

The CAPEX of the Balance of Plant is ██████████ ██████████ as shown in Table 6.9. With a £/€ exchange rate of 1.16 as of September 18 2023 [67], this leads to a CAPEX of ██████████/MW. For a wind farm of 450 MW, the total CAPEX of the BoP is ██████████.

Table 6.9: 15 MW IEA BoP CAPEX.

Category	██████████
Array cables	██████████
Export cables	██████████
Cable accessories	██████████
Offshore substation	██████████
Onshore substation	██████████
Total	██████████

6.2.1.4 CAPEX 15 MW IEA I&C

The CAPEX of the installation and commissioning is ██████████ ██████████ as shown in Table 6.10. With a £/€ exchange rate of 1.16 as of September 18 2023 [67], this leads to a CAPEX of ██████████. For a wind farm of 450 MW, the total CAPEX of the installation and commissioning is approximately ██████████.

Table 6.10: 15 MW IEA I&C CAPEX.

Category
Inbound transport
Offshore cable installation
Export cable installation
Array cable installation
Cable pull in
Electrical testing & termination
Mooring & anchoring pre-installation
Floating substructure & turbine assembly
Heavy lifting equipment
Technician services
Marshalling port
Other
Floating substructure turbine installation
Offshore substation installation
Onshore export cable installation
Offshore logistics
Sea-based support
Marine coordination
Weather forecasting & metocean data
Marine safety & rescue
Total

6.2.1.5 CAPEX 15 MW IEA total

When the CAPEX of the four separate categories are combined, the total CAPEX for the 15 MW IEA can be calculated. The CAPEX summary of the 15 MW IEA is shown in Table 6.11. The total CAPEX of the 15 MW IEA is [REDACTED].

Table 6.11: 15 MW IEA CAPEX.

Category
Turbine & floater
Foundations
BoP
I&C
Total

6.2.2 CAPEX 15 MW X1 Wind PivotBuoy

6.2.2.1 CAPEX 15 MW X1 Wind PivotBuoy Turbine

The wind turbine consists of several main parts.

6.2.2.1.1 Nacelle

The costs of the nacelle of the 15 MW X1 Wind PivotBuoy was based on the costs of the nacelle of the 15 MW turbine from [41] and the more detailed guide on a 10 MW offshore wind project [68]. As the X1 Wind PivotBuoy does not have an active yaw system, it can be removed from the costs. The guide on a 10 MW offshore wind project describes all cost components in more detail, including the yaw system and the yaw bearings. Removing these from the 10 MW nacelle leads to a [REDACTED] cost reduction. It is assumed that the costs of the 15 MW nacelle from BVG Associates used for the CAPEX of the 15 MW IEA floater are also reduced by [REDACTED], leading to a CAPEX of [REDACTED] per turbine.

6.2.2.1.2 Rotor

According to [14], a downwind configuration wind turbine can lead to a 5% mass reduction of the rotor blades. It is assumed that this mass reduction leads to a 5% cost reduction. Therefore, the CAPEX for the blades is 95% of those of the BVG 15 MW blades, leading to a CAPEX of ██████████ per turbine.

6.2.2.1.3 Tower

The PivotBuoy design does not consist of a tower since the RNA is supported by the triangular three-mast design. The costs of this design are included in the costs of the substructure. Therefore the costs of the tower are considered to be €0.

6.2.2.1.4 Floating substructure

The floating substructure is determined based on the weights of the steel profiles needed to construct this element. These weights are determined in section 4.2. With the weights and the cost per kg for these steel profiles, the total cost for the substructure can be calculated. Table 6.12 shows the weight and cost per element.

Table 6.12: Substructure costs 15 MW X1 Wind PivotBuoy (R&D TotalEnergies internal information, 2023).

Element	Weight [kg]	Cost/Weight [€/kg]	Total cost	
			Low [€]	High [€]
Pivot column	██████████	██████████	██████████	██████████
Nacelle columns	██████████	██████████	██████████	██████████
Horizontal pontoons	██████████	██████████	██████████	██████████
Vertical masts	██████████	██████████	██████████	██████████
Diagonal mast	██████████	██████████	██████████	██████████
Total	██████████	-	██████████	██████████

6.2.2.1.5 PivotBuoy

As the size of the SPM system is mainly dependent on the bearings, they are used for the price calculation. For a 15MW turbine, this came down to a bearing inside diameter of 1.1 m section 4.7. From this, the size of the turret column within is calculated. This column is tested for shear strength, to assure the right wall thickness. The weight of the housing and shock breakers is assumed to be similar to the turret and bearings it holds. Note, that this is the housing of the turning bearing and turret system, not the entire buoy, as that cost is already incorporated in the substructure weight. The total weight can then be multiplied by the cost per kg, ██████████ (R&D TotalEnergies internal information, 2023). This results in a total cost of ██████████ per turbine

6.2.2.2 CAPEX 15 MW X1 Wind PivotBuoy Foundations

6.2.2.2.1 Mooring lines

The mooring lines for the 15 MW X1 Wind PivotBuoy are the tendons that connect the gravity anchor to the pivotfloater. For this TLP system to be adequate, it is assumed that the floater must always create tension in the tendons to guarantee a horizontal restoring force in the TLP system. For this, the buoyancy force in the PivotBuoy needs to be more than the maximum compressive force caused by the floating substructure. In section 4.2 the floating substructure was designed to ensure no tension would occur in the PivotBuoy during maximum wind to preserve the turret system. Because of this, a maximum compressive force (4.72 MN) can be found in the PivotBuoy during no wind conditions. This maximum compressive force in combination with the weight of the turret (0.4 MN) combines into the total downward force which needs to be at least equal to the buoyancy force (5.12 MN). This buoyancy force will be counteracted by the tension force in the tendons.

These tendons are calculated by comparing the tensile strength to the maximum tension in order to find the surface area. The tensile force that can be used for tendons is 1770 N/mm^2 according to [69]. Dividing the maximum tension by this tensile strength gives a surface area of 5788 mm^2 . Taking a redundancy of two other tendons into account for safety, this gives a total surface area of 17364 mm^2 . Given the length of the tendons of 80 meters and a steel density of 7850 kg/m^3 , this gives a total weight of 10905 kg. with a cost per kilo of [REDACTED] (R&D TotalEnergies internal information, 2023), this gives a total cost of [REDACTED] per wind turbine.

6.2.2.2.2 Anchor systems

As mentioned in the former paragraph, the anchor system consists of a ground anchor produced out of concrete. The dimensions of these anchors need to be such that they provide enough tension in the tendons to counteract the buoyancy in the TLP floater and ensure tension in the tendons. For this reason, the self-weight of the anchor needs to be equal to 5.12 MN + the self-weight of the submerged tendons. According to [70], the self-weight of underwater concrete is 14 kN/m^3 and the cost is [REDACTED]. With this, the necessary amount of concrete comes down to 381 m^3 , which will cost around [REDACTED] per turbine.

6.2.2.2.3 Jewellery

The jewelry consists of all parts that are attached to mooring lines. Since in the case of a TLP there are only vertical tendons present, there is no need for parts such as connectors, clump weights, and load reduction devices. Only the buoyancy elements will be temporarily present during the installation stage to keep the tendons vertical and tensioners are used to set the TLP to a certain tension. Because of the temporary and scaled-down character of these parts, it is assumed that only 10% of the standard jewelry cost is applicable for the pivot buoy. This comes down to [REDACTED] per turbine.

6.2.2.2.4 Topside connection

The topside connection is PivotBuoys patented easy connection system. For this analysis, this system is simplified as a hollow rod based on the patent with a diameter of 1m, a thickness of 0.08m and a height of 1.5 m [26]. This in combination with a steel weight of 7850 kg/m^3 gives a weight of 2723 kg. With a cost per kilo of [REDACTED] (R&D TotalEnergies internal information, 2023), this comes down to [REDACTED] per turbine.

6.2.2.2.5 Installation aids

Since both the reference and the PivotBuoy are floating offshore wind structures, it is deemed that the installation aids are the same. The cost for this is [REDACTED] per turbine.

6.2.2.3 CAPEX 15 MW X1 Wind PivotBuoy BoP

6.2.2.3.1 Array cable

Since the usable plot size, total rated power, and the number of turbines do not change, the costs for the array cables will not change when compared to the IEA 15 wind farm. This cost will stay at [REDACTED] for the 450 MW wind farm. This gives a cost of [REDACTED] per turbine.

6.2.2.3.2 Export cable

The same goes for the export cable as the array cables. Since the total rated power and the distance to shore between the IEA 15 and PivotBuoy windfarm do not change, the export cable stays the same and thus the affiliated costs. This will stay at [REDACTED]. This gives a cost of [REDACTED] per turbine.

6.2.2.3.3 Cable accessories

The 15 MW X1 Wind PivotBuoy is expected to require mostly the same types and amounts of cable accessories as the BVG benchmark. For example, the cable protection, buoyancy regulators,

and connectors need to be similar. However, because of the extra implementation of a slip ring, the cost is increased by 10% when compared to the 15 MW IEA to a cost of [REDACTED] per turbine. accessories for the entire 450 MW farm.

6.2.2.3.4 Offshore substation

Since the number of turbines and the rated power per turbine stay the same, the offshore substation can stay the same as the one in the 15 MW IEA wind farm. Therefore, the cost will stay at [REDACTED]. This gives a cost of [REDACTED] per turbine.

6.2.2.3.5 Onshore substation

The same goes for the onshore substation. Since the rated power of the total wind farm and the export cable stays the same, the onshore substation will stay at [REDACTED]. This gives a cost of [REDACTED] per turbine.

6.2.2.4 CAPEX 15 MW X1 Wind PivotBuoy I&C

6.2.2.4.1 Inbound transport

Inbound transport is calculated based on the different elements that need to be imported to the fictional assembly port in Lorient, France. The elements that will be imported, plus their fictional location of production and travel distance are portrayed in Tab Table 6.13 The location of production for all the steel elements (all profiles, jacket structure, and mooring lines) is set to a steel mill in England with water access, namely Pulhalm steels. The location of production for the nacelle, electrical cables, and offshore substation is the General Electric factory in Saint Nazaire. Finally, the location of production for the rotors is the LM wind power factory in Cherbourg-en-Cotentin. These ten elements for the major imports for the production of the wind farm. The general production of these locations is simplified in this investigation and it is acknowledged that more specific, specialized production locations would supply these elements in a real-world setting. However, for reasons of simplified inbound transport calculations, these three locations are used;

Table 6.13: Imported elements.

Element	Production location	Distance to Brest [km]	Volume/weight of elements
Mast+Horizontal profiles	Pulhalm steels, England	400 km	5011 m^3
Upper column profiles	Pulhalm steels, England	400 km	10677 m^3
Base column profiles	Pulhalm steels, England	400 km	2972 m^3
Jacket structure	Pulhalm steels, England	400 km	5000t [71]
Mooring lines	Pulhalm steels, England	400 km	21 m^3
TLP anchors	Pulhalm steels, England	400 km	2972 m^3
Nacelle	Saint Nazaire, France	300 km	7288 m^3
Cables	Saint Nazaire, France	300 km	1822 m^3
Substation	Saint Nazaire, France	300 km	3000t [41]
Rotors	Cherbourg-en-Cotentin, France	350 km	5466 m^3

To transport these elements, this study focuses on two seafaring transportation modes: a 1000 TEU cargo vessel and a semi-subconstruction vessel. Table 6.14 gives important information about these boats from [72] and [73].

Table 6.14: Used transportation vessels.

Ship	Speed [km/h]	Day-rate [€]
Cargo vessel	37.4	[REDACTED]
Semi-sub construction vessel	12.9	[REDACTED]

Based on the amount of volume/ weight of the different elements in Table 6.13 and the capacity of the boats in Table 6.14, Table 6.15 shows the sort and amount of ships needed for the transport.

Table 6.15: Needed ships.

Element	Ship type	Ships needed
Mast + Horizontal pontoon profiles	Cargo vessel	2.75
Upper column profiles	Cargo vessel	5.85
Base column profiles	Cargo vessel	1.63
Jacket structure	Semi-sub construction vessel	1
Mooring lines	Cargo vessel	0.01
TLP anchors	Cargo vessel	1.63
Nacelle	Cargo vessel	3
Cables	Cargo vessel	1
Substation	Semi-sub construction vessel	1
Rotors	Cargo vessel	3
Total needed	Cargo vessel	21
	Semi-sub construction vessel	2

Table 6.15 combined with the distances from Table 6.13 and the day rates from Table 6.14 gives the total rent cost. Assuming that each ship needs a day for on/offloading in the respective ports, these total costs will be ██████████ for the cargo ships and ██████████ for the semi-sub construction vessel. From [74], the cost of using landside cranes is ██████████ per TEU. When assuming the cargo ships are 85% filled, this gives a total amount of TEU of 16150 TEU, which results in a total cost of ██████████. This combines into a total cost for inbound transport of ██████████. This gives a cost of ██████████ per turbine. For the complete calculation, the Excel cost model is supplied.

6.2.2.4.2 Offshore cable installation

Since the amount and the type of offshore cables stay the same, the offshore cable installation is considered the same as the IEA 15 benchmark. The cost will therefore stay at ██████████. This gives a cost of ██████████ per turbine.

6.2.2.4.3 TLP and turbine installation

To install the PivotBuoy's elements, anchor handling vehicles are used. These vessels have a certain day rate, a speed with which they can transport the anchors, a distance to the installation plot, an installation time, and a (faster) return speed. By combining these characteristics, the installation cost for the TLP as the turbine assembly can be estimated. Table 6.16 gives all these characteristics for a single 15 MW turbine.

Table 6.16: All needed characteristics for installation of TLP and turbine.

Element	TLP	Turbine
Price/day [€] [41]	████████	████████
Needed anchor handling vehicles [75]	1	2
Pull speed [km/day] [40]	216	216
Distance [km]	60	170
Installation time [hour]	4	4
Return speed [km/day] [40]	648	648
Total installation time [day]	0.54	1.22
Total cost [€]	████████	████████

6.2.2.4.4 Turbine assembly

For the turbine assembly, all the different elements that need to be lifted and assembled are investigated. For these elements, it is investigated to what height they need to be lifted. With this information, a heavy-lifting crane is found to perform this job. The most critical part here is the hub, since this is a highly heavy part that needs to be lifted to a high height, in this case, the Liebherr 13000 is necessary for this element. From this crane, the lifting table is investigated which gives a clear image of how much weight can be lifted to a certain height. This table is shortly given for the investigated lifting heights in Table 6.17. Besides this crane, a smaller support crane is also used for the assembly. It is assumed that this support crane has the same working hours as the primary crane. E.g., the support crane is always deployed in tandem with the primary crane.

Table 6.17: Condensed lifting table Liebherr 13000 [76].

Height [m]	Reach [m]	Capacity [t]
143	26	472.5
74	16	1826
71.5	16	1826

For the support crane, a 300-ton crawler crane is used. This crane has a day rate of [REDACTED]. Extrapolating this to the 3000-ton Liebherr 13000, the day rate will be [REDACTED]. Besides this, the hoisting speed of the Liebherr crane is 20 m/s, and it is assumed that it takes two hours to connect and disconnect an element. Also, the crane will have 10-hour operating days. With this, Table 6.18 is constructed. In here all elements are described based on their weight, heave height, attach height (which can be different), and the needed lift. With this, the total heave duration for one element can be found, which can be combined into a cost given the day rate and duration of an operating day. A large assumption here is that the nacelle can be made modular and lifted in multiple lifts. As of now, this has not been performed before.

Table 6.18: Elements to be lifted for 15 MW.

Elements	Weight [t]	Heave height [m]	Attach height [m]	Needed lifts	Heave duration [min]
Masts	785	143	71.5	2	259
Pivot mast	866	143	71.5	1	130
Nacelle	647	143	143	2	259
Hub	69	143	143	1	130
Rotors	206	148	74	3	390
Total hours					19
Cost per turbine					[REDACTED]

6.2.2.4.5 Offshore substation installation

This cost post will be the same as in the IEA 15 benchmark since the same sub-station will be installed. This cost will come down to [REDACTED]. This gives a cost of [REDACTED] per turbine.

6.2.2.4.6 Onshore export cable installation

Since nothing changes in the design or amount of onshore export cables, the installation of this will stay the same as well. This will amount to [REDACTED]. This gives a cost of [REDACTED] per turbine.

6.2.2.4.7 Offshore logistics

The offshore logistics cost category consists of sea-based support and safety vessels, and the management of heightened marine traffic due to the offshore construction site. Short-term weather forecasting and metocean data collection. This post is dependent on the amount of vessels used

and the size of the wind park. These elements are assumed to be similar between the BVG benchmark and the X1 Wind PivotBuoy wind farm. The cost is therefore considered equal to the BVG benchmark, [REDACTED]. This gives a cost of [REDACTED] per turbine.

6.2.2.5 CAPEX 15 MW X1 Wind PivotBuoy total

When the CAPEX of the four separate categories is combined, the total CAPEX for the 15 MW X1 Wind PivotBuoy wind farm can be calculated. The CAPEX summary of the 15 MW X1 Wind PivotBuoy is shown in Table 6.19. The total CAPEX of the 15 MW X1 Wind PivotBuoy is € [REDACTED].

Table 6.19: 15 MW X1 Wind PivotBuoy CAPEX.

Category	Cost [€]
Turbine & floater	[REDACTED]
Foundations	[REDACTED]
BoP	[REDACTED]
I&C	[REDACTED]
Total	[REDACTED]

6.2.3 CAPEX 30 MW solution

6.2.3.1 CAPEX 30 MW solution Turbine

6.2.3.1.1 Nacelle

The cost of the nacelle of the 30 MW solution is based on the costs of the nacelles from reference projects [78] and [41]. In these reference projects, the costs are compared to the rated power. This is used to extrapolate the cost for a 30 MW nacelle. Table 6.20 shows these reference projects with their rated power and costs. Figure 6.6 shows the extrapolation based on these projects and the cost of [REDACTED] for a 30 MW nacelle. Since the downwind configuration does not have an active yaw system, this post can be removed in the same way this was done for the 15 MW (reduction of [REDACTED]). This gives a cost of [REDACTED] per turbine.

Table 6.20: Nacelle costs used to extrapolate 30 MW nacelle.

Rated power [kW]	Cost [€]
1500	[REDACTED]
3000	[REDACTED]
15000	[REDACTED]

6.2.3.1.2 Rotor

The cost of the rotors of the 30 MW solution is found based on costs found in reference projects [79] and [41]. In these reference projects, the costs are compared to the rotor length. This is used to extrapolate the cost for a 30 MW nacelle. Table 6.21 shows these reference projects with their rated power and costs. Figure 6.7 shows the fitted curve on these projects and the cost of [REDACTED] for a 30 MW rotor. According to [14], a downwind configuration wind turbine can lead to a 5% mass reduction of the rotor blades. It is assumed that this mass reduction leads to a 5% cost reduction. This gives a cost of [REDACTED] per turbine.

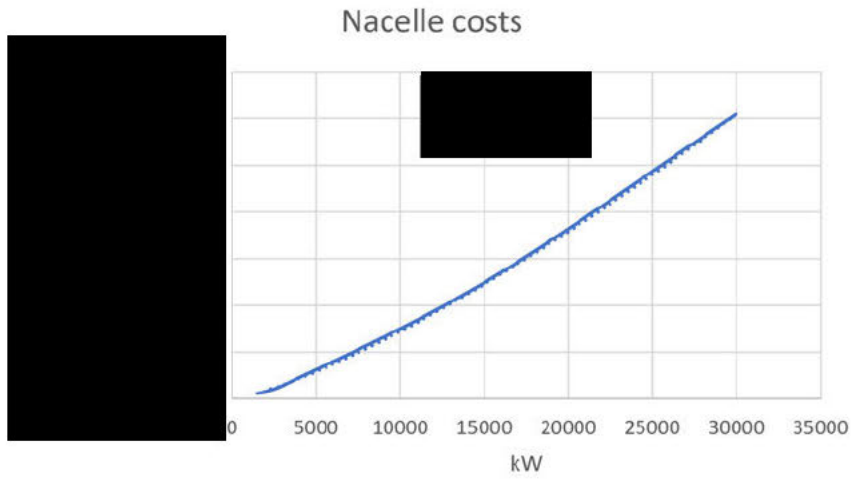


Figure 6.6: Extrapolated costs from reference projects to find cost 30 MW nacelle.

Table 6.21: Rotor costs used to apply a curve to find 30 MW rotor.

Rotor span [m]	
33.3	
61.5	
63	
95	
100	
117	

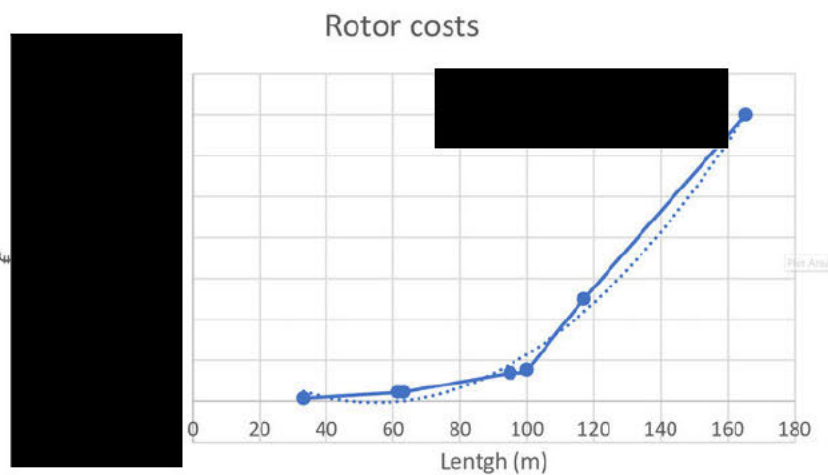


Figure 6.7: Fitted costs from reference projects to find the cost of 30 MW rotors.

6.2.3.1.3 Tower

The 30 MW solution does not consist of a tower since the RNA is supported by the triangular three-mast design. The costs of this design are included in the costs of the substructure. Therefore the costs of the tower are considered to be [REDACTED]

6.2.3.1.4 Floating substructure

The floating substructure is determined based on the weights of the steel profiles needed to construct this element. These weights are determined in section 4.2. With the weights and the cost per kg for these steel profiles, the total cost for the substructure can be calculated. Table 6.22 shows the weight and cost per element.

Table 6.22: Substructure costs 30 MW PivotBuoy (R&D TotalEnergies internal information, 2023).

Element	Weight [kg]	Cost/Weight [€/kg]	Total cost	
			Low [€]	High [€]
Pivot column				
Nacelle columns				
Horizontal pontoons				
Vertical masts				
Diagonal mast				
Total		-		

6.2.3.1.5 PivotBuoy

As the size of the SPM system is mainly dependent on the bearings, they are used for the price calculation. For a 30MW turbine, this comes down to an inner bearing diameter of 1.8 m. From this, the size of the turret column is calculated. This column is tested for shear strength, to assure the right wall thickness. The weight of the housing and shock breakers is assumed to be similar to the turret and bearings it holds. Note, that this is the housing of the turning bearing and turret system, not the entire buoy, as that cost is already incorporated in the substructure weight. The total weight can then be multiplied by the cost per kg, [REDACTED] (R&D TotalEnergies internal information, 2023). This results in a total cost of [REDACTED] per turbine

6.2.3.2 CAPEX 30 MW solution Foundations

6.2.3.2.1 Mooring lines

The mooring lines for the 30 MW solutions are similar to the 15 MW pivot buoy system and therefore follow the same methodology to calculate the costs. In section 4.2 the floating substructure was designed to ensure no tension would occur in the pivot buoy during maximum wind to preserve the turret system. Because of this, a maximum compressive force (17 MN) can be found in the PivotBuoy during no wind conditions. This maximum compressive force in combination with the weight of the turret (1.62 MN) combines into the total downward force which needs to be at least equal to the buoyancy force (18.62 MN). This buoyancy force will be counteracted by the tension force in the tendons.

The tendons are calculated in the same manner as for the 15 MW X1 Wind PivotBuoy, this gives a total cost of [REDACTED] per wind turbine.

6.2.3.2.2 Anchor systems

The dimensions of the anchor need to be such that they provide enough tension in the tendons to counteract the buoyancy in the TLP floater and ensure tension in the tendons. This is calculated in the same manner as in the PivotBuoy and comes down to [REDACTED] per turbine.

6.2.3.2.3 Jewellery

For the jewelry, an increase of the 15 MW X1 Wind PivotBuoy cost is taken based on the increase in weight of the TLP tendons. This increase in weight is [REDACTED] This factor multiplied with the cost of the 15 MW gives [REDACTED] per turbine.

6.2.3.2.4 Topside connection

The same analysis as for the 15 MW X1 Wind PivotBuoy is performed here. For this analysis, the system is seen as a hollow rod with a diameter of 1.8m, a thickness of 0.1m, and a height of 2 m [26]. With these dimensions and the same approach as before, this comes down to ██████ per turbine.

6.2.3.2.5 Installation aids

It is deemed that the installation aids are double for the 30 MW solution when compared to the 15 MW X1 Wind PivotBuoy because of the increased size. The cost for this ██████ per turbine.

6.2.3.3 CAPEX 30 MW solution BoP

6.2.3.3.1 Array cable

It is assumed the 15 MW X1 Wind PivotBuoy and 30 MW solution farm will have comparable layouts with the main difference in the amount of turbines. Table 6.23 gives the characteristics of 66 and 132 kV array cables. With this information, the amount of array cables in the 15 MW X1 Wind PivotBuoy farm can be calculated. This can be used to find the needed array cable length for the 30 MW wind farm layout.

Table 6.23: Characteristics of array cables (R&D TotalEnergies internal information, 2023).

Element	66kV	132kV
Installation cost [€/m]	████	████
Supply cost [€/m]	████	████
Current [A]	800	800
Rated power(voltage*current* $\sqrt{3}$)	91.5	182.9
15 MW connections/cable	6	12
30 MW connections/cable	3	6

With the information about the two types of array cables, the length of cable in the 15 MW X1 Wind PivotBuoy wind farm can be estimated as ██████ (array cable cost 15 MW X1 Wind PivotBuoy farm) / ██████ (cost 66kV cable/m) = ██████. Assuming that the 30 MW solution will use 132 kV array cables for efficiency reasons, the same amount of connections per cable can be made with half the turbines. This gives a needed array cable length of ██████ m. This gives a total cost of ██████, which amounts to a cost of ██████.

6.2.3.3.2 Export cable

Since the total rated power and the distance to shore between the PivotBuoy 15 MW and 30 MW wind farm do not change, the export cable stays the same and thus the affiliated costs. This will stay at ██████, which is ██████ per turbine.

6.2.3.3.3 Cable accessories

The cost of the cable accessories is expected to increase with a factor depending on the increase in the diameter of the connection system. This factor is $1.5/1.0 = 1.5$. This gives a new cost of ██████ per turbine.

6.2.3.3.4 Offshore substation

Since the rated power stays the same, the offshore substation can stay the same as the one in the 15 MW IEA and 15 MW X1 Wind PivotBuoy wind farm. Therefore, the cost will stay at ██████ which comes down to a cost of ██████ per turbine.

6.2.3.3.5 Onshore substation

The same goes for the onshore substation. Since the rated power of the total wind farm and the export cable stays the same, the onshore substation will stay at [REDACTED] which comes down to a cost of [REDACTED] per turbine.

6.2.3.4 CAPEX 30 MW solution I&C

6.2.3.4.1 Inbound transport

Inbound transport is calculated based on the different elements that need to be imported to the fictional assembly port in Lorient, France, as done in the analysis for the 15 MW X1 Wind PivotBuoy. Here a comparison is made between the total weight needed to be transported between the 15 MW X1 Wind PivotBuoy and the 30 MW solution. This increase in weight is assumed to be directly responsible for the increase in shipping cost. This increase over the total weight is 213 [REDACTED]. This gives a total shipping cost of [REDACTED] = €8,568,108 which gives a cost of [REDACTED] per turbine.

6.2.3.4.2 Offshore cable installation

The offshore cable installation is calculated in the same manner as the array cable calculation earlier in paragraph 6.2.3.3.1. The installed length of cable in the 15 MW X1 Wind PivotBuoy windfarm can be estimated as [REDACTED] array cable installation cost 15 MW X1 Wind PivotBuoy farm) / [REDACTED] (installation cost 66kV cable/m) = [REDACTED]. Assuming that the 30 MW solution will use 132 kV array cables for efficiency reasons, the same amount of connections per cable can be made with half the turbines. This gives a needed array cable length of [REDACTED]. This gives a total cost of [REDACTED], which amounts to a cost of [REDACTED].

6.2.3.4.3 TLP and turbine installation

To install the 30 MW solutions elements, a similar approach is used as for the 15 MW X1 Wind PivotBuoy. The main difference is the amount of anchor-handling vehicles used. This is shown in Table 6.24 for a single 30 MW turbine.

Table 6.24: Characteristics for installation of TLP and turbine for 30 MW solution.

Element	TLP	Turbine
Price/day [€] [41]	[REDACTED]	[REDACTED]
Needed anchor handling vehicles [75]	1	3
Pull speed [km/day] [40]	216	216
Distance [km]	60	170
Installation time [hour]	4	4
Return speed [km/day] [40]	648	648
Total installation time [day]	0.54	1.22
Total cost [€]	[REDACTED]	[REDACTED]

6.2.3.4.4 Turbine assembly

For the turbine assembly, a similar approach to the 15 MW X1 Wind PivotBuoy is applied. The main difference is the crane used, in this case, the Sarens 250. From this crane, the lifting table is investigated which gives a clear image of how much weight can be lifted to a certain height. This table is shortly given for the investigated lifting heights in Table 6.25. Besides this crane, a smaller support crane is also used for the assembly. It is assumed that this support crane has the same working hours as the primary crane. E.g., the support crane is always deployed in tandem with the primary crane.

For the support crane, a 300-ton crawler crane is used. This crane has a day rate of [REDACTED] [77]. Extrapolating this to the 4250-ton Sarens 250, the day rate will be [REDACTED]. Besides this, the hoisting speed of the Sarens crane is 20 m/s, and it is assumed that it takes three hours to

Table 6.25: Condensed lifting table Sarens 250 [80].

Height [m]	Reach [m]	Capacity [t]
210	48.5	491
200	48.5	522
102.5	48.5	1525
100	48.5	1771

connect and disconnect an element. Also, the crane will have 10-hour operating days. With this, Table 6.26 is constructed. In here all elements are described based on their weight, heave height, attach height (which can be different), and the needed lift. With this, the total heave duration for one element can be found, which can be combined into a cost given the day rate and duration of an operating day. A large assumption here is that the nacelle can be made modular and lifted in multiple lifts. As of now, this has not been performed before.

Table 6.26: Elements to be lifted for 30 MW.

Elements	Weight [t]	Heave height [m]	Attach height [m]	Needed lifts	Heave duration [min]
Masts	1916	200	100	2	400
Pivot mast	3751	200	100	3	600
Nacelle	1847	215	210	4	806
Hub	405	200	200	1	200
Rotors	388	205	102.5	3	601.5
Total hours					43.46
Cost per turbine					

6.2.3.4.5 Offshore substation installation

This cost post will be the same as in the IEA 15 benchmark and 15 MW X1 Wind PivotBuoy since the same substation will be installed. This cost will come down to [REDACTED].

6.2.3.4.6 Onshore export cable installation

Since nothing changes in the design or amount of onshore export cables, the installation of this will stay the same as well. This will amount to [REDACTED].

6.2.3.4.7 Offshore logistics

The offshore logistics is dependent on the amount of vessels used and the size of the wind park. Since there is an increase in the amount of vessels used between the 30 MW and 15 MW X1 Wind PivotBuoy, this cost will increase. It is calculated that the ships installing the TLP and floater solution for the 15 MW will spend 2.97 days offshore per turbine. This is 4.19 for the 30 MW solution, which gives an increase factor of 1.41. This multiplied with the offshore logistics cost for the 15 MW X1 Wind PivotBuoy gives a cost of [REDACTED] per turbine.

6.2.3.5 CAPEX 30 MW Solution total

When the CAPEX of the four separate categories are combined, the total CAPEX for the 30 MW solution can be calculated for the whole wind farm. The CAPEX summary of the 30 MW solution is shown in Table 6.27. The total CAPEX of the 30 MW X1 Wind PivotBuoy is [REDACTED].

6.2.4 CAPEX Comparison

Finally, the three CAPEX are compared with each other and visualized in Table 6.28. From here it can be seen that in almost every category a reduction can be found in comparison with the 15

Table 6.27: 30 MW solution CAPEX.

Category	Cost [€]
Turbine & floater	
Foundations	
BoP	
I&C	
Total	

MW IEA. This is except for the category of the turbine and floater. This can be explained by the shortcomings of the design cycle performed in this study. The elements that form the structure are represented through singular circle hollow sections with very large diameters and thicknesses. Because of this, there actually is no weight reduction and the relative weight actually increases a significant amount in the 30 MW solution. Recommendations here for future research are to focus on a weight reduction of these elements through the use of for example trusses instead of circular hollow section beams.

Table 6.28: Comparison between CAPEX of wind farms.

Category	15 MW IEA		15 MW PivotBuoy			30 MW solution		
	Cost [€]	% of CAPEX	Cost [€]	Diff. [%]	% of CAPEX	Cost [€]	Diff. [%]	% of CAPEX
Development		12						
Turbine								
Substructure								
Foundations								
BoP								
I&C								
Total		100		-10	100		+52	100

6.2.5 CAPEX Uncertainties

This economic evaluation is based on reference projects and figures from research. The costs are not the exact costs. For example, a wind turbine manufacturer would provide an official fabrication request in reality, which gives an exact cost. Therefore, uncertainties are introduced in this evaluation where exact numbers are not available. There are many ways in which the cost component in this study was calculated. For example by curve fitting through known costs, extrapolating for larger sized components. Many other methods for determining the CAPEX and OPEX were applied. An example of how the CAPEX of the Array Cables supply (BoP component) for the 30 MW solution was determined can be found below:

- The 90% confidence interval of the supply cost [€/m] is expected to be able to deviate from its value with 10%
- The 90% confidence interval of the current capacity (A) is expected to be able to deviate from its value with 10%

In turn, the variances are added and calculated back to a 90% confidence interval, leading to, in this array cable supply case, a confidence interval of [] the expected value.

After determining the 90% confidence interval of all sub-cost posts, these intervals are combined through their variances into the 90% confidence interval for the main posts. These confidence intervals are presented in box plots. **Note that the vertical axis is represented logarithmic.** To find the spread of the total costs, the variance of each main cost is added together. The costs per part are all assumed to be distributed normally. The distribution of the total CAPEX is then:

$$N(\mu, \sigma^2) = N(\Sigma\mu, \Sigma\sigma^2) \quad (6.2)$$

The same method is applied for determining the uncertainties of the OPEX.

6.2.5.1 CAPEX Uncertainty 15 MW X1 Wind PivotBuoy

Figure 6.8 displays the spread on the CAPEX of the 15 MW X1. Note that the foundations have a large spread. This is due to the large expected uncertainties in the costs for cable jewellery, topside connection (turret host) and installation aids. Also, the CAPEX for the installation and commissioning is uncertain.

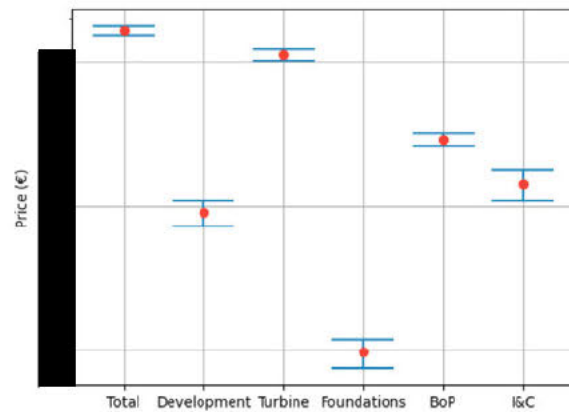


Figure 6.8: Box plot of 90% confidence interval of 15 MW X1 Wind PivotBuoy CAPEX cost components, and total.

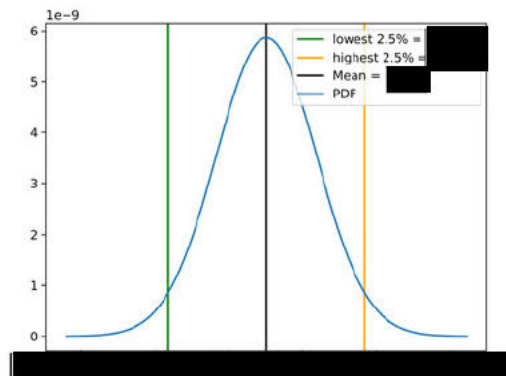


Figure 6.9: Normal distribution of the CAPEX of 15MW solution.

6.2.5.2 CAPEX Uncertainty 30 MW Solution

Just like for the 15 MW X1 Wind, the CAPEX for the foundations is highly uncertain. The same goes for the Installation and Commissioning, mostly because the turbine assembly introduces large uncertainties.

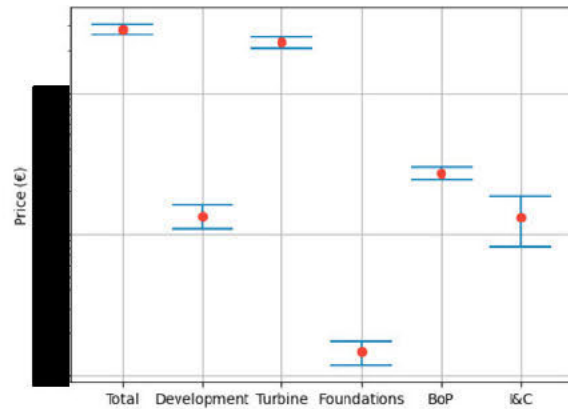


Figure 6.10: Box plot of 90% confidence interval of 30 MW solution CAPEX cost components, and total.

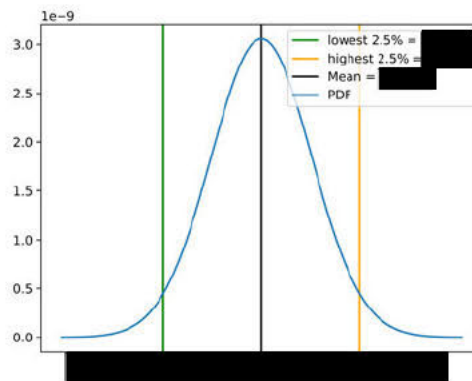


Figure 6.11: Normal distribution of the CAPEX of 15MW solution.

6.3 OPEX

OPEX are the costs an entity incurs over time through its normal business operations. It includes rent, inventory and equipment costs, payroll, R&D, and maintenance costs, amongst other things [81]. In the case of a floating offshore wind farm, most of these costs fall under operations and maintenance. The OPEX consists of an operation control centre, training, onshore logistics, technical resources, admin & support staff, insurance, BoP maintenance, statutory inspections, offshore logistics and vessels, O&M port. The categories of costs in the OPEX formula are based on the Guide to a Floating Offshore Wind Farm by BVG Associates [41].

6.3.1 OPEX 15 MW IEA

The OPEX for the IEA 15 MW reference wind turbine is based on the 2023 'Guide to a Floating Offshore Wind Farm' by BVG-associates [41]. The costs in £per MW per year per category are given in Table 6.29. This amounts to an OPEX of [redacted] per MW per year with an exchange rate of 1.16 (September 2023). For a wind farm of 450 MW, the OPEX is [redacted] per year.

Table 6.29: 15 MW IEA OPEX parameters.

Category	
Operations	
Operations control centre	
Training	
Onshore logistics	
Technical resource	
Admin & support staff	
Insurance	
Maintenance	
Turbine maintenance	
BoP maintenance	
Statutory inspections	
Offshore logistics & vessels	
O&M port	
Total	

6.3.2 OPEX 15 MW X1 Wind PivotBuoy

6.3.2.1 Operations

The costs for operations for the 15 MW X1 Wind PivotBuoy are assumed to be the same as for the IEA 15 MW semi-sub floater. This is because they are both 15 MW solutions in a 450 MW farm, requiring similar staff and equipment. The insurance of the PivotBuoy is also assumed to be around the same as for the 15 MW IEA, although the CAPEX is lower, the technology is more novel, levelling out the insurance cost. The costs for operations for the 15 MW X1 Wind PivotBuoy are estimated to be ██████████ per year.

6.3.2.2 Maintenance

6.3.2.2.1 Turbine Maintenance

The maintenance of the turbines will reduce drastically for the X1 Wind PivotBuoy case when compared with the IEA reference turbine. This is in large part due to the possibility of the tow-to-shore maintenance strategy enabled by the quick-connect system of the PivotBuoy. Without the tow to shore strategy, offshore maintenance is needed, and the large offshore cranes and vessels required for this, have large costs, low availability, and need specific weather conditions to operate. ECN predicts a maintenance cost decrease of 35% in some cases [82]. Besides this decrease, the PivotBuoy concept uses a TLP mooring system, which is the most accessible mooring type to maintain [83], except for the caveat that disconnection with TLP systems can be hard [84]. This caveat has been remedied however by the quick-connect system introduced by PivotBuoy [5]. The quick-connect system significantly reduces the time and effort required to (dis)connect the turbine from the mooring solution. The PivotBuoy solution also has no active yaw and ballast systems eliminating maintenance for said systems. The X1 Wind PivotBuoy floater tripod substructure also distributes the forces better, resulting in less stress on single points. Finally, there is reduced fatigue on the dynamic cable due to the lower sway of the cable when compared to other floating offshore wind solutions [85]. The combination of these factors lead to an assumed reduction of ██████████ in turbine maintenance costs. This means that the turbine maintenance cost will be ██████████ per year for the X1 Wind PivotBuoy wind farm.

6.3.2.2.2 Balance of Plant Maintenance

The BoP maintenance elements, such as the maintenance of the substations and export cable will not change. This is because the substations and export cables that are used do not change between the IEA 15 MW and X1 Wind PivotBuoy 15 MW wind farms. The BoP maintenance will thus stay at ██████████ per year.

6.3.2.2.3 Statutory inspections

The statutory inspections are assumed to be similar between the two 15 MW turbines. The costs of these inspections for the 15 X1 Wind PivotBuoy are thus [REDACTED] per year.

6.3.2.3 Offshore logistics & vessels

As for the offshore logistics and vessels, the same type of vessels can be used to perform minor maintenance. For major maintenance activities, tugboats can be used to tow the turbines back to port. The costs of these vehicles and the logistics to manage them are considered the same as the BVG benchmark. The cost of the offshore logistics and vessels are thus [REDACTED] per year.

6.3.2.4 O&M port

For the operations and maintenance port, the port in Lorient can be used as a base of operations for smaller maintenance activities. To accommodate the tow to shore and maintenance activities on shore, the port in Brest needs to be used. Using the same yard as for the construction can be quite expensive if it is used solely for maintenance for the Sud de la Bretagne I site. However, if it is used as a maintenance (and/or construction) base for a wide range of floating offshore wind farms, costs for the land can be split between the farms. To account for the tow to shore strategy, a [REDACTED] factor is used when compared to the IEA. This leads to an O&M port cost of [REDACTED] per year.

6.3.3 OPEX 30 MW solution

6.3.3.1 Operations

Most of the operation procedures do not differ much between the 15 and 30 MW turbines. This will lead to a saving for the 30 MW since the number of turbines is halved when compared to the 15 MW turbine wind farms. The costs for support staff per turbine will increase slightly. The insurance for the turbines will increase with the increased CAPEX. The increase of the insurance cost is calculated in Equation 6.3.

$$OPEX(insurance30MW) = OPEX(insurance15MW) * \frac{CAPEX(Total15MW)}{CAPEX(Total30MW)} \quad (6.3)$$

The total costs for operations of the 30 MW solution are estimated to be [REDACTED] per year.

6.3.3.2 Maintenance

6.3.3.2.1 Turbine Maintenance

The calculation of the turbine maintenance of the 30 MW solution is based on the turbine maintenance of the 15 MW X1 Wind PivotBuoy and the heavy lifting operations needed for certain replacements. As with the 15 MW version, the tow to-shore maintenance strategy can save money for the 30 MW solution. However, the expensive heavy lifting operations needed to replace the nacelle, blades and hub, are added. This is done by multiplying the major replacement rates found in Table 5.6 with the costs of heavy lifting operations found in Table 6.26. This gives the costs of major replacements per year, this amounts to [REDACTED] per turbine per year. Combining this with the [REDACTED] for the general turbine maintenance gives a total of [REDACTED] turbine per year. For the whole farm, the costs associated with turbine maintenance are then € [REDACTED].

6.3.3.2.2 Balance of Plant Maintenance

The BoP maintenance elements, such as the maintenance of the substations and export cable will not change. This is because the substations and export cables that are used do not change between the IEA 15 MW and 30 MW solution wind farms. The BoP maintenance will thus stay at [REDACTED] per year.

6.3.3.2.3 Statutory inspections

The statutory inspections for the 30 MW are assumed to be slightly more expensive per turbine due to the size increase. The cost per turbine is assumed to be approximately 1.5 times the costs of the 15 MW turbine. This leads to a cost of 1.5 per turbine per year. The cost of these inspections for the 30 MW solution farm are thus 1.5 per year.

6.3.3.3 Offshore logistics & vessels

As for the offshore logistics and vessels, the same type of vessels can be used to perform minor maintenance. For major maintenance activities, tugboats can be used to tow the turbines back to port. The tow to shore activities require an extra tug boat. The cost of the offshore logistics & vessels increases thus per turbine. But due to the lower number of turbines required, the total costs go down. The cost of offshore logistics and vessels is estimated to be 1.5 per year.

6.3.3.4 O&M port

The operations and maintenance port is the same for the 15 X1 Wind PivotBuoy and the 30 MW solution. The port in Lorient is used as a base of operations for smaller maintenance activities, and the port in Brest is used for the maintenance activities on shore. Using the same yard as for the construction can be quite expensive if it is used solely for maintenance for the Sud de la Bretagne I site. However, if it is used as a maintenance (and/or construction) base for a wide range of floating offshore wind farms, costs for the land can be split between the farms. To account for the tow to shore strategy, a 1.5 is used when compared to the IEA. This leads to an O&M port cost of 1.5 per year.

6.3.4 OPEX Comparison

The OPEX of both the 15 MW X1 Wind PivotBuoy and the 30 MW solution are lower than the OPEX of the 15 MW IEA. For the 15 MW X1 Wind PivotBuoy, this is mainly because of the removal of the yaw systems, and the tow to shore strategy with the quick connect system. The per turbine operation and maintenance costs for the 30 MW solution are higher, but due to the fact that only half the number of turbines are serviced, the total OPEX is expected to be lower.

Table 6.30: Comparison of OPEX of three 450 MW wind farm designs in € per year.

Category	15 MW IEA	15 MW PivotBuoy		30 MW solution	
	Cost [€]	Cost [€]	Diff. [%]	Cost [€]	Diff. [%]
Operations	1.5	1.5	0	1.5	0
Maintenance	1.5	1.5	0	1.5	0
Offshore l&v	1.5	1.5	0	1.5	0
O&M port	1.5	1.5	0	1.5	0
Total	1.5	1.5	-14.6	1.5	-2.9

6.3.5 OPEX Uncertainties

Similarly to the uncertainties introduced in the CAPEX evaluation, the OPEX also comes with many assumptions and uncertainties. The same method as for the 15 MW X1 Wind is used for representing these uncertainties. This means that again the 90% confidence intervals are determined. These are presented below.

6.3.5.1 OPEX Uncertainty 15 MW X1 Wind PivotBuoy

Note that the operations and maintenance port cost component is expected to have large uncertainty. This is attributable to the uncertainty on to what extent ports need adaptation to host the platforms.

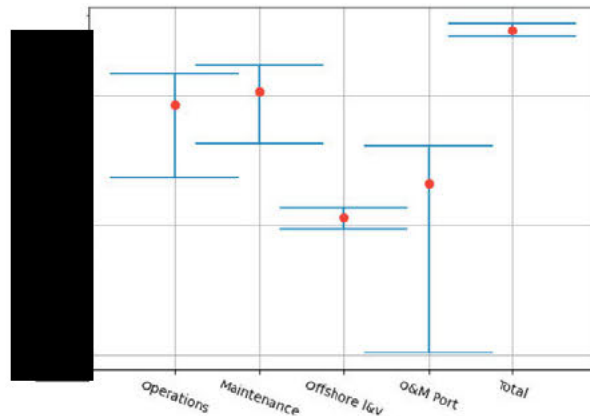


Figure 6.12: Box plot of 90% confidence interval of 15 MW X1 Wind PivotBuoy OPEX cost components, and total.

6.3.5.2 OPEX Uncertainty 30 MW Solution

Note that the operations and maintenance port cost component is expected to have large uncertainty. This is attributable to the uncertainty on to what extent ports need adaptation to host the platforms. Also, the maintenance costs are expected to have a large spread.

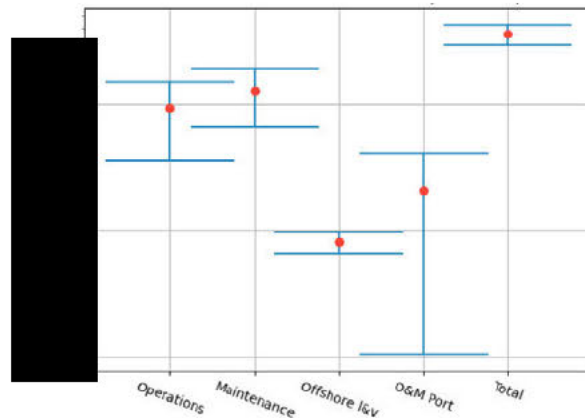


Figure 6.13: Box plot of 90% confidence interval of 30 MW PivotBuoy OPEX cost components, and total.

6.4 ABEX

ABEX are costs incurred by an entity for closing down, decommissioning, abandoning or removing assets. It also includes restoration of land and/or seabed [86]. In the case of a floating offshore wind farm, it consists of the decommissioning of the floating substructure & turbine, mooring & anchoring, cables, and substations. These categories are based on the 'Guide to a Floating Offshore Wind Farm' by BVG Associates 2023 [41]. The ABEX is often considered separately from the CAPEX, as the cost occurs at the end of the project, and this influences the net present value (NPV).

6.4.1 ABEX 15 MW IEA

The ABEX of the IEA 15 MW reference wind farm is ██████████ per MW according to BVG associates [41]. For the whole wind farm, this would amount towards a total of ██████████.

6.4.2 ABEX 15 MW X1 Wind PivotBuoy

For decommissioning purposes, specialized equipment needs to be deployed. Even though the PivotBuoy itself is easily detached from its turret mooring point, significantly more effort is necessary to remove the TLP mooring system. For this reason, it is chosen that the costs will be similar to the decommissioning of the IEA 15 semi-sub. For this design, removing the floater from the anchors is harder, but the anchors are more easily removed. The total cost will therefore be [REDACTED]

6.4.3 ABEX 30 MW solution

The decommissioning of a singular 30 MW X1 Wind PivotBuoy will be harder than that of a 15 MW turbine, due to its size. However, only half of the turbines will need to be decommissioned. The cost to decommission the 30 MW solution is based on a report from TNO [87]. Figure 6.14, taken from the TNO report, displays the costs per MW for different wind turbine sizes and distances to shore. The report investigated two distances to shore, namely 20 km and 500 km. In this research, the set project site is situated 40 km from the shore, so the values are interpolated.

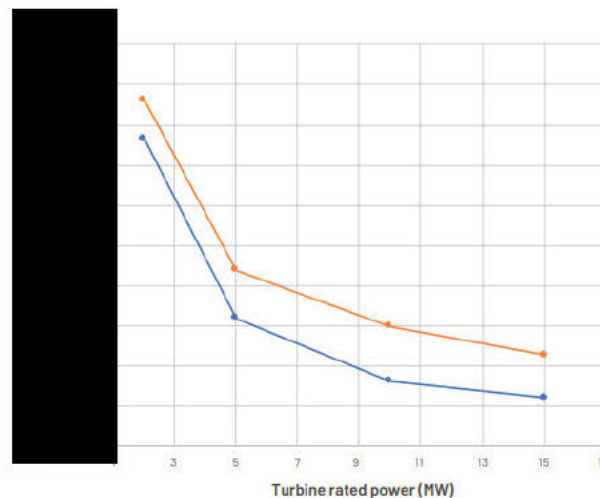


Figure 6.14: Costs of decommissioning for different turbine sizes and distances to shore, from [87].

This interpolation and subsequent extrapolation to 30 MW led to Figure 6.15. This shows that, according to extrapolating this research, the 30 MW turbine has a decommissioning cost of [REDACTED] per MW [REDACTED]. The decommissioning of a 450 MW wind farm with 15 MW turbines costs [REDACTED], according to this research. As this research is on bottom fixed wind turbines and the [41] is based on floating wind, the decommissioning costs are compared to get a scaling. BVG states that the decommissioning of a 450 MW floating wind farm costs [REDACTED]. The difference is [REDACTED]. Multiplying the extrapolation to 30 MW, visualised in Figure 6.15, by [REDACTED] gives a final expected decommissioning cost for the 30 MW wind farm of [REDACTED].

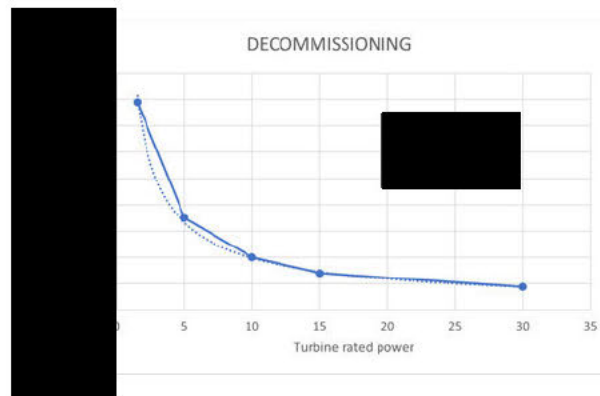


Figure 6.15: Interpolated and extrapolated costs per MW.

6.4.4 ABEX Comparison

Table 6.31 shows a comparison of the costs for decommissioning the three 450 MW wind farms. It shows that the costs for decommissioning the 30 MW solution are lower than the 15 MW turbines in a farm sense.

Table 6.31: Comparison of ABEX of three 450 MW wind farm designs.

Category	15 MW IEA	15 MW PivotBuoy		30 MW solution	
	Cost [€]	Cost [€]	Diff. [%]	Cost [€]	Diff. [%]
ABEX			+0		-38.0

6.5 LCOE

The LCOE is a measure of the average net present cost of electricity production for a wind turbine over its lifetime. It uses the NPV of both the costs incurred during the lifetime and the NPV of the energy produced during the lifetime. It can be used as a comparative measure between different methods of electricity generation. In this investigation, it will be used as such. In order to calculate the LCOE of a wind farm, multiple different performance indicators need to be identified: the CAPEX, OPEX, ABEX, and AEP. The LCOE is calculated in the following way, Eq. (6.4) uses a Fixed Charge Rate (FCR) method [88, ■], where the CAPEX is multiplied by a certain number to cover all expenses over a year. This includes R&D, interest on loans and other company costs that need to be covered to make a profit [90].

$$\begin{aligned}
 LCOE &= \frac{\sum (NPV) \text{ of costs over lifetime}}{\sum (NPV) \text{ of electrical energy produced over lifetime}} \\
 &= \frac{(CAPEX * FCR) + OPEX}{AEP}
 \end{aligned}
 \tag{6.4}$$

As the calculations for the CAPEX came with a lot of uncertainties, it is hard to state one final number for the LCOE. To tackle this problem, a Monte Carlo simulation is done with the normal distribution found for the CAPEX in subsection 6.2.5. These values are generated a million times, with which the LCOE is then calculated. This gives a better idea of the spread of required energy costs to turn a profit. The results for the 15 and 30 MW downwind design are shown below, in Figure 6.16 and Figure 6.17.

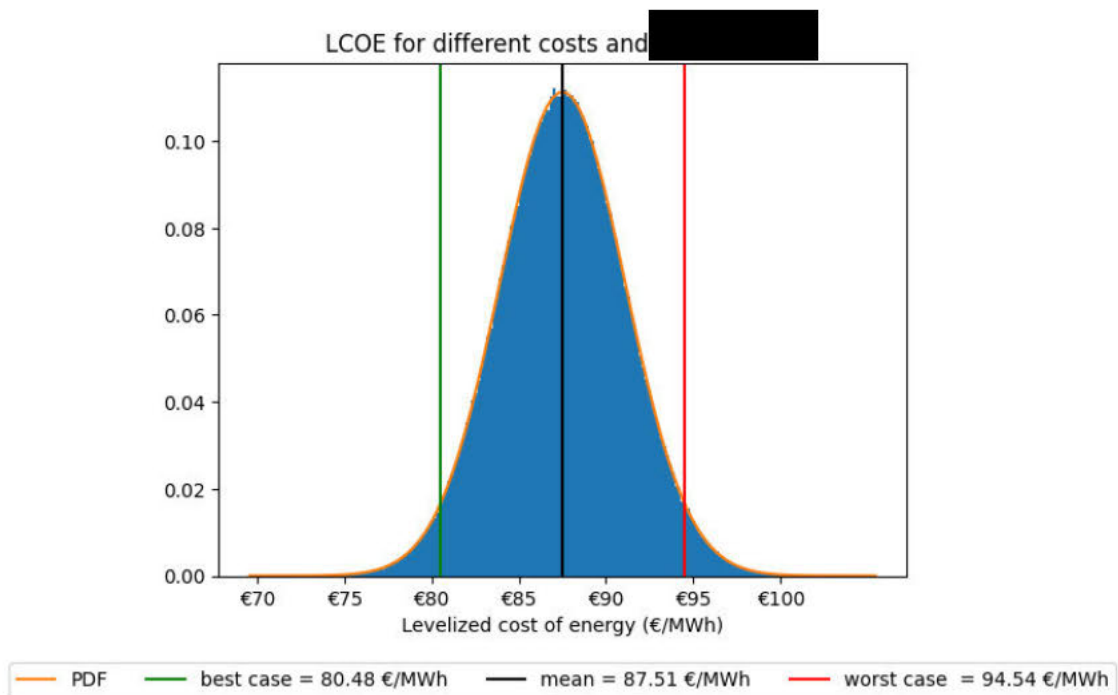


Figure 6.16: Levelized cost of energy for 15MW design.

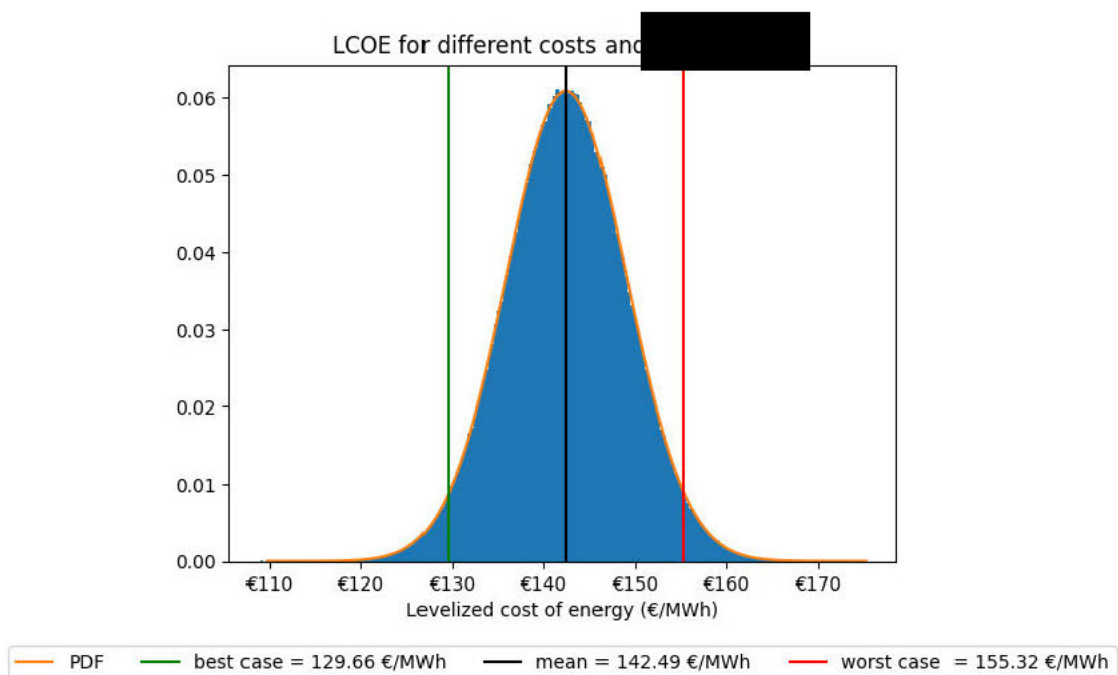


Figure 6.17: Levelized cost of energy for 30MW design.

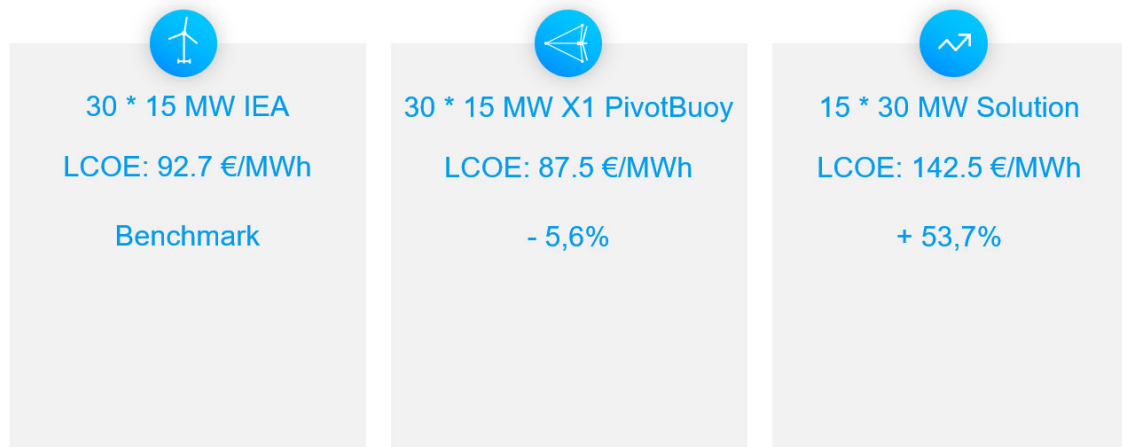


Figure 6.18: Comparisson of the mean LCOE for the three wind farm designs.

From Figure 6.18, it can be seen that the 15MW PivotBuoy design, on a farm scale, has a lower LCOE when compared to the 15 MW IEA and 30 MW solution. This can be justified by the fact that this is taking into account a fixed output. With the 30MW design, there seems to be more space left to place extra turbines, whereas there is no space left in the wind farms consisting of 30 times 15 MW turbines. Next to this, the 30MW turbine is much bigger and therefore needs novel solutions to be assembled, which is more costly. An example of this could be the cranes which are not as readily available. Furthermore, as many of the parts are not yet available, this would require significant investments from the industry, and the price of parts is noticeably higher. Due to the economy of scale, this difference could be reduced in the future.

6.6 Conclusion

The goal of the economic evaluation was to investigate whether the 15 MW and 30 MW downwind solutions are economically feasible when compared to the 15 MW IEA. In Figure 6.19, a short recap of the conclusions can be found.

15 MW X1 PivotBuoy	
AEP	↘
CAPEX	↘
OPEX	↘
ABEX	—
LCOE	↘
Economic feasibility	✓
30 MW solution	
AEP	—
CAPEX	↗
OPEX	↘
ABEX	↘
LCOE	↗
Economic feasibility	✗

Figure 6.19: Conclusion economic evaluation.

From the results, it can be concluded that for the 15 MW X1 Wind PivotBuoy, the AEP goes down. However, both the CAPEX and OPEX also go down and the ABEX stays the same. In the end, the LCOE is lower when compared to the 15 MW IEA wind farm, for this reason, this solution is deemed economically feasible.

For the 30 MW solution, the AEO is comparable to the 15 MW IEA. However, the CAPEX is significantly higher. Both the OPEX and ABEX are lower, but in the end, the LCOE is significantly higher when compared to the 15 MW IEA. For this reason, this solution is deemed unfeasible as of now.

Opportunities could arise by maximizing the plot by incorporating more 30 MW solutions. It is seen that more of these solutions fit, which could create an increase in AEP and thus decrease the LCOE. Besides this, implementing the downwind solutions in more sheltered areas where wind and waves are less misaligned will decrease the yaw misalignment, increase AEP thus decrease LCOE which would improve the feasibility

Chapter 7

Summary of results

In this study, the feasibility of upscaling floating offshore wind turbines is investigated. For this, three wind turbine designs are examined: the IEA 15 MW, the 15 MW X1 Wind PivotBuoy (both deemed feasible today), and a newly created 30 MW solution. These three designs are reviewed through a structural-, lifecycle-, and economic analysis for a fixed 450 MW wind farm. In this chapter, the key results of these studies are discussed.

7.1 Structural analysis

A structural analysis is performed to find a design for the 30 MW solution and perform checks on this design. For this, the base characteristics of the 30 MW solution are determined and shown in Table 7.1. This analysis consists of the following four parts.

Table 7.1: Base characteristics of 30 MW solution used for structural analysis.

Element	Size [m]
Rotor diameter	358
Hub height	204

7.1.1 Preliminary design

A preliminary design model was set up to find the preliminary dimensions of the structure based on buoyancy, local Euler buckling stability, and global stability. From this, the results in Table 7.2 are found.

Table 7.2: Dimension results from preliminary design.

Element	Diameter [m]	Thickness [m]	Freeboard [m]
Pivot column	19	0.07	10
Nacelle column	27.5	0.07	8
Pontoon	3.69	0.06	-
Nacelle masts	3.47	0.06	-
Pivot mast	5.47	0.09	-
Center to center width of platform [m]		207	-
Draft [m]		8	-

7.1.2 Global stability analysis

After the preliminary design, this design is checked for global stability using openFAST. In this study, the dynamic responses due to DLCs are compared to certain movement boundaries. The

most critical result of these can be seen in Table 7.3.

Table 7.3: Simulation results DLC 6.1 (most critical load case).

Motion	Max	Min	Mean	Std
Platform Surge (m)	5.913	-3.457	1.580	1.549
Platform Sway (m)	16.810	-20.540	-0.661	5.692
Platform Heave (m)	6.183	-6.472	0.162	2.446
Platform Roll (deg)	0.166	-0.215	-0.002	0.046
Platform Pitch (deg)	2.210	-2.496	-0.025	0.851
Platform Yaw (deg)	5.714	-7.042	-0.221	2.008

7.1.3 FEM analysis

After the global stability analysis, a FEM analysis is performed towards the design. The goal of this is to find the most important eigenfrequencies, deflections, and stresses and check this with the wave and wind spectrum, 1P, 6P, and steel strengths. Key results are found in Figure 7.1 and Table 7.4.

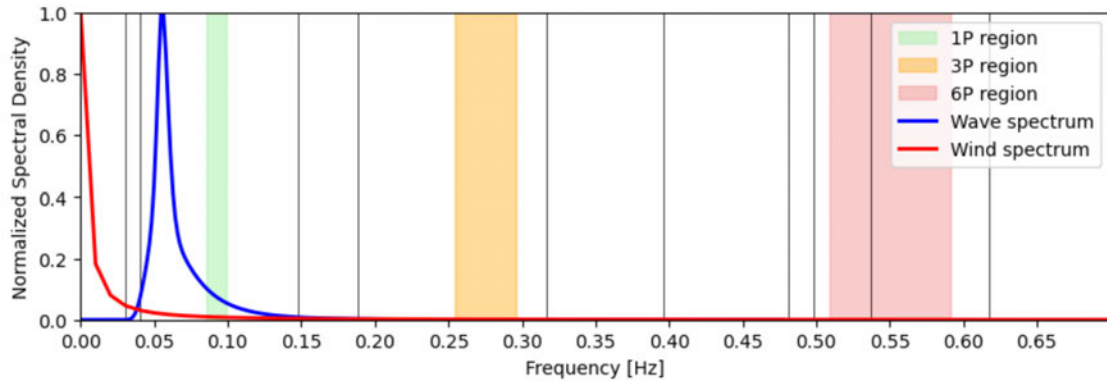


Figure 7.1: Natural frequencies structure (vert. lines) compared to present spectra. Important: the one nat. freq. in the 6P region does not have deflections in the masts and thus will not form a structural problem.

Table 7.4: Comparison of unity check for the Combined axial forces and moments between the standard and proposed improvement method models.

Element	First model U.C. [-]	Proposed improved model U.C.[-]
Left and right pontoons	5.13	2.57
Front pontoon	6.95	11.63
Left and right masts	2.06	1.76
Pivot mast	12.64	4.93

7.1.4 Turret analysis

After the global and local structural analysis, a more detailed study is performed on the turret system. From this, the dimensions as portrayed in Table 7.5.

Table 7.5: Final dimensions for the turret.

Element	D [m]	t [m]	H [m]
Turret	1.95	0.05	10
Bearing	1.95	-	-

7.2 Lifecycle assessment

In the lifecycle assessment, the 30 MW solution was analysed to find potential bottlenecks and pitfalls in six different categories. Supply chain, construction, transport, installation, operations & maintenance, and decommissioning. The main bottlenecks and results found are the following:

7.2.1 Supply chain

The upscale to a 30 MW turbine requires major commitments from the supply chain. Especially for the RNA, the pontoons and the PivotBuoy. The components for the RNA will be come so big, that the dimensions of most current factories are not sufficient to accommodate them. The question arises if OEMs are willing to take the risk to develop nacelles and blades of this size in the future. The PivotBuoy is a novel concept, and the forces exerted on this upscaled version are so high, that very specialized equipment will be needed to manufacture it. It could be a bottleneck that either OEMs are not willing to produce it, or for a too high price.

7.2.2 Construction

Heavy lifting equipment is required for the construction of the platform and the installation of the RNA. The installation of the pivot mast is the most challenging part of the construction of the substructure. For the RNA, there is currently no crane that can lift a weight as heavy as the 30 MW nacelle to the required height.

7.2.3 Transport

For the specific site used as a baseline in this report (Sud de la Bretagne I), the main locations for assembly, marshalling and maintenance of the platforms are identified. Brest is best suited for the assembly. Rade de Brest or Baia de Douarnenez are well suited for marshalling before the platforms are towed to their production location. Lorient is most fitting for maintenance in the water, whereas Brest is the only possible location for onshore maintenance of the platforms. Towing from the marshalling anchorages to the site takes approximately 23 hours.

7.2.4 Installation

In the installation, no real bottlenecks are identified. The foundation is placed and then the tendons and pivot base are added. These activities can be done first. In a later stage, the floater and turbine are connected through a quick connection system. The connection activity is assumed to be approximately four hours.

7.2.5 Operation & Maintenance

The maintenance strategy is mostly proactive, with both inspections and data-driven analysis being input for maintenance activities. For large replacements, the turbines will be towed to Brest, or another maintenance harbour. This is expected to be once every five years per turbine. Bottlenecks in O&M are replacements of the generator / nacelle. And the availability of a maintenance harbour.

7.2.6 Decommissioning

The turbines will be towed to shore for decommissioning. The anchors have to be lifted from the ground, or new turbines will have to be attached to the anchors. No real bottlenecks have been identified for the decommissioning.

7.3 Economic Analysis

7.3.1 CAPEX OPEX ABEX

The CAPEX OPEX and ABEX are set up based on structural and lifecycle analysis. The end results are portrayed in Table 7.6.

Table 7.6: CAPEX & OPEX & ABEX of a 450 MW wind farm.

Category	15 MW IEA	15 MW PivotBuoy		30 MW solution	
	Cost	Cost	Diff. [%]	Cost	Diff. [%]
CAPEX [€]			-10.7		+52.2
OPEX [€/year]			-14.6		-2.9
ABEX [€]			+0		-38.0

7.3.2 AEP

For all three platform configurations, the AEP was calculated for a 450 MW wind farm. The results are presented in Table 7.7.

Table 7.7: AEP estimation for the three platform configurations in a 450 MW farm.

Turbine type	Number of turbines	AEP (GWh)
15 MW IEA	30	
15 MW DW	30	
30 MW up-scale DW	15	

7.3.3 Wind-current misalignment effect on AEP

When calculating AEP for an active yaw system in PYWAKE, one would normally use an average misalignment of 5 degrees. The downwind design does not yaw actively, and is therefore subject to changes in wind direction and its reaction to these changes, while also being influenced by waves. From the calculations based on earlier research, an average loss in AEP of about 5.5% was found. When calculating AEP in PYWAKE, this would be the same as calculating with an average yaw misalignment of 17°.

Table 7.8: Influence of mean yaw misalignment on AEP for the IEA 15 MW wind farm.

Yaw (degrees)	AEP (GWh)
0	
5	
10	
20	
45	

7.3.4 LCOE

In the end, using all results from the prior analysis, the LCOE calculations are statistically performed for the 15 MW X1 Wind PivotBuoy and the 30 MW solution. The results of these are

found in Figure 7.2. The LCOE for the 15 MW IEA is ████████ MWh (Figure 6.18).

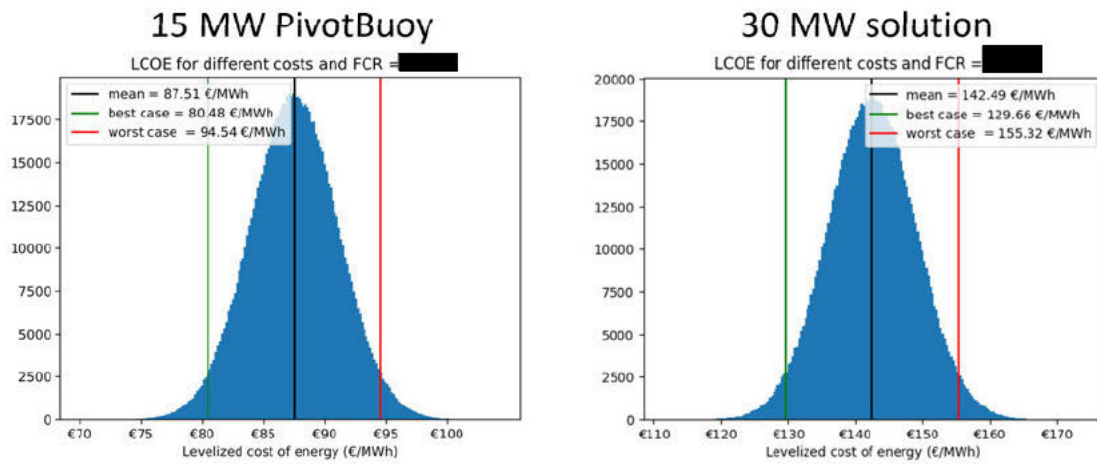


Figure 7.2: Comparison between the 15 MW X1 Wind PivotBuoy and 30 MW solution LCOE.

Chapter 8

Discussion and conclusion

In this chapter, the results are interpreted and discussed and conclusions are drawn.

8.1 Project outline

This study investigates the feasibility of upscaling the 15 MW X1 Wind PivotBuoy concept to a 30 MW DWT solution. Currently, there is no public 30 MW floating DWT design available. Therefore, first, a design for a 30 MW DWT, based on the 15 MW X1 Wind PivotBuoy concept was made in this study.

A structural analysis was performed to identify the complications that come with this upscaling. This structural analysis consists of several parts. The analysis goes into the global stability of the new design. A FEM analysis is performed to get insight into the natural frequencies and modal shapes of the structure. This analysis is in turn compared to the wind, wave, 1P, 3P, and 6P spectra. Another part of this structural analysis is the stress checks in the individual members of the substructure.

Besides a structural analysis, a life cycle assessment is performed to determine the bottlenecks and to see what kind of commitments the current industry should make to realize a 30 MW offshore floating wind turbine. The life cycle assessment consists of six main parts: it evaluates the supply chain, construction, transport, installation, operation & maintenance, and decommissioning.

Lastly, an economic feasibility study is performed for the 15 MW X1 Wind PivotBuoy and for the 30 MW downwind design. This study consists of an AEP simulation based on a 450 MW wind farm and a CAPEX, OPEX and ABEX analysis. This economic study is subsequently compared to the 15 MW IEA benchmark. This benchmark is based on a floating wind farm with 15 MW UWT. The different configurations are compared through the LCOE.

8.2 Discussion

8.2.1 Structural analysis

Global stability

From the global stability analysis, it can be concluded that the designed 30 MW platform is stable because the movement of the platform stays within the specified movement boundaries. The platform was modelled and simulated using the software OpenFAST. A simulation does however not completely accurately model the real life behaviour. Also, many assumptions were made to be able to model the platform. One of the main assumptions is that aerodynamic forces are not

calculated on the substructure but only on the rotors. Besides that, the horizontal connectors connecting the columns are assumed to not contribute to the buoyancy in the model due to model limitations. Another assumption is the roughness length k is assumed to lie between two reference values, leading to inaccuracies in the calculation of the hydrodynamic drag forces on the platform. Consequently, the model does not fully represent reality, and in practice, the movement of the platform could be higher.

Natural frequency analysis

The FEM analysis indicates that only one natural frequency falls into the wind, wave, 1p, 3p, and 6p spectra. This natural frequency is checked. Since the deflection of the corresponding modal shape is minor, this natural frequency does not influence the structural integrity. However, this will highly depend on the properties of the structure. The natural frequency of the structure depends on the mass and stiffness. Adapting the structure by implementing extra structural members or by adjusting the diameters and thicknesses of the members causes new natural frequencies of the entire structure. This should be checked in case a new design is proposed.

Member stress analysis

The stress checks performed in this report indicate that the 30 MW solution does not provide the prescribed structural integrity. However, the stress determination in the FEM analysis has some limitations. The first one is that the FEM model assumes that the structure does not move in space. The 30 MW solution however is able to move with the wind and waves. Because of this assumption, the wave force on the structure is overestimated. This approach is considered to be valid for an accidental limit state, as these forces could occur when the turret is out of use and no weathervaning is possible. Furthermore, since the wave forces are a time series, they depend on time. For the unity check of the stress in the beams, the axial force and the bending moment in the y-axis and z-axis do not have to be maximum at the same time. In this study, it is assumed that all the forces are maximum at the same time which can lead to an overestimation of the forces.

8.2.2 Life cycle assessment

In the table where the ratings are compared between the 15 MW X1 Wind PivotBuoy and the 30 MW solution regarding the supply chain of certain components, is stated that the industry needs to invest in developing and producing the RNA, pivot top, main columns, and blades for the 30 MW turbines. However, during the study of the upscale of the 30 MW solution, there was no contact with potential manufacturers of these elements. It is assumed that it is going to be hard for the industry since the commitments are major. The ratings are based on personal interpretation, it might be that certain manufacturers are further in the developing process than expected as of now.

Besides this, it is assumed that in the case of construction, the identified ports in Lorient and Brest are available and will not cause any problems. However, these two ports will also have busy shipping traffic and it will be a big commitment for a port to provide space for the construction of the large structure of the 30 MW solution.

8.2.3 Economic evaluation

AEP

The difference between the simulated AEP yield for the three platforms and turbine configurations is mainly caused by the misalignment between wind and waves/current. The misalignment was calculated based on a previous study and on a metocean report that contains data from a site not exactly at the plot assessed in this study. This could lead to differences in the misalignment between reality and this calculation, leading to a different AEP. Also, the wake model used for calculating the AEP of the farm for the three different configurations is calibrated on a different turbine. This causes inaccuracies in the simulated AEP result. Lastly, the misalignment due to tilt is not assessed in this study, whilst this could have major impacts.

CAPEX

It turns out that the wind farm consisting of the 15 MW X1 Wind PivotBuoy turbines has a reduced CAPEX. This can be attributed mostly to reduced costs for the turbine, substructure, foundations and I&C. The foundations reduce in costs most drastically because the 15 MW IEA semi-sub uses drag-anchors which are costly. The downwind designs make use of relatively cheap gravity anchors. The CAPEX of the 30 MW solution downwind farm, however, is significantly higher compared to the benchmark IEA 15 MW. This is mainly due to an increase in the size of the floating substructure, leading to an increased CAPEX. The CAPEX is based on many assumptions and extrapolation and interpolation methods. For example, it is assumed that the nacelle can be installed in parts as it is currently impossible to lift the 30 MW nacelle to the hub height. The costs for the assembly are based on this and are therefore not accurate.

Also, the CAPEX of the floating substructure of both the 15 MW X1 Wind PivotBuoy and the 30 MW design are based on a preliminary design based on buckling made in this study. The profiles could therefore be larger or smaller, which would influence the CAPEX.

OPEX

The OPEX for the 15 X1 Wind MW PivotBuoy farm is 14.6% lower compared to the benchmark. This is a result of a decrease in maintenance costs. Because, contrary to the IEA turbines, the 15 MW X1 Wind PivotBuoy can be towed to shore easily due to its quick-connect system. The OPEX for the 30 MW downwind solution reduces slightly compared to the benchmark. This reduction is mainly due to the same quick-connect system. Also, the amount of offshore logistics and vessels is expected to be less because there are only half the amount of turbines in the farm. It is however not certain to what extent the quick-connect system will reduce the OPEX.

ABEX

The ABEX for the 15 MW X1 Wind PivotBuoy is the same as for the benchmark turbine. This is however inaccurate as the structure is not the same. Therefore it can deviate from this value. The same inaccuracy holds for the ABEX of the 30 MW downwind design.

8.3 Conclusion

This study focuses on the feasibility of upscaling the X1 Wind PivotBuoy concept to a 30 MW downwind solution for an offshore floating wind turbine. This study has the following objective:

“Evaluate the feasibility of a 30 MW upscaled DWT and compare it economically to a 15 MW X1 Wind PivotBuoy DWT and a benchmark 15 MW IEA Umaine VoltturnUS-S UWT in the Bay of Biscay based on a 450 MW wind farm.”

In the first part of this study, the structural analysis is performed to investigate the structural integrity of the 30 MW solution. In this analysis a preliminary design is made to determine the dimensions and weight of the substructure, these properties are used as an input for OpenFAST to access the global stability of the structure. This does not cause any difficulties. Furthermore, a FEM analysis is performed to get insight into the natural frequencies and modal shapes of the structure. This is compared to the wind, wave, 1P, 3P, and 6P spectra. These are sufficient for the structural integrity. From this, the displacements and stresses can be obtained. The stresses in the members are checked based on steel strength. However, using circular hollow sections does not provide the prescribed structural integrity. Therefore, A direct upscale of the X1 Wind PivotBuoy is structurally unfeasible.

The life cycle assessment of the 30MW upscale evaluated six aspects: supply chain, construction, installation, transport, operation and maintenance, and decommissioning. Regarding these aspects, the following can be concluded:

- Supply chain: The industry needs to invest in developing and producing the RNA, pivot top, main columns, and blades for the 30MW turbines, which are not available yet.
- Construction: The lifting of the nacelle, which weighs 1400 tons, to a height of 210 meters requires larger cranes or new techniques.
- Operation and maintenance: The large maintenance operations involve heavy and high lifting, which might be difficult and costly. The use of nearby ports could reduce the O&M costs.
- Decommissioning: No major problems are expected, as the operations are well-known and the industry has 30 years to adapt to the larger turbines.

The other aspects (installation, transport) are not likely to pose new problems, as they are similar to existing operations. From this, it can be concluded that the life cycle assessment of the 30 MW solution causes major difficulties and the industry is not ready for it as of now.

In the last part of this study, the economic evaluation is done. In this part, the 30 MW solution and the 15 MW X1 Wind PivotBuoy are compared to the IEA 15 MW UMaine VoltturnUS-S. The comparison is performed on a wind farm level. The comparison looked at AEP, CAPEX, OPEX, ABEX and LCOE. The 15 MW X1 Wind PivotBuoy appeared to be economically feasible because it had a lower LCOE than the 15 MW IEA. However, The 30 MW downwind solution appeared to have an increase of the LCOE of 53%. Therefore, it is not economically feasible to upscale the X1 Wind PivotBuoy to 30 MW. The main driver of this increase in LCOE is the costs of the substructure of the 30 MW solution.

It can be concluded that the proposed 30 MW solution, in comparison with the two other turbine concepts, is deemed unfeasible today. Upscaling the substructure of the 30 MW causes problems regarding the structural integrity. Moreover, it is not feasible to build such a large structure since the industry is not ready for the manufacturing and construction of such heavy and large structures. Focusing on the economical evaluation of the concept, the LCOE of the 30 MW solution is 53.7% higher compared to the IEA 15 MW wind turbine designs.

8.4 Opportunities

This study towards the upscale of a 30 MW also provides some opportunities and recommendations for the future:

1. No structural optimization is performed for the 30 MW solution. Singular hollow tubes are deemed to be unfeasible. However, using trusses instead of hollow beams can lead to better stress distribution and reduction of the weight of the substructure.
2. The 15 MW X1 Wind PivotBuoy is deemed to be more economically feasible when compared to a semi-submersible floater. Since the structural analysis in the report only focused on the 30 MW solution, it would be interesting to look more in detail into the structural analysis and life cycle assessment of the 15 MW X1 Wind PivotBuoy to investigate future possibilities and cost reductions.
3. As of now, no crane is available to lift a nacelle of 1400 tons. It would be interesting to investigate the possibilities of modular nacelles. The nacelle will be lifted in parts and installed at the top of the structure.
4. To reduce the LCOE of a wind park, it could be interesting to investigate the possibilities of creating a construction and maintenance yard that serves several wind farms to reduce the OPEX and thus the LCOE.

5. This study assumes a fixed power tender of 450 MW, which corresponds to 15 * 30 MW turbines. However, the study also shows that the available space could accommodate at least 19 * 30 MW turbines, which would lower the LCOE. Therefore, a future research direction could be to optimize the space utilization and consider a fixed space tender instead of a fixed power tender.
6. The misalignment of the downwind turbine is caused by the wind and currents. The AEP decreases when the average misalignment of the 30 MW turbine increases. This can be prevented by accessing the downwind turbines in sheltered waters to reduce the average misalignment.

Appendix A

TOPFARM and PyWake

A.1 Wind Farm Optimization

As previously stated, `PyWake` and `TOPFARM` play an important role in optimizing wind farm spacing. Achieving this optimization requires the customization of default settings to align with specific wind turbine characteristics, site conditions, constraints, drivers, and cost models. Lastly, implementing the wake model's sensitivity to see how variations in the wind model's complexity affect the overall outcome.

A.1.1 Wind turbine

A new class `WindTurbine` is created with distinctive attributes of each of the three turbine types examined in this project. This class incorporates essential properties such as rotor diameter and hub height. Additionally, it incorporates parameters relating to power generation and thrust coefficient corresponding to specific wind speeds for each turbine type. This class will subsequently find application within the engineering wake model `PyWake` optimization tool `TOPFARM`, contributing to the calculation of the optimal spacing between wind turbines.

A.1.2 Site

To create a site, a new class is designed to encapsulate critical information about environmental conditions and correlate them with specific types of power generation. The initial step involves analyzing wind data, focusing on the frequency and directionality of wind from 12 equally divided sectors spanning 0 to 360 degrees. This wind data is represented using a Weibull distribution, with shape and scale parameters derived from the actual data. This distribution faithfully mirrors the real environmental conditions prevalent in the Celtic Sea, precisely at the project's location.

Subsequently, the wind farm's parameters are defined, including details such as its geographical boundaries, the number of wind turbines it consist of, and the predetermined initial positions for these turbines within the specified boundaries.

This class will subsequently find application within the optimization tool `TOPFARM`, contributing in the calculation of the optimal spacing between wind turbines.

A.1.3 Constraints

The model primarily incorporates physical constraints, with two key constraints in focus. The first constraint relates to spacing, ensuring a minimum distance between wind turbines because of the influence of wake. The second constraint is related to boundaries, specifying that turbines must remain within the defined boundary limits and cannot be positioned outside of them.

This class subsequently finds application within the optimization tool `TOPFARM`, contributing in the calculation of the optimal spacing between wind turbines.

A.1.4 Driver

In this research the gradient-based optimization technique employing the SciPy algorithm known as Sequential Least Squares Quadratic Programming is used as the driver behind the optimization. The OpenMDAO library offers various built-in drivers that leverage open-source optimization algorithms. Gradient-based drivers are iterative algorithms that utilize gradient information of the objective function concerning the design variables. They systematically explore the design space to identify improved designs. The optimization process employs the `EasyScipyOptimizeDriver` as the driver.

This optimization procedure aims to enhance the wind farm's economic performance and overall efficiency by strategically positioning the turbines.

A.1.5 Cost-model

TOPFARM employs a cost-based model to optimize the layout of a wind farm, considering factors such as the AEP and the IRR. The functions for AEP and cost calculations are established. In this context, the IRR serves as the primary financial metric for the optimization. The turbines' positions are static, so alterations in AEP due to changes in turbine placement become the key factor influencing IRR. By experimenting with various parameters, the optimization outcome varies accordingly.

A.1.6 Wake-model

The wake model is included in the `PyWake` packages. A wake is characterized by a mean wind decrease (i.e. wake deficit) and turbulence increase behind a turbine. The primary motivation for a detailed modeling of wind turbine wakes is that wind turbines located in wind farms experience inflow wind conditions that is substantially modified compared to the ambient wind field that apply for stand-alone wind turbines due to upstream emitted wakes. So, wake-models become interesting when multiple wind turbines are placed in a certain space, because they can influence each other, which can cause a decrease of generated energy. In this report different wake-models will be compared to each other, so see what the effect of the wake-models are

The `PyWake` package incorporates a wake model that characterizes the phenomenon of wind turbine wakes. A wake is defined by a reduction in mean wind speed and an increase in turbulence levels behind a turbine. The primary reason for accurately modeling wind turbine wakes is that wind turbines situated within wind farms experience altered inflow wind conditions compared to standalone turbines. This variation occurs due to the wakes generated upstream by other turbines. Therefore, wake models become crucial when multiple turbines are placed in close range to each other because they can mutually influence each other, potentially resulting in reduced energy generation. This report will compare various wake models to assess their effects and implications on wind farm performance.

The first one is N.O. Jensen deficit model which is only valid for far wake [91]:

$$V = U \left(1 - 2\alpha \left(\frac{r_0}{r_0 + \alpha x} \right)^2 \right) \quad (\text{A.1})$$

Where:

U = free stream velocity

r_0 = wake radius

x = downstream distance

α = the entrainment distance (with a value of 0.1)

The second one is Bastankhah Gaussian deficit model [92], which is only valid for far wake

$$\frac{\Delta U}{U_\infty} = \left(1 - \sqrt{1 - \frac{C_T}{8(k^*x/d_0 + \varepsilon)^2}} \right) \times \exp \left(-\frac{1}{2(k^*x/d_0 + \varepsilon)^2} \left\{ \left(\frac{z - z_h}{d_0} \right)^2 + \left(\frac{y}{d_0} \right)^2 \right\} \right) \quad (\text{A.2})$$

Where:

$\frac{\Delta U}{U_\infty}$ = normalised velocity deficit

C_T = thrust coefficient of turbine

k^* = wake growth rate

x = downstream distance

d_0 = diameter of turbine

ε = 0.2β , with β being a parameter function of the turbine's C_T

z = vertical coordinate

z_h = hub height of the turbine

y = spanwise coordinate

The third one is Fuga[93], which is valid for near wake, far wake and blockage deficit.

The FugaDeficit model calculates the wake deficit based on a set of look-up tables computed by a linearized RANS solver. The look-up tables are created in advance. The most important parameters to create the look-up tables are:

- Wind turbine diameter
- Wind turbine hub height
- Terrain roughness length
- Lower and upper height of output domain

A wake deficit model is a model used to compute the deficit caused by a single turbine [10]. In order to validate the results and to provide a bandwidth for the AEP, three different wake deficit models were implemented in the simulations. Figure A.1 displays the diverse wake deficit models that can be implemented in PyWake. Using this figure, three models with very distinguishable wake deficit over the center line were selected. These models are NOJDeficit, FugaDeficit and BastankhahGaussianDeficit.

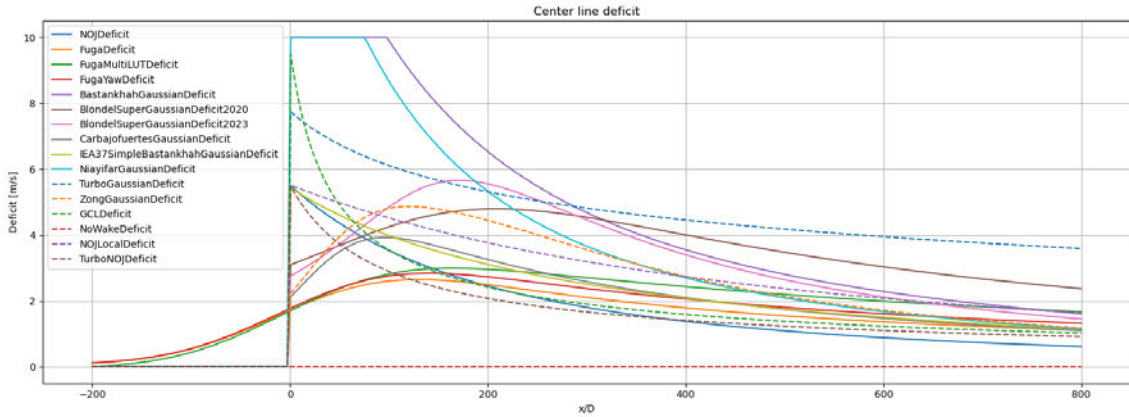


Figure A.1: Deficit along center line from different models, [10].

A.1.7 Optimizing the farm level

In order to attain insight into optimizing the AEP of a wind farm, various parameters come into play. The initial stage involves optimizing the layout of the wind turbines within the predefined boundaries while ensuring that the wind farm generates a target output of 450 MW of energy, as detailed in the boundaries outlined in (section 1.4). The initial positions of the wind turbines are predetermined. This optimization process is grounded in maximizing the IRR, aiming to position the wind turbines to maximize power generation.

The subsequent step involves the implementation of various models to validate the AEP and evaluate the sensitivity of the created model. These models predominantly includes wake models and optimization drivers.

In the final phase, a comprehensive analysis is conducted to determine the energy output of each turbine under varying wind speeds and directions. This analysis provides insights into the individual contributions of each turbine within the wind farm's layout.

To optimize the spatial arrangement of wind turbines and maximize the IRR, a solver relying on the AEP and IRR is employed. Initially, the NOJ wake model is used, in which the specific wind turbine and site parameters are incorporated. As this report progresses, various wake models will be used to assess the model's sensitivity. The site characteristics, as detailed in chapter 3, serve as the foundation for this optimization.

Appendix B

Numerical modelling

B.1 Approach

Step 1: Define Equation of motion

First, the equations of motion regarding an Euler-Bernoulli beam for a given element are given by their respective PDEs

Step 2: Construct Lagrangian

Next, the EOMs of the system need to be obtained, whose individual bodies have to satisfy certain constraints. For this, the Lagrangian (L) is defined as the difference between the kinetic and potential energies:

$$L = T - U \tag{B.1}$$

where T is the total kinetic energy and U is the total potential energy.

Step 3: Take derivatives

To derive the final matrix form, The Euler-Lagrange equation is used which relates the Lagrangian to the equations of motion. Applying this equation to each degree of freedom, the equations are obtained. These prescribe that the energy in the system is conserved.

Solving these equations results in an equation for each of the 12 degrees of freedom. This will yield the complete matrix equation (the strong form):

$$M \cdot \ddot{U} + C \cdot \dot{U} + K \cdot U = F \tag{B.2}$$

However, if damping is included in the system, the equations cannot be easily decoupled and solved using modal analysis. The generic damping matrix, when transformed to the modal coordinates, does not result in a diagonal matrix. This means that the equations cannot be decoupled, and solving for the modal responses becomes more complex.

The modal analysis approach is used for several reasons.

- Modal analysis allows obtaining the modal response of each mode, which is similar to a Single Degree of Freedom system. Solving these coupled differential equations for each mode is relatively easier and faster when compared to solving a system of coupled ordinary differential equations for all degrees of freedom simultaneously. This simplification facilitates a more efficient computation of the dynamic response.
- The highest frequency modes tend to be the least accurate in the analysis because of numerical errors and assumptions made during the modeling process. Excluding these modes from the analysis does not significantly impact the overall accuracy of the results, allowing for computational efficiency.

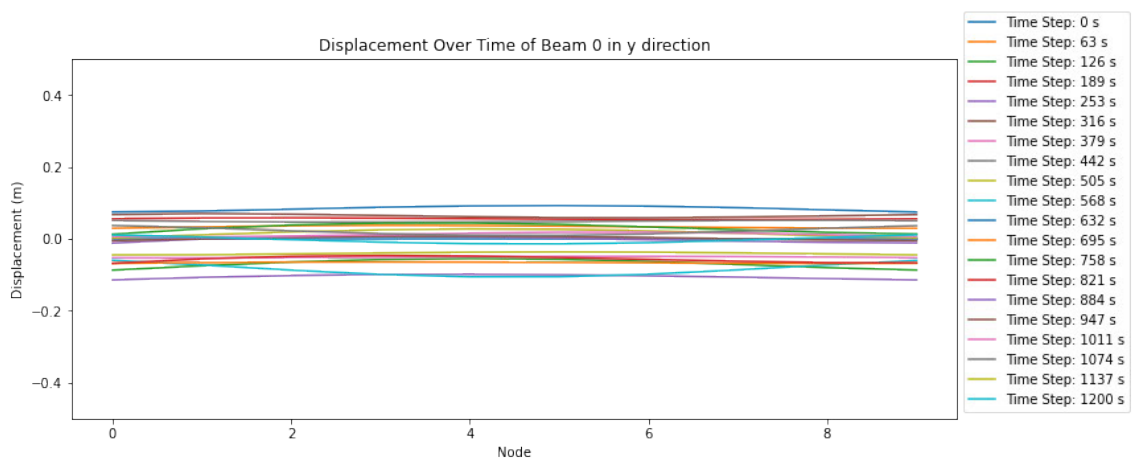
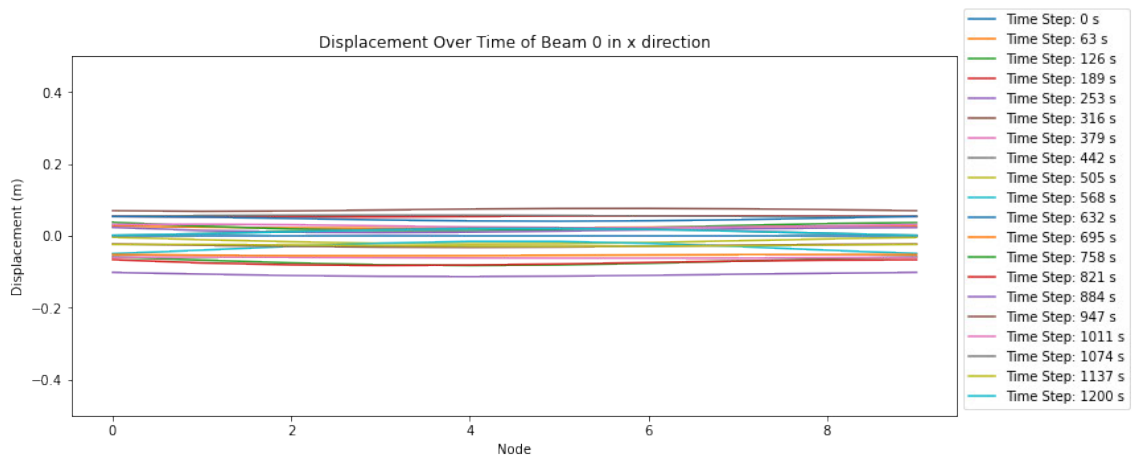
Therefore the damping matrix (C) is excluded from the equation of motion, resulting in:

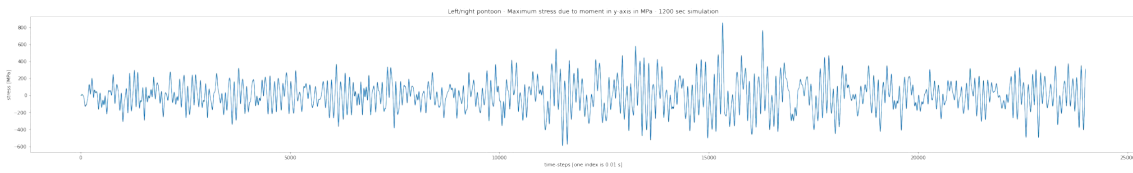
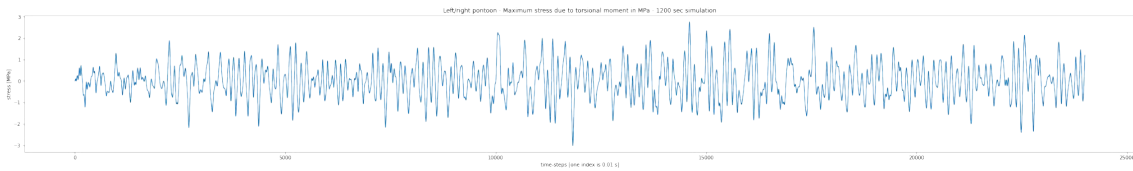
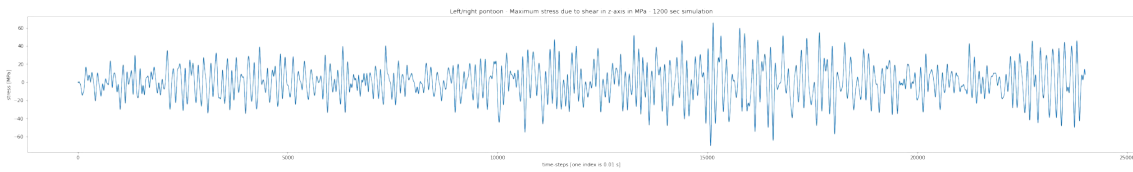
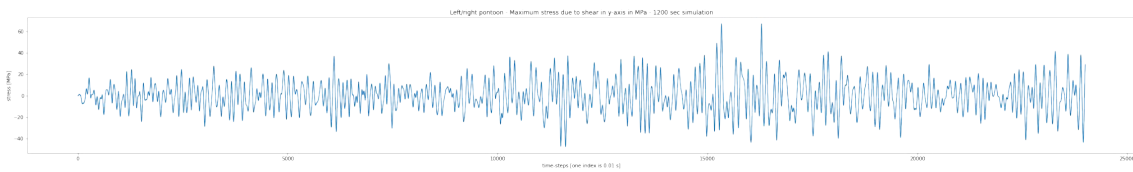
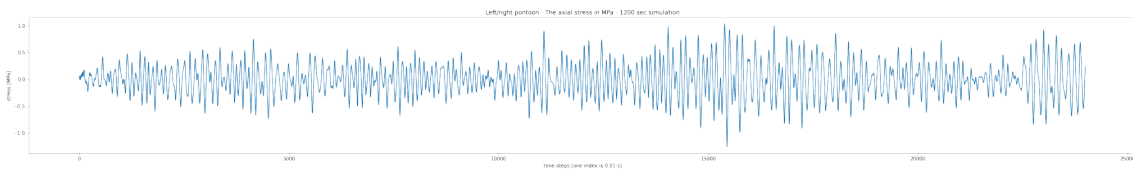
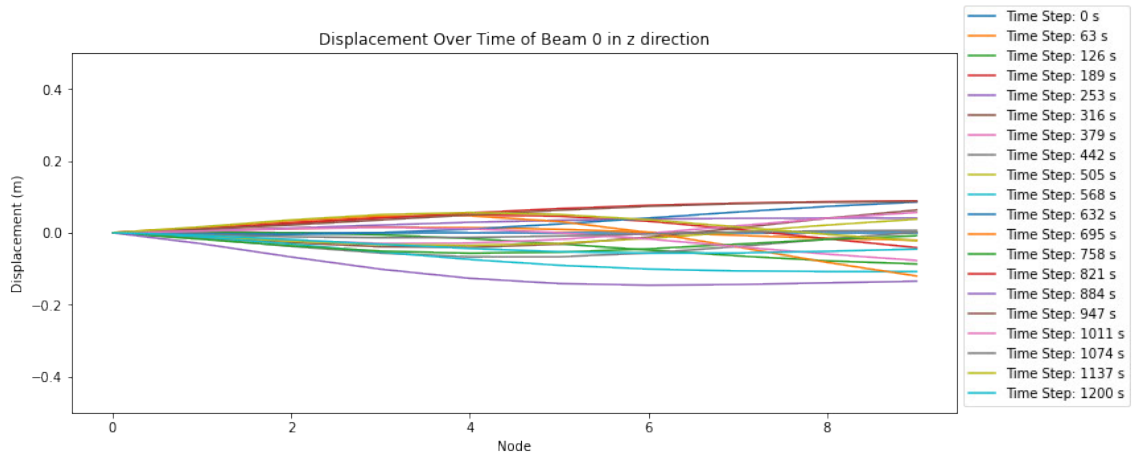
$$M \cdot \ddot{U} + K \cdot U = F \quad (\text{B.3})$$

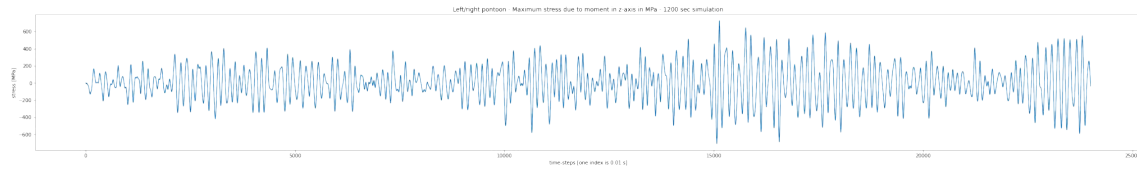
Damping is later re-introduced using modal damping, which assumes that each mode of vibration in the system has associated damping. The modal damping approach allows for the inclusion of damping effects by defining damping associated with each mode shape (as a percentage of the critical damping). The damping matrix (C) is added as a diagonal matrix with the modal damping coefficients on the diagonal.

B.2 Results

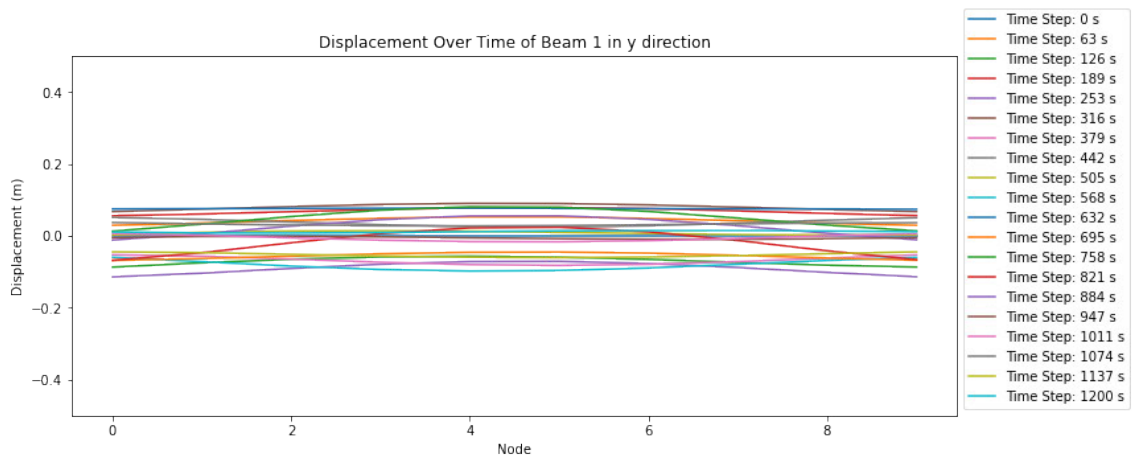
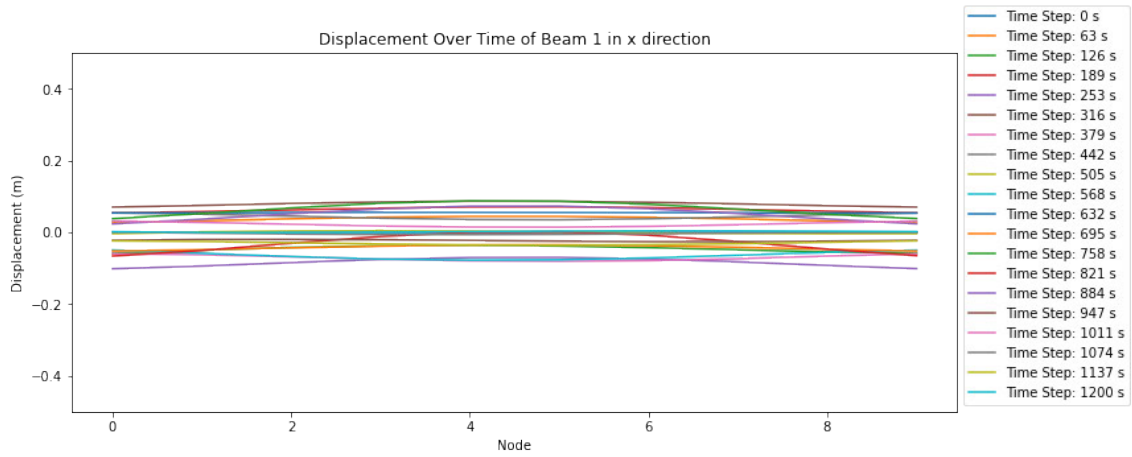
B.2.1 Pontoon left

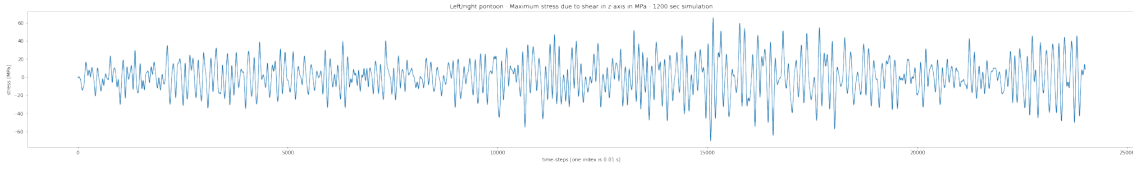
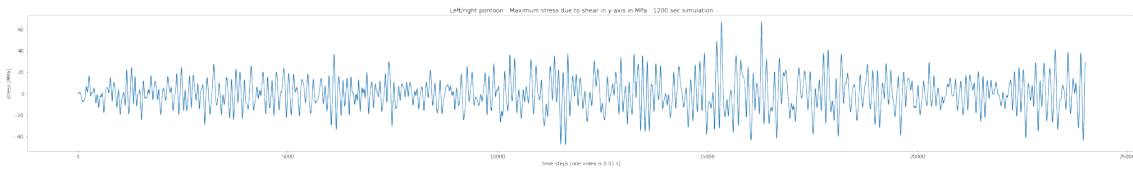
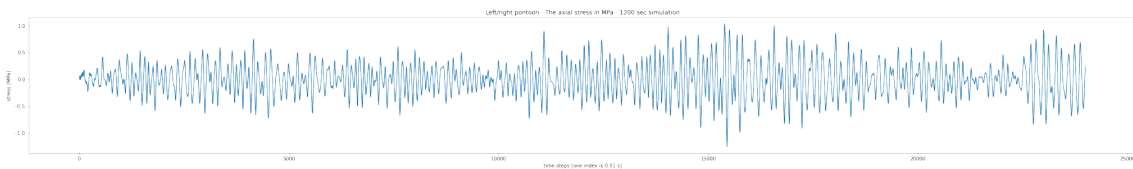
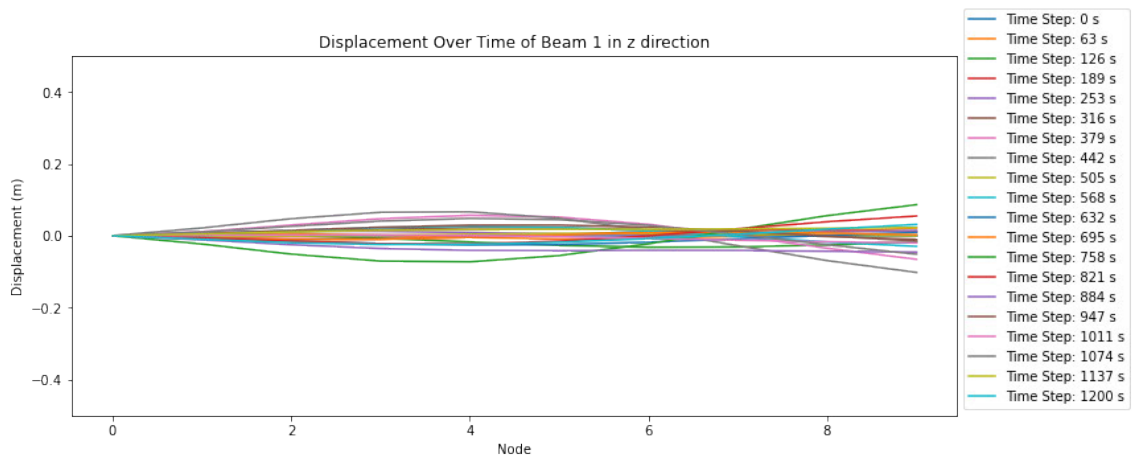


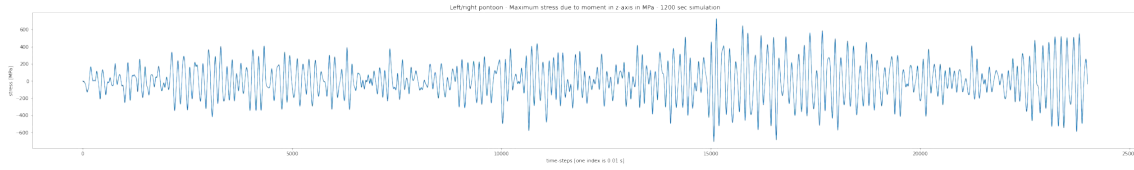




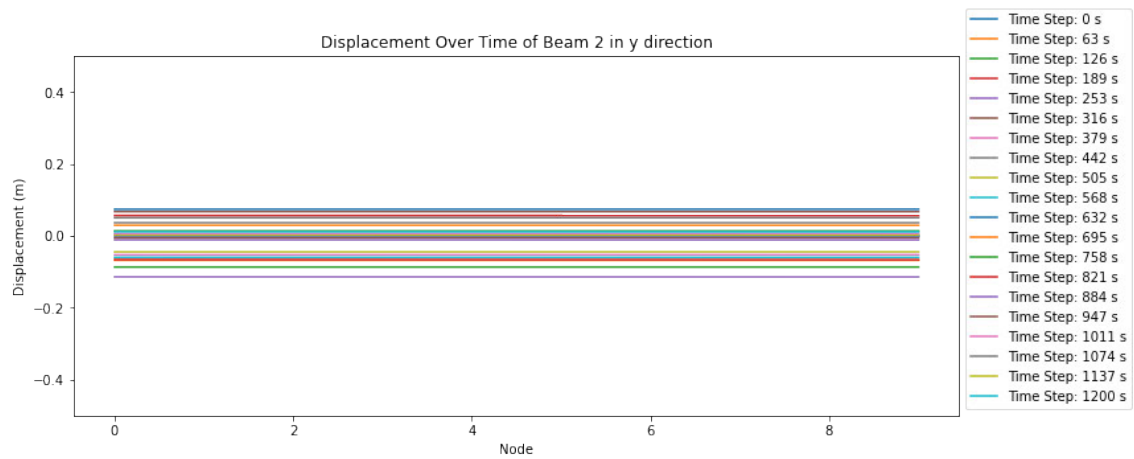
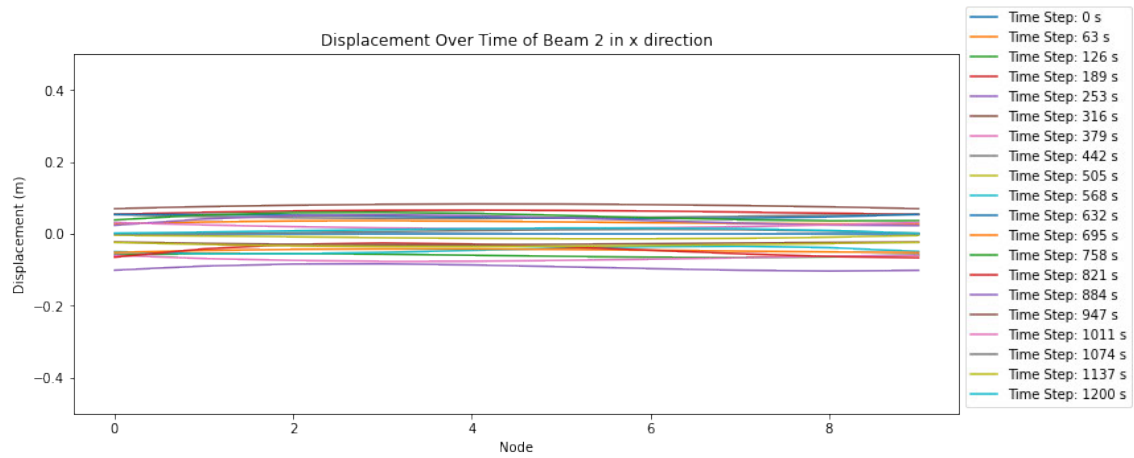
B.2.2 Pontoon right

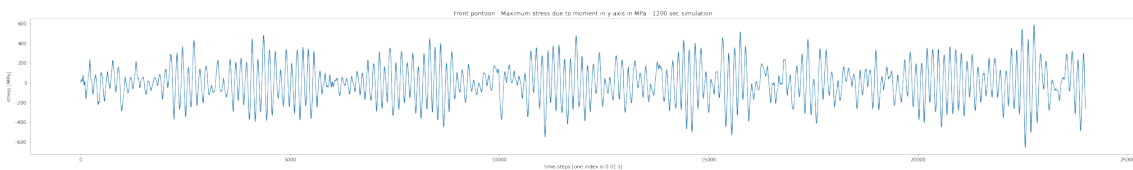
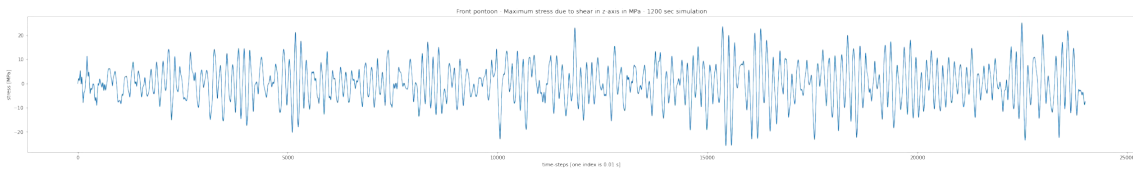
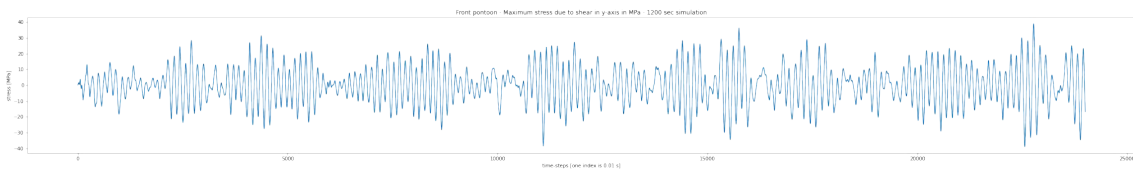
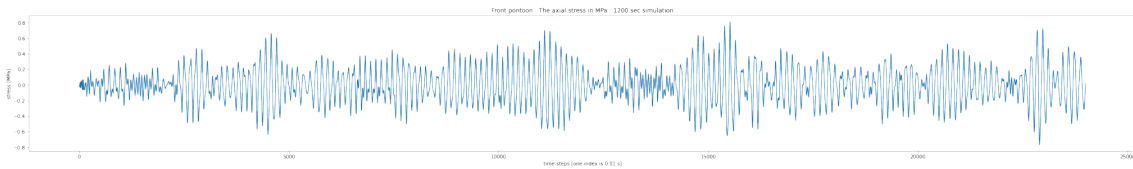
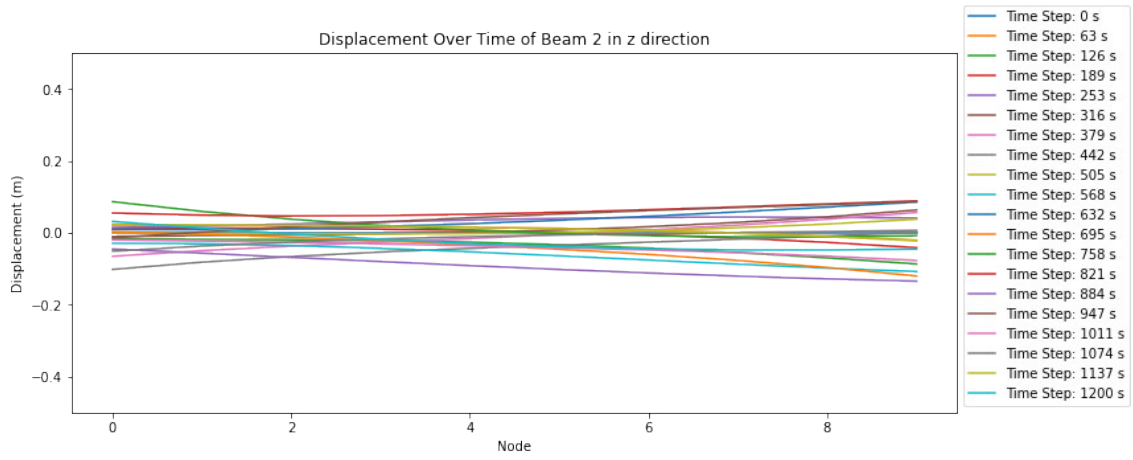






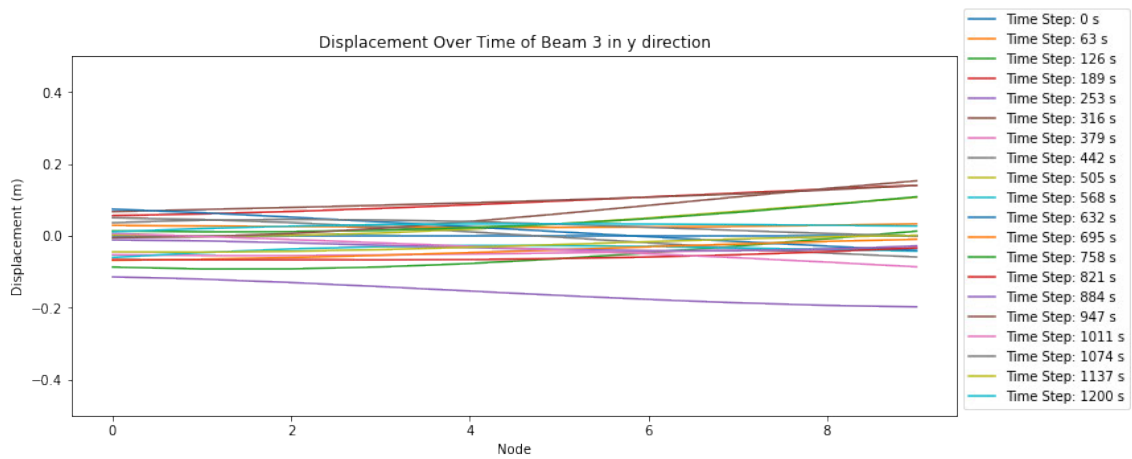
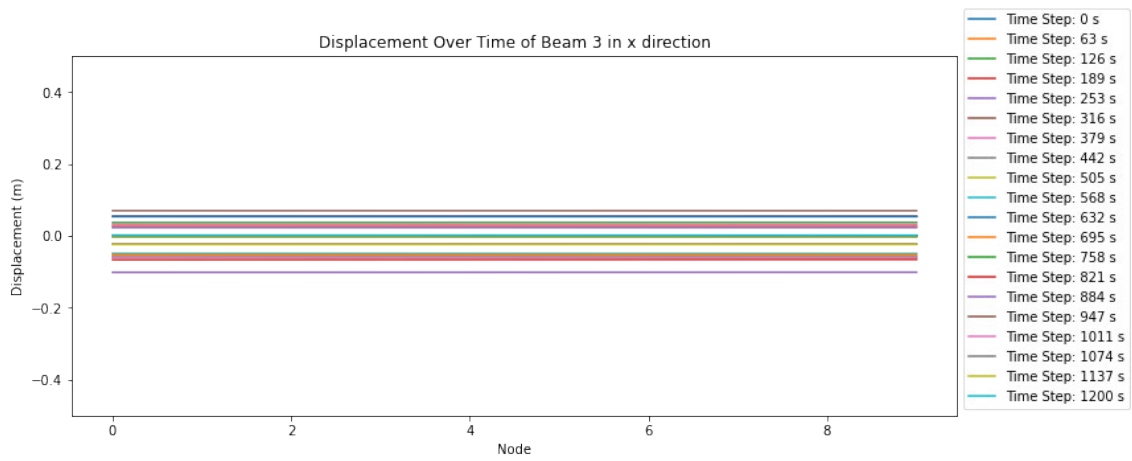
B.2.3 Pontoon front

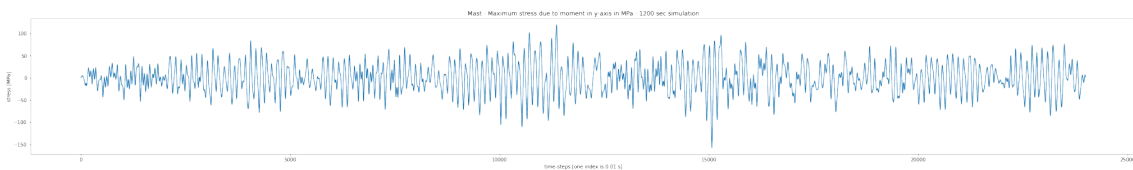
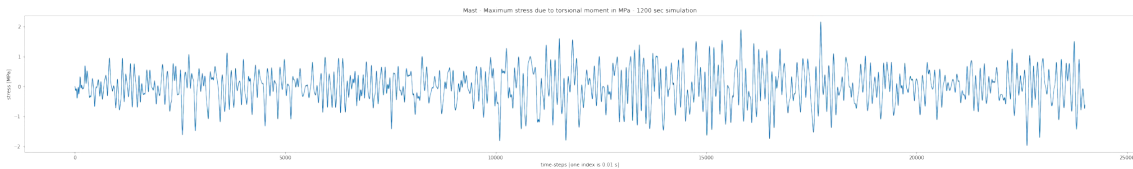
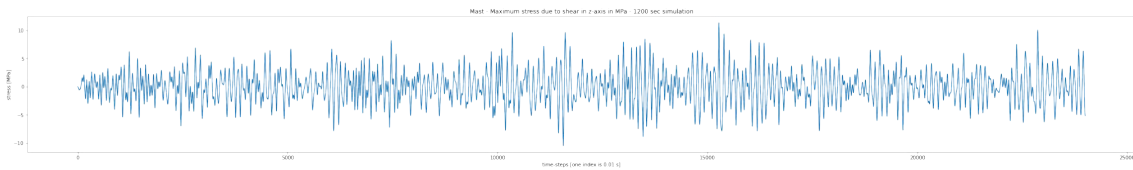
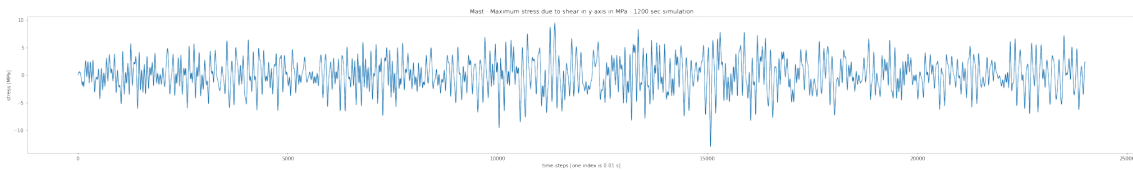
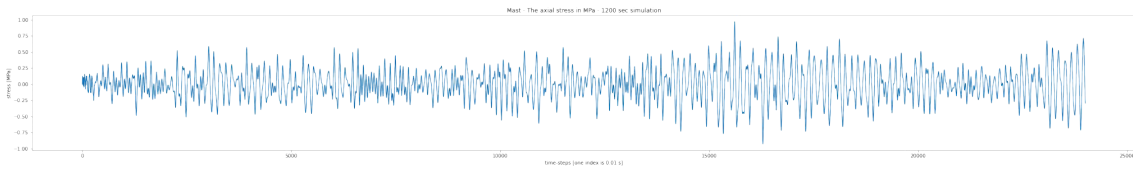
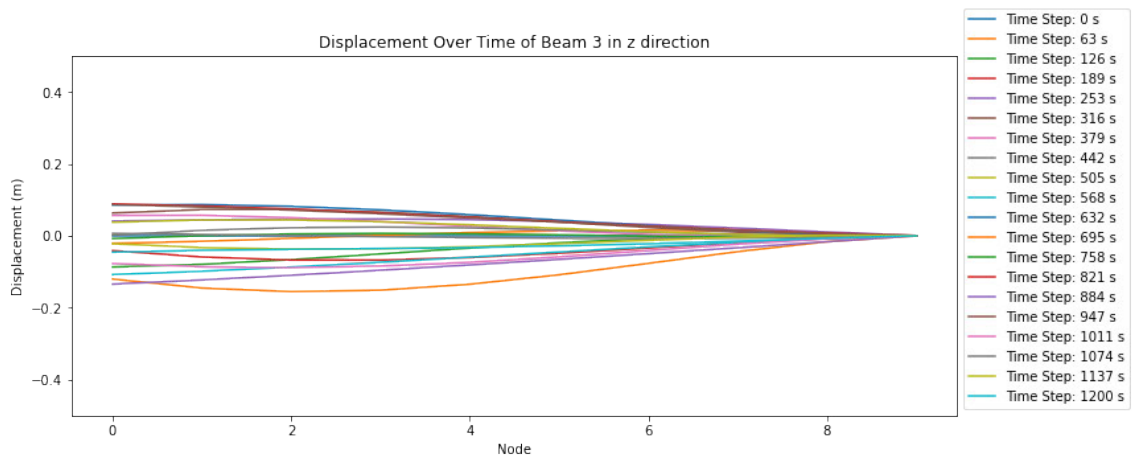


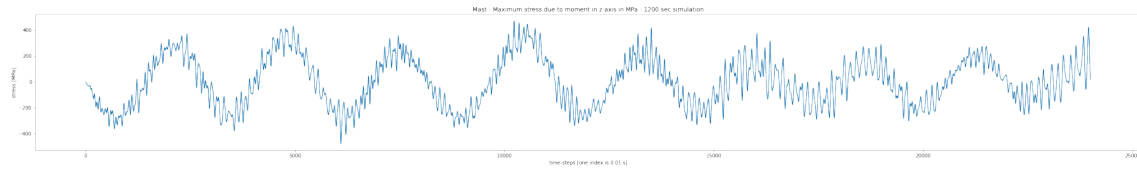




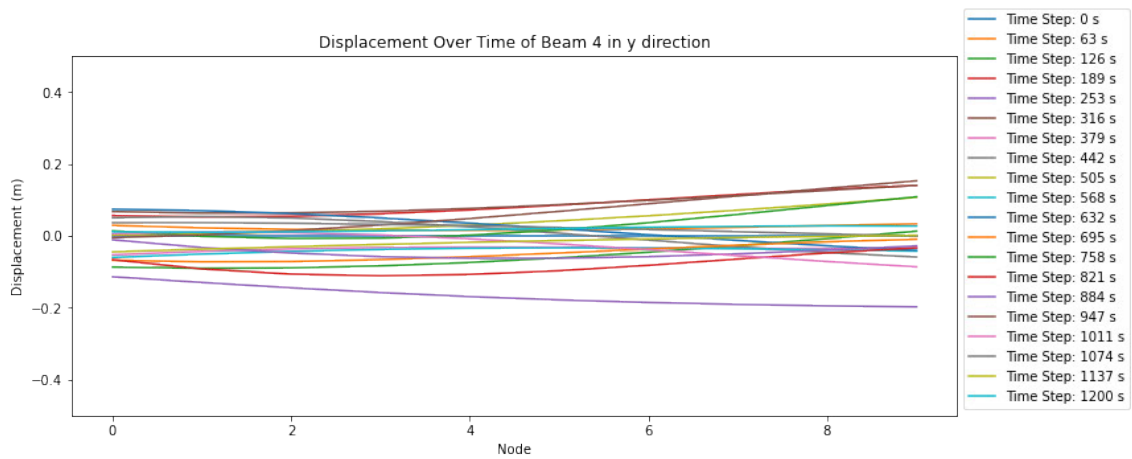
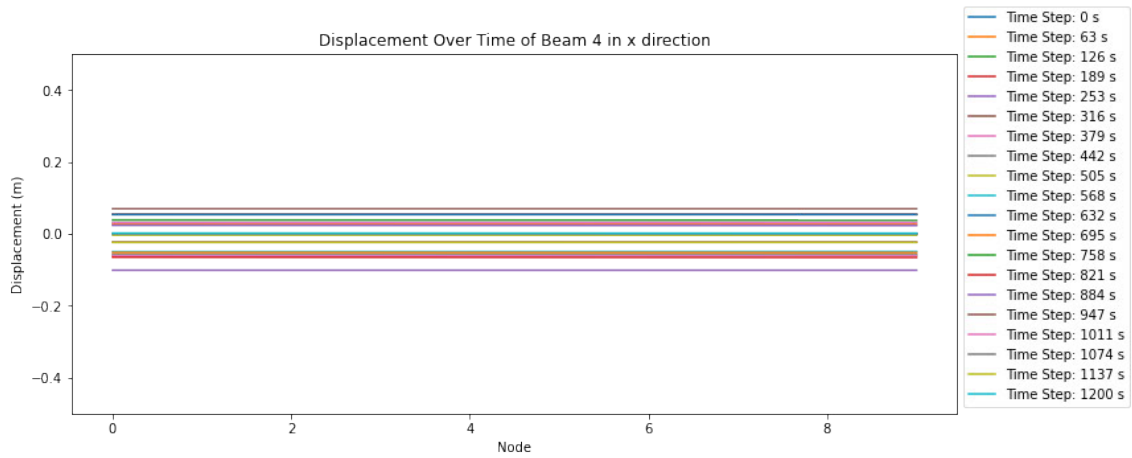
B.2.4 Mast front right

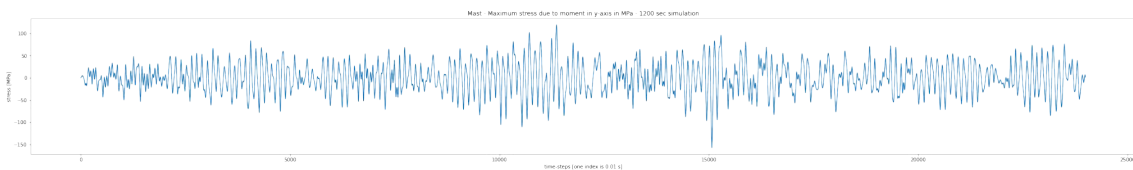
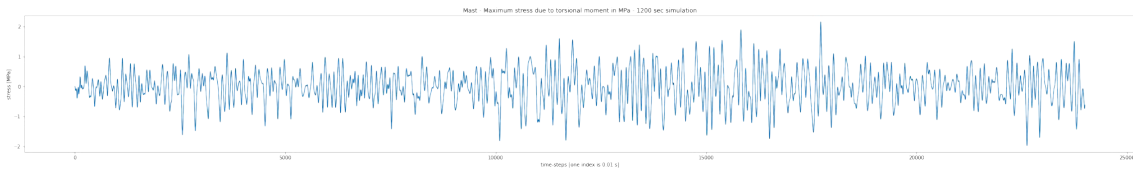
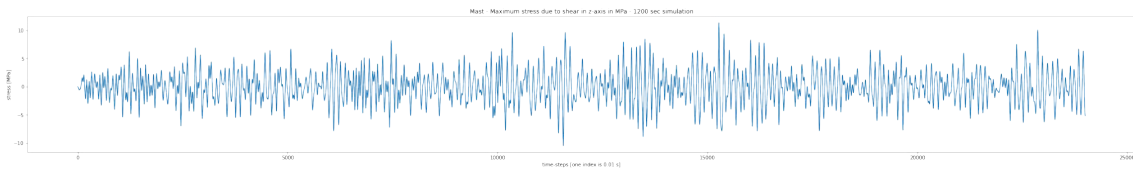
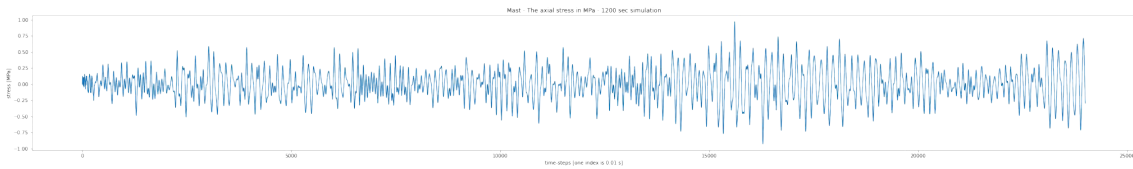
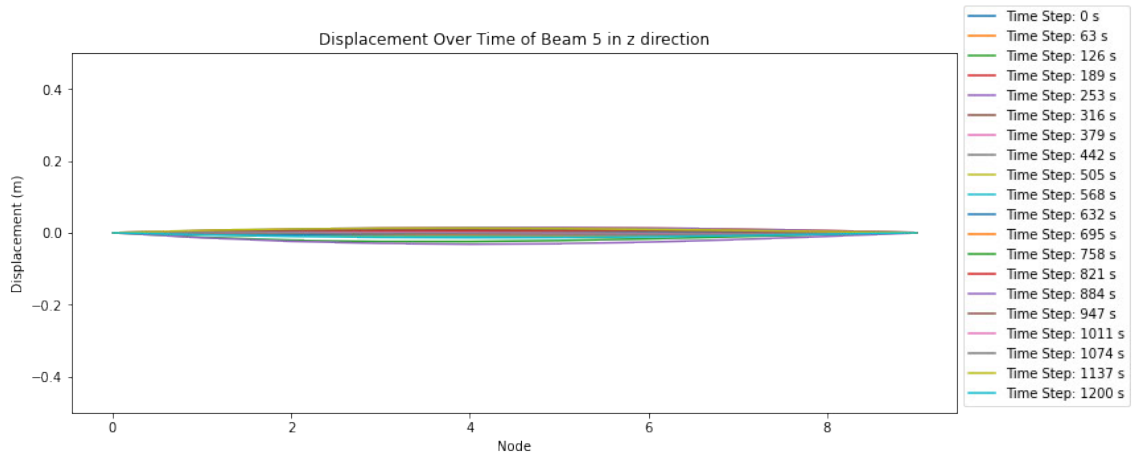


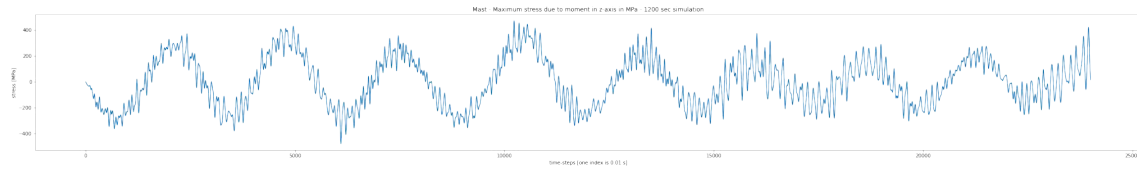




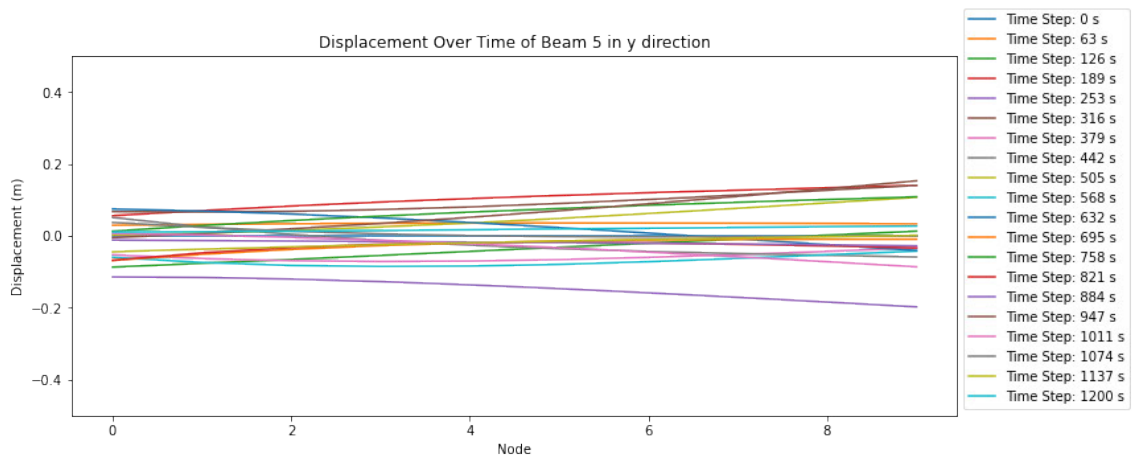
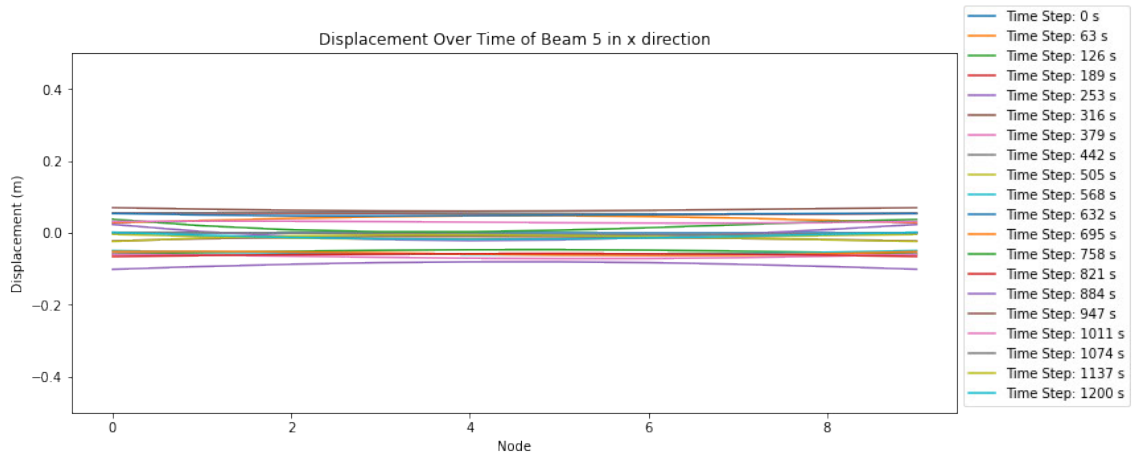
B.2.5 Mast front left

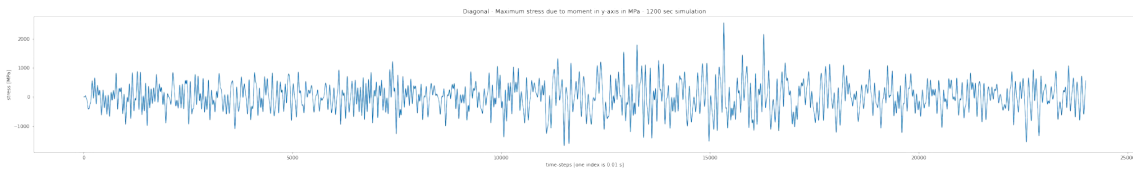
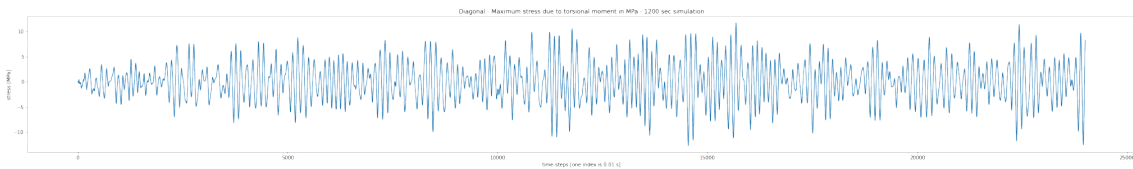
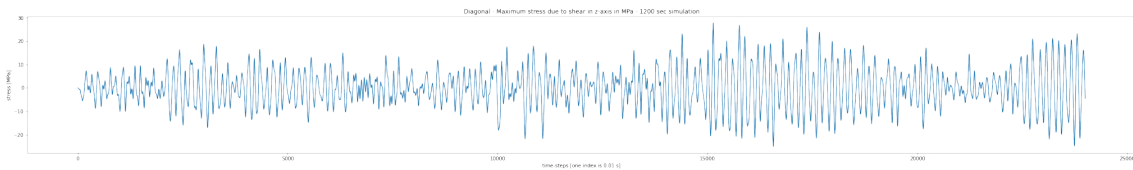
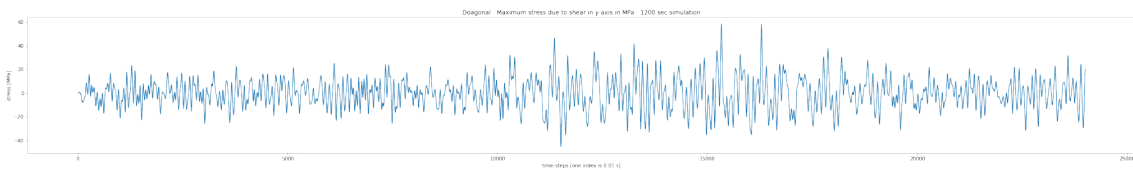
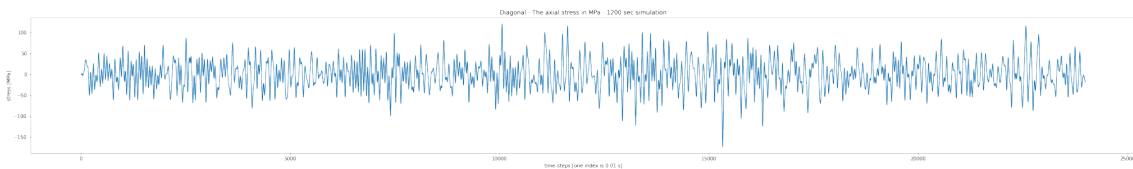
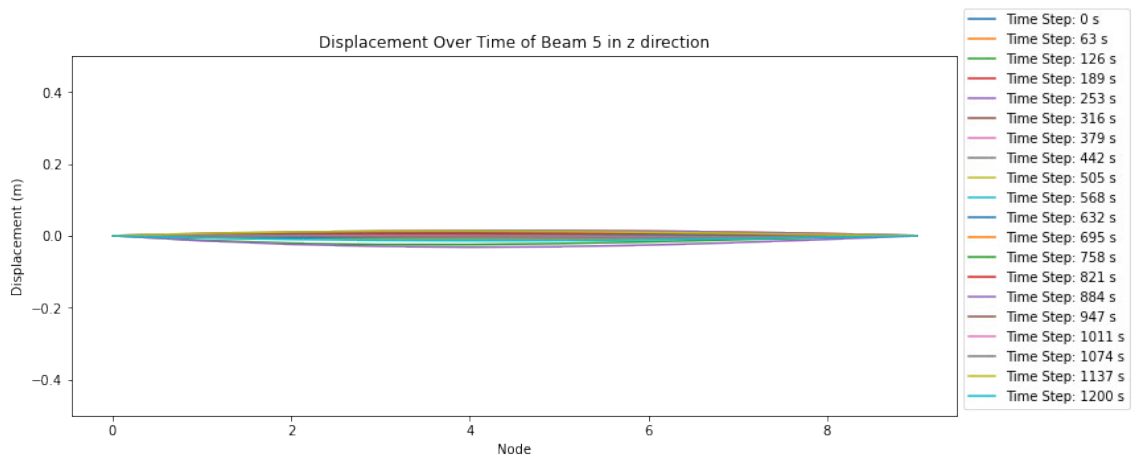


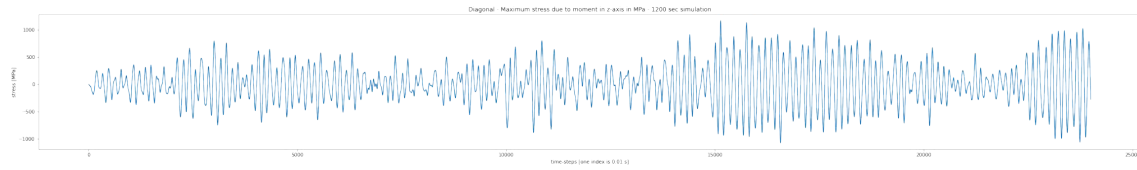




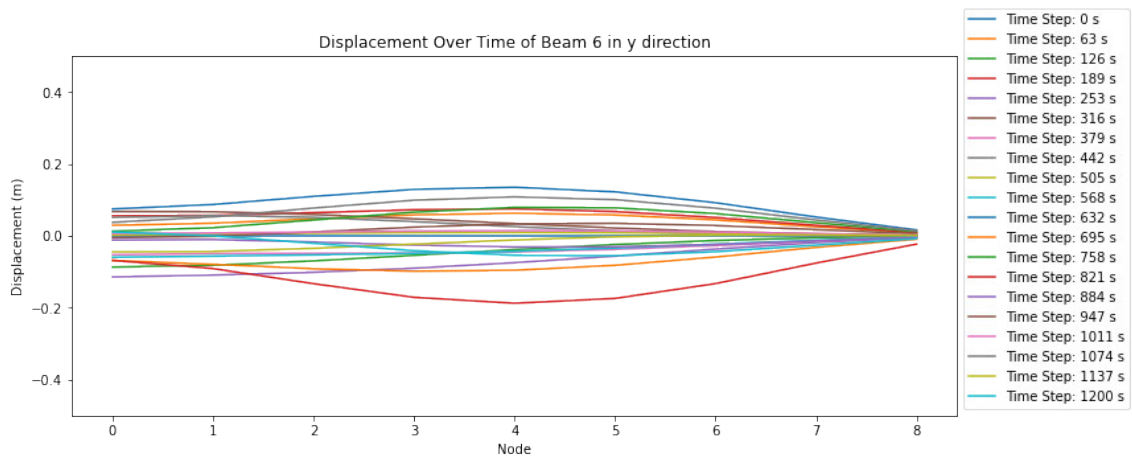
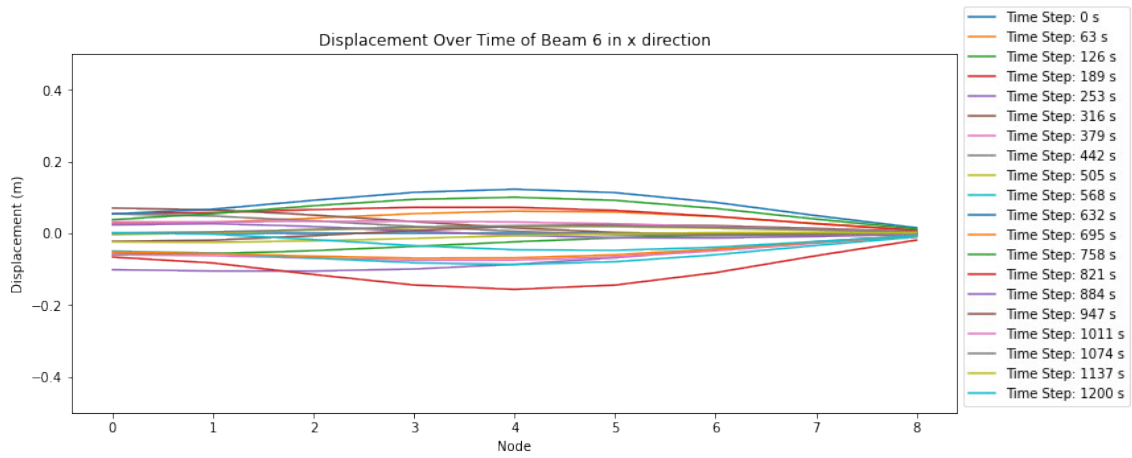
B.2.6 Pivot mast (diagonal)







B.2.7 TLP



Appendix C

Turret failure modes

Table C.1: Types of primary and secondary bearing failures.

Primary Damage	Damage	Cause	Countermeasures
Wear	Wear on the contact surfaces	Vibrations / contaminated lubricant	Apply enough lubricant of high quality
Indentations	Raceways and rollers become dented	Abnormal loadings when not spinning / foreign material	Improve sealing / improving mounting procedures
Smearing	Roughening of surface	Improper lubrication / slipping (high speed and low load)	Choose right lubrication and pretension of bolts
Corrosion	Rust partially covering bearing surface	Bad sealing / no dry storage	Improve sealing and storage
Electric current damage	Pitting on raceways or contact surface	High electrical current traveling through bearing balls/rollers	Insulation of bearings / provide bypass for current
Secondary Damage	Damage	Cause	Countermeasures
Flaking	Material is removed in flakes from raceway or rolling elements	contact surface fatigue	Increase clearance, improve mounting procedure
Cracks	Cracking on outer ring or rolling elements	Heavy impact load / advanced flaking	Re-examine load conditions

Appendix D

30 MW details OpenFAST

Table D.1: Location of joints final design.

Joint	x-location	y-location	z-location	Joint description
1	0.000000	-103.5000	-7.90000	Nacelle side Heaveplate 1 top
2	0.000000	103.5000	-7.9000	Nacelle side Heaveplate 2 top
3	-174.6000	0.000000	-9.50000	PivotBuoy Heaveplate top
4	0.000000	-103.5000	8.00000	Nacelle side buoy 1 top
5	0.000000	103.5000	8.00000	Nacelle side buoy 2 top
6	-174.6000	0.000000	8.00000	Hor. Connectors & diag. mast PivotBuoy
7	0.000000	-103.5000	8.00000	Nacelle side connection vertical mast 1
8	0.000000	103.5000	8.00000	Nacelle side connection vertical mast 2
9	-174.6000	0.000000	10.00000	Pontoon PivotBuoy top
10	0.000000	0.000000	199.0000	Top of substructure
11	0.000000	-103.5000	-8.00000	Pontoon nacelle side 1 bottom
12	0.000000	103.5000	-8.00000	Pontoon nacelle side 2 bottom
13	-174.6000	0.000000	-10.0000	PivotBuoy Heaveplate bottom

List of Figures

1.1	Schematic of UWT and DWT [4].	2
1.2	Overview of project structure.	3
1.3	Overview of location, adapted from 4C offshore [6].	3
1.4	Location of wind farm relative to Bretagne, adapted from 4C offshore [6].	4
2.1	UMaine IEA 15 MW turbine with VoltturnUS-S semi-submersible floating platform [13].	8
2.2	X1 Wind PivotBuoy concept.	9
2.3	X1 Wind PivotBuoy concept schematic representation, adapted from [5].	11
3.1	Annual wind rose at 100 meter height [16].	13
3.2	Threshold significant wave height.	15
3.3	Extreme value significant wave height.	15
3.4	Return period significant wave height.	15
3.5	Threshold zero-crossing wave period.	16
3.6	Extreme values zero-crossing wave period.	16
3.7	Extreme values zero-crossing wave period.	16
3.8	Location of Sud de la Bretagne I and SEM-REV Site [6].	17
3.9	Current velocity distribution [16].	17
4.1	Forces and moments.	21
4.2	Optimization process which ensures no tension in the connector.	22
4.3	Full submergence of pontoon B analysis.	22
4.4	3D representation of 30 MW PivotBuoy design.	23
4.5	Three cross sections of the PivotBuoy necessary for the representative distances to find the pitch, roll, and yaw inertias.	24
4.6	Different moments of inertia based on axis for circular hollow sections [17].	25
4.7	Visualization of design of the 30 MW PivotBuoy in ParaView.	26
4.8	Visualization of how drag coefficients are applied [20].	29
4.9	Dimensions of the 30 MW PivotBuoy visualized using ParaView.	31
4.10	The final floating model consisting of 7 elements.	34
4.11	x-y plot of the first 12 modes.	38
4.12	y-z plot of the first 12 modes.	39
4.13	JONSWAP spectrum based on wave conditions.	40
4.14	Swept distance between the two masts in white (heart to heart) (Dist = 177.8 m).	41
4.15	Spectrum analysis.	41
4.16	Modal excitation of mode 20 which occurs in 6P region.	42
4.17	JONSWAP sea-level elevation time series for swell waves.	43
4.18	the amplitude spectrum for swell waves.	43
4.19	Velocities on structural components of variant one.	44
4.20	Accelerations on structural components of variant one.	44
4.21	Forces on structural components of variant one.	44
4.22	Time-series of the displacement at the corner points of the floater.	45

4.23	Displacement of every single node.	45
4.24	Time-series of the displacement of every single node.	46
4.25	Time-series of the displacement of every single node.	46
4.26	Improved structural configuration to resist occurring stresses.	49
4.27	Model set-up for truss analysis.	49
4.28	Overview method of sections.	50
4.29	Detail of floater to TLP connection, including the quick connector and the turret [26].	51
4.30	Extrapolation of bearing capacity and diameter size.	53
4.31	Conclusion Structural Analysis.	54
5.1	30 MW blade compared to General Electric blade factory, Cherbourg, adapted from Apple Maps [30].	56
5.2	Steps of construction.	61
5.3	Map of Bretagne with proposed MRE ports Brest and Lorient [32].	61
5.4	Map of Lorient (left) with the proposed yard (top right) and access channel width (bottom right), adapted from Navionics [34].	62
5.5	Map of Bay of Brest with proposed yard in green in the top right, adapted from Navionics [36].	63
5.6	Map of Brest construction yard with preliminary layout for 15 and 30 MW X1 Wind PivotBuoy, adapted from Navionics [36].	64
5.7	Map of possible marshalling anchorages near Brest, adapted from Navionics [36]. .	65
5.8	Map of possible emergency anchorages near site, adapted from Navionics [34]. . . .	66
5.9	Installation sequence: 1) Foundation, 2) Tendons & Pivot Base, 3) Floater [29]. . .	68
5.10	Maintenance strategies.	69
5.11	Failure rates of components identified by Carroll et al. [55].	70
5.12	Weather window available for installation.	72
5.13	Results of life cycle analysis.	73
6.1	Comparison of 15 MW IEA Wind Turbine Positions.	77
6.2	Comparison of Wind Turbine Positions.	78
6.3	Histogram alignment for misalignment [$^{\circ}$] and wind speed [m/s].	81
6.4	AEP of individual wind turbine.	82
6.5	AEP distribution based on wind speeds and directions.	82
6.6	Extrapolated costs from reference projects to find cost 30 MW nacelle.	92
6.7	Fitted costs from reference projects to find the cost of 30 MW rotors.	92
6.8	Box plot of 90% confidence interval of 15 MW X1 Wind PivotBuoy CAPEX cost components, and total.	98
6.9	Normal distribution of the CAPEX of 15MW solution.	98
6.10	Box plot of 90% confidence interval of 30 MW solution CAPEX cost components, and total.	99
6.11	Normal distribution of the CAPEX of 15MW solution.	99
6.12	Box plot of 90% confidence interval of 15 MW X1 Wind PivotBuoy OPEX cost components, and total.	103
6.13	Box plot of 90% confidence interval of 30 MW PivotBuoy OPEX cost components, and total.	103
6.14	Costs of decommissioning for different turbine sizes and distances to shore, from [87].	104
6.15	Interpolated and extrapolated costs per MW.	105
6.16	Levelized cost of energy for 15MW design.	106
6.17	Levelized cost of energy for 30MW design.	106
6.18	Comparisson of the mean LCOE for the three wind farm designs.	107
6.19	Conclusion economic evaluation.	107

7.1	Natural frequencies structure (vert. lines) compared to present spectra. Important: the one nat. freq. in the 6P region does not have deflections in the masts and thus will not form a structural problem.	110
7.2	Comparison between the 15 MW X1 Wind PivotBuoy and 30 MW solution LCOE.	113
A.1	Deficit along center line from different models, [10].	121

List of Tables

2.1	15 MW IEA Reference Wind Turbine Parameters [13, 12].	7
2.2	15 MW X1 Wind PivotBuoy Wind Turbine Parameters [5], [15].	10
2.3	30 MW DWT Parameters, dimensions determined in section 4.1.	12
3.1	Annual direction of sample distribution (%) [16].	14
3.2	Return period of significant wave height.	15
3.3	Return period of zero-crossing period.	16
3.4	Annual direction of sample distribution (%) [16].	18
4.1	Overview parameters.	21
4.2	Dimension results from preliminary design.	23
4.3	Pitch, roll and yaw moment of inertias.	25
4.4	Movement boundaries of the platform.	26
4.5	DLC 6.1 wind and waves input.	27
4.6	DLC 1.6 wind, waves and current input.	27
4.7	DLC 1.2 wind, waves and current input.	27
4.8	Surface roughness for different materials.	30
4.9	Hydrodynamic drag coefficients for different members for different load cases.	30
4.10	Simulation results from DLC 6.1.	32
4.11	Simulation results from DLC 1.6.	32
4.12	Simulation results DLC 1.2.1.	32
4.13	Simulation results DLC 1.2.2.	33
4.14	Point masses present in model.	34
4.15	Added mass present in model.	35
4.16	Diameters of the respective cross-sections.	36
4.17	Properties of the elements.	37
4.18	Maximum forces acting on the structural elements in the combined swell and wind wave conditions.	44
4.19	Maximum Stresses for different components.	47
4.20	Comparison of unity check for the Combined axial forces and moments between the standard and proposed improvement method models.	48
4.21	Comparison of unity check for the Combined axial forces and moments between the standard and proposed improvement method models.	48
4.22	Applied loads for 30 MW WT.	52
4.23	Factors for bearing fatigue.	52
5.1	Components analyzed in industrialization plan.	56
5.2	Component rating comparison for 15 MW X1 Wind PivotBuoy [29] and 30 MW solution.	60
5.3	Port of Brest information [35].	63
5.4	Speeds of vessels in knots.	66
5.5	Distances between locations in km [34, 36].	67
5.6	Major replacements per component per turbine per year, adapted from [55, 56].	70

5.7	Weather windows with alpha 0.78 for waves and 0.8 for wind.	73
6.1	Prices of Energy.	76
6.2	Parameters for optimization of 15 MW turbine.	76
6.3	Parameters for optimization of 30 MW turbine.	77
6.4	Influence of mean yaw misalignment on AEP for the IEA 15 MW wind farm. . . .	78
6.5	Misalignment [°] under wind [m/s] - current [m/s] offset.	80
6.6	AEP estimation.	81
6.7	15 MW IEA Turbine CAPEX.	83
6.8	15 MW IEA Foundation CAPEX.	84
6.9	15 MW IEA BoP CAPEX.	84
6.10	15 MW IEA I&C CAPEX.	85
6.11	15 MW IEA CAPEX.	85
6.12	Substructure costs 15 MW X1 Wind PivotBuoy (R&D TotalEnergies internal information, 2023).	86
6.13	Imported elements.	88
6.14	Used transportation vessels.	88
6.15	Needed ships.	89
6.16	All needed characteristics for installation of TLP and turbine.	89
6.17	Condensed lifting table Liebherr 13000 [76].	90
6.18	Elements to be lifted for 15 MW.	90
6.19	15 MW X1 Wind PivotBuoy CAPEX.	91
6.20	Nacelle costs used to extrapolate 30 MW nacelle.	91
6.21	Rotor costs used to apply a curve to find 30 MW rotor.	92
6.22	Substructure costs 30 MW PivotBuoy (R&D TotalEnergies internal information, 2023).	93
6.23	Characteristics of array cables (R&D TotalEnergies internal information, 2023). . .	94
6.24	Characteristics for installation of TLP and turbine for 30 MW solution.	95
6.25	Condensed lifting table Sarens 250 [80].	96
6.26	Elements to be lifted for 30 MW.	96
6.27	30 MW solution CAPEX.	97
6.28	Comparison between CAPEX of wind farms.	97
6.29	15 MW IEA OPEX parameters.	100
6.30	Comparison of OPEX of three 450 MW wind farm designs in € per year.	102
6.31	Comparison of ABEX of three 450 MW wind farm designs.	105
7.1	Base characteristics of 30 MW solution used for structural analysis.	109
7.2	Dimension results from preliminary design.	109
7.3	Simulation results DLC 6.1 (most critical load case).	110
7.4	Comparison of unity check for the Combined axial forces and moments between the standard and proposed improvement method models.	110
7.5	Final dimensions for the turret.	111
7.6	CAPEX & OPEX & ABEX of a 450 MW wind farm.	112
7.7	AEP estimation for the three platform configurations in a 450 MW farm.	112
7.8	Influence of mean yaw misalignment on AEP for the IEA 15 MW wind farm. . . .	112
C.1	Types of primary and secondary bearing failures.	139
D.1	Location of joints final design.	140

Bibliography

- [1] TotalEnergies. *A Net Zero Company by 2050, Together With Society*. 2023. URL: <https://totalenergies.com/company/transforming/ambition/net-zero-2050>.
- [2] U.S. Department of Energy, Office of Energy Efficiency and Renewable Energy. *Offshore Wind Market Report: 2022 Edition*. U.S. Department of Energy, Office of Energy Efficiency and Renewable Energy, 2022. URL: <https://www.example.com/wind-energy-report-2022>.
- [3] H.J. Wagner and J. Mathur. “Design Considerations”. In: *Introduction to Wind Energy Systems: Basics, Technology and Operation*. Berlin, Heidelberg: Springer Berlin Heidelberg, 2013. DOI: 10.1007/978-3-642-32976-0_5. URL: https://doi.org/10.1007/978-3-642-32976-0_5.
- [4] A.M. Eltamaly, M.A. Mohamed, and A.G. Abo-Khalil. “Maximum Power Point Tracking Strategies of Grid-Connected Wind Energy Conversion Systems”. In: *Control and Operation of Grid-Connected Wind Energy Systems*. Ed. by A.M. Eltamaly, A.Y. Abdelaziz, and A.G. Abo-Khalil. Cham: Springer International Publishing, 2021, pp. 193–225. ISBN: 978-3-030-64336-2. DOI: 10.1007/978-3-030-64336-2_8. URL: https://doi.org/10.1007/978-3-030-64336-2_8.
- [5] PivotBuoy and X1 Wind. *D2.5: Preliminary design for 10-20MW systems*. Tech. rep. H2020-LC-SC3-RES-11-2018. PivotBuoy, 2022. URL: https://pivotbuoy.eu/wp-content/uploads/2023/05/PB_D2.5_Preliminary-design-for-10-20MW-systems_V1.1_sent.pdf.
- [6] 4C Offshore. *Global Offshore Renewable Map*. 2023. URL: <https://map.4coffshore.com/offshorewind/>.
- [7] C. Lamiroux. *Floating Offshore Wind Turbines in the Bay of Biscay*. 2023. URL: <https://www.ogj.com/home/article/17217122/operators-renewing-exploration-in-offshore-basins-of-france>.
- [8] Bretagne Ocean Power. *Bretagne a strategic location in the heart of Offshore Wind & Marine Energies Market*. 2022. URL: <https://bretagneoceanpower.fr/wp-content/uploads/2022/08/plaquette-emr-2022-page-a-page.pdf>.
- [9] R. Riva et al. *Welcome to TOPFARM*. 2018. URL: <https://topfarm.pages.windenergy.dtu.dk/TopFarm2/index.html>.
- [10] M.M. Pedersen et al. *PyWake 2.5.0: An open-source wind farm simulation tool*. Feb. 2023. URL: <https://gitlab.windenergy.dtu.dk/TOPFARM/PyWake>.
- [11] OpenFAST. *OpenFAST documentation*. URL: <https://openfast.readthedocs.io/en/main/>.

- [12] E. Gaertner et al. *Definition of the IEA 15-Megawatt Offshore Reference Wind Turbine*. Tech. rep. International Energy Agency, 2020. URL: <https://www.nrel.gov/docs/fy20osti/75698.pdf>.
- [13] C. Allen et al. *Definition of the UMaine VoltturnUS-S Reference Platform Developed for the IEA Wind 15-Megawatt Offshore Reference Wind Turbine*. Tech. rep. International Energy Agency, 2020. URL: <https://www.nrel.gov/docs/fy20osti/76773.pdf>.
- [14] G. Wanke et al. “Redesign of an upwind rotor for a downwind configuration: design changes and cost evaluation”. In: *Wind energy science* 6.1 (Feb. 2021), pp. 203–220. DOI: 10.5194/wes-6-203-2021. URL: <https://doi.org/10.5194/wes-6-203-2021>.
- [15] L. Trezza. *PivotBuoy weathervaning floating technology: benefits, drawbacks and comparison to a standard semi-sub*. 2023.
- [16] O. Thilleul and Y. Perignon. *SEM-REV Metocean design basis*. Tech. rep. Centrale Nantes SEM-REV - LHEEA, 2022.
- [17] E. Oberg et al. *Machinerys Handbook*. Industrial Press Inc, 2016, p. 238.
- [18] G. Hassan. *Tip Speed Trends*. URL: <https://www.wind-energy-the-facts.org/tip-speed-trends.html>.
- [19] DNV. *Environmental conditions and environmental loads*. Tech. rep. DNV-RP-C205. DNV, 2010. URL: https://www.researchgate.net/publication/276069456_New_DNV_Recommended_Practice_DNV-RP-C205_on_Environmental_Conditions_and_Environmental_Loads.
- [20] M. Bohm et al. “Optimization-based calibration of hydrodynamic drag coefficients for a semisubmersible platform using experimental data of an irregular sea state”. In: (2020).
- [21] WEAMEC. *HP_Flow: heaveplates modelling for floating wind*. URL: https://www.weamec.fr/en/projects/hp_flow/.
- [22] DSA Ocean. *Why the added mass force can be confusing*. 2023. URL: <https://dsaocean.com/now-you-see-me/>.
- [23] S.M. Vazirizade. “An Intelligent Integrated Method for Reliability Estimation of Offshore Structures Wave Loading Applied in Time Domain”. In: (2019).
- [24] N.M.C. Dacunha, N. Hogben, and K.S. Andrews. “Wave climate synthesis worldwide”. In: *Wave Climate Syn. using NMINET: A Trilogy of Published Papers 11 p(SEE N 84-28127 18-42)* (1984).
- [25] X.K. Zou et al. “Design and Construction of High-Performance Long-Span Steel Transfer Twin Trusses Applied in One Hospital Building in Hong Kong”. In: *Buildings* 13.3 (2023). ISSN: 2075-5309. DOI: 10.3390/buildings13030751. URL: <https://www.mdpi.com/2075-5309/13/3/751>.
- [26] C. Casanovas Bermejo, S. Canedo Pardo, and S. González Poveda. *A quick connector coupling an offshore floating structure to a pre-laid mooring system and a method therefor*. May 2023. URL: <https://patentimages.storage.googleapis.com/d7/0e/5f/ca8207a413a485/W02023084375A1.pdf>.
- [27] Jtekt. *Large Size Ball & Roller Bearings (Technical Section)*. 2022.
- [28] Afnor. *NF ISO 76*. 2006.

- [29] Intecsea BV, PivotBuoy, and X1 Wind. *D3.5: Industrialization plan for serial production of large farms*. Tech. rep. H2020-LC-SC3-RES-11-2018. PivotBuoy, 2022. URL: <https://pivotbuoy.eu/wp-content/uploads/2023/05/D3.5-Industrialization-plan-for-serial-production-of-large-farms.pdf>.
- [30] Apple Maps. *Cherbourg, France*. 2023. URL: https://satellites.pro/France_map#49.649383,-1.598216,18.
- [31] R. Millard. *Wind power industry faces size problem as blades get longer than football pitches*. 2023. URL: <https://www.ft.com/content/565c21bf-25a0-4fc6-9f47-c7483671d43a>.
- [32] Bretagne Ocean Power. *2 ports in the core of 6GW of new French wind farms*. 2023. URL: <https://bretagneoceanpower.fr/en/bretagne-mre/ports/?cn-reloaded=1>.
- [33] Bretagne Ocean Power. *MRE Port of services of Lorient*. 2022. URL: https://bretagneoceanpower.fr/wp-content/uploads/2022/08/2204082-bdi-emr-seanergy-2022-fiche-port_lorient_v5.pdf.
- [34] Navionics. *Lorient, France*. 2023. URL: <https://webapp.navionics.com/?lang=en#boating@14&key=axebH~apS>.
- [35] Bretagne Ocean Power. *Port of Brest MRE Terminal*. 2022. URL: <https://bretagneoceanpower.fr/wp-content/uploads/2022/08/brest-et-lorient.pdf>.
- [36] Navionics. *Brest, France*. 2023. URL: <https://webapp.navionics.com/#boating@11&key=%7BtcfHpupZ>.
- [37] MHPA. 2021. URL: <https://www.mhpa.co.uk/media/gavmx12p/towage-guidelines-2021.pdf>.
- [38] NGA. *Sailing Directions (Enroute): WEST COAST OF EUROPE AND NORTHWEST AFRICA*. Tech. rep. Pub. 143. NGA, 2022. URL: <https://msi.nga.mil/api/publications/download?key=16694491/SFH00000/Pub143bk.pdf&type=view>.
- [39] M.A. El-Reedy. “Chapter 5 Fabrication and Installation”. In: *Offshore Structures*. Ed. by M.A. El-Reedy. Boston: Gulf Professional Publishing, 2012, pp. 293–381. ISBN: 978-0-12-385475-9. DOI: <https://doi.org/10.1016/B978-0-12-385475-9.00005-5>. URL: <https://www.sciencedirect.com/science/article/pii/B9780123854759000055>.
- [40] R.C. Ramachandran et al. “Floating offshore wind turbines: Installation, operation, maintenance and decommissioning challenges and opportunities”. In: 2021. URL: <https://api.semanticscholar.org/CorpusID:239950685>.
- [41] BVG Associates. *Guide to a floating offshore wind farm*. Tech. rep. BVG Associates, 2023. URL: <https://guidetofloatingoffshorewind.com/>.
- [42] C. Le et al. “Towing Performance of the Submerged Floating Offshore Wind Turbine under Different Wave Conditions”. In: *Journal of Marine Science and Engineering* 9.6 (2021). ISSN: 2077-1312. DOI: 10.3390/jmse9060633. URL: <https://www.mdpi.com/2077-1312/9/6/633>.
- [43] PivotBuoy and WavEC - Offshore Renewables. *D6.4: Optimal maintenance strategies for single point mooring systems*. Tech. rep. H2020-LC-SC3-RES-11-2018. PivotBuoy, 2019. URL: <https://pivotbuoy.eu/wp-content/uploads/2020/01/D6.4-Optimal-maintenance-strategies-for-single-point-mooring-systems.pdf>.

- [44] PivotBuoy and PLOCAN. *D4.6: Recommendations for the installation and operation of floating systems*. Tech. rep. H2020-LC-SC3-RES-11-2018. PivotBuoy, 2023. URL: https://pivotbuoy.eu/wp-content/uploads/2023/05/D4.6_Recommendations-for-the-installation-and-operation.pdf.
- [45] Bourbon Offshore. *Bourbon Theia*. 2008. URL: <https://www.bourbonoffshore.com/sites/default/files/documents-associés/pdf/ahts-bourbon-theia.pdf>.
- [46] United Offshore Support. *UT vessel specification*. 2020. URL: <https://uos.ag/wp-content/uploads/2020/08/UT-Vessel-Specification.pdf>.
- [47] Y. Dalgic, I. Lazakis, and O. Turan. “Investigation of Optimum Crew Transfer Vessel Fleet for Offshore Wind Farm Maintenance Operations”. In: *Wind Engineering* 39.1 (2015), pp. 31–52. ISSN: 0309524X, 2048402X. URL: <https://www.jstor.org/stable/90006858> (visited on 10/24/2023).
- [48] TGS. *An introduction to crew transfer vessels*. 2023. URL: <https://www.4coffshore.com/support/an-introduction-to-crew-transfer-vessels-aid2.html>.
- [49] B. Cerfontaine et al. “Anchor geotechnics for floating offshore wind: Current technologies and future innovations”. In: *Ocean Engineering* 279 (July 2023), p. 114327. DOI: 10.1016/j.oceaneng.2023.114327.
- [50] M.G. Deighton. “Chapter 5 - Maintenance Management”. In: *Facility Integrity Management*. Ed. by M.G. Deighton. Boston: Gulf Professional Publishing, 2016, pp. 87–139. ISBN: 978-0-12-801764-7. DOI: <https://doi.org/10.1016/B978-0-12-801764-7.00005-X>. URL: <https://www.sciencedirect.com/science/article/pii/B978012801764700005X>.
- [51] L. Mishnaevsky. “Maintenance and repair of wind turbine blades”. English. In: *Advances in Wind Turbine Blade Design and Materials*. Ed. by Povl Brøndsted, Stergios Goutianos, and Rogier Nijssen. 2nd. Woodhead Publishing Series in Energy. United Kingdom: Elsevier, 2023, pp. 475–484. DOI: 10.1016/B978-0-08-103007-3.00003-3.
- [52] N.A.J. Hastings. “Maintenance Organization and Budget”. In: *Physical Asset Management: With an Introduction to ISO55000*. Cham: Springer International Publishing, 2015, pp. 317–341. ISBN: 978-3-319-14777-2. DOI: 10.1007/978-3-319-14777-2_19. URL: https://doi.org/10.1007/978-3-319-14777-2_19.
- [53] Z. Li, K. Wang, and Y. He. “Industry 4.0 - Potentials for Predictive Maintenance”. In: Jan. 2016. DOI: 10.2991/iwama-16.2016.8.
- [54] C. Okoh, R. Roy, and J. Mehnen. “Predictive Maintenance Modelling for Through-Life Engineering Services”. In: *Procedia CIRP* 59 (2017), pp. 196–201. ISSN: 2212-8271. DOI: <https://doi.org/10.1016/j.procir.2016.09.033>. URL: <https://www.sciencedirect.com/science/article/pii/S2212827116309726>.
- [55] J. Carroll, A. McDonald, and D. Mcmillan. “Failure rate, repair time and unscheduled O&M cost analysis of offshore wind turbines”. In: *Wind Energy* 19 (Aug. 2015). DOI: 10.1002/we.1887.
- [56] J.M.P. Pérez et al. “Wind turbine reliability analysis”. In: *Renewable & Sustainable Energy Reviews* 23 (July 2013), pp. 463–472. DOI: 10.1016/j.rser.2013.03.018. URL: <https://doi.org/10.1016/j.rser.2013.03.018>.
- [57] S.M. Maxwell et al. “Potential impacts of floating wind turbine technology for marine species and habitats”. In: *Journal of Environmental Management* 307 (2022), p. 114577. ISSN: 0301-

4797. DOI: <https://doi.org/10.1016/j.jenvman.2022.114577>. URL: <https://www.sciencedirect.com/science/article/pii/S0301479722001505>.
- [58] R. Lacal Arantegui, J. Yusta, and J.A. Domínguez Navarro. “Offshore wind installation: Analysing the evidence behind improvements in installation time”. In: *Renewable and Sustainable Energy Reviews* 92 (Sept. 2018). DOI: 10.1016/j.rser.2018.04.044.
- [59] EPEX. *Market Data Continuous Energy Prices Sep 14 2023*. Sept. 2023. URL: https://www.epexspot.com/en/market-data?market_area=FR&trading_date=&delivery_date=2023-09-14&underlying_year=&modality=Continuous&sub_modality=&technology=&product=60&data_mode=graph&period=month&production_period=.
- [60] Haya Energy Solutions. *French Market Analysis - Haya energy Solutions*. Sept. 2023. URL: <https://hayaenergy.com/french-power-and-gas-markets-analysis/>.
- [61] Trading Economics. *France Electricity price - 2023 data - 2011-2022 historical - 2024 forecast - quote*. Sept. 2023. URL: <https://tradingeconomics.com/france/electricity-price>.
- [62] A. Hernandez. *TotalEnergies defends price paid for German offshore wind lease*. July 2023. URL: <https://www.reuters.com/business/energy/totalenergies-defends-price-paid-german-offshore-wind-lease-2023-07-27/>.
- [63] SRD. *France: electricity price 2023 monthly | Statista*. Sept. 2023. URL: <https://www.statista.com/statistics/1267546/france-monthly-wholesale-electricity-price/#statisticContainer>.
- [64] S. Netzband, C.W. Schulz, and M. Abdel-Maksoud. “Passive self-aligning of a floating offshore wind turbine”. In: *Journal of Physics: Conference Series* 1618.5 (2020), p. 052027. DOI: 10.1088/1742-6596/1618/5/052027.
- [65] J. Cruse et al. “Design of Floating Offshore Wind Turbine (FOWT)”. In: (Nov. 2020), pp. 55–67. DOI: 10.1007/978-981-15-8350-6_5.
- [66] J. Fernando. “Capital Expenditure (CAPEX) Definition, Formula, and Examples”. In: *Investopedia* (May 2023). URL: <https://www.investopedia.com/terms/c/capitalexpenditure.asp>.
- [67] Bloomberg. *GBP to EUR exchange rate (2023 September 18)*. Sept. 2023. URL: <https://www.bloomberg.com/quote/GBPEUR:CUR#xj4y7vzkg>.
- [68] BVG Associates. *Guide to an offshore wind farm*. 2019. URL: <https://guidetoanoffshorewindfarm.com/wind-farm-costs>.
- [69] Pfeifer. *Wire ropes technical information*. Tech. rep. Pfeifer, 2018. URL: https://www.pfeifer.info/out/assets/PFEIFER_WIRE-ROPES-TECHNICAL-INFO_PPEN.PDF.
- [70] J. Wagner. *Research on armour units breakwaters IJmuiden, The Netherlands*. Tech. rep. TU Delft, 2004. URL: <https://repository.tudelft.nl/islandora/object/uuid:19aac834-9022-4d01-85b1-46806b3f796c/datastream/OBJ>.
- [71] Mammoet. *Jacket Handling for offshore wind projects*. 2023. URL: <https://www.mammoet.com/offshore-wind/jacket-handling/>.
- [72] Z. Jiang. “Instalation of offshore wind turbines: a technical review”. In: *Renewable and Sustainable Energy Reviews* (Nov. 2020). URL: <https://www.sciencedirect.com/science/article/pii/S1364032120308601>.

- [73] Tsuneishi Shipbuilding. *1091 TEU Type Container Carrier*. 2023. URL: <https://www.tsuneishi.co.jp/english/products/1091teu/>.
- [74] Australian Competition and Consumer Commission. *Container stevedoring monitoring report*. Tech. rep. 978 1 920702 38 0. ACCC, 2018. URL: https://www.accc.gov.au/system/files/1465_Container%20stevedoring%20monitoring%20report%202017-18_D08.pdf.
- [75] R. Bosnjak et al. “Concept Of Present Practice In Choosing Of Optimal Number Of Tugs”. In: *Pedagogika-Pedagogy* 93 (Sept. 2021), pp. 7–21. DOI: 10.53656/ped21-7s.01conc.
- [76] Liebherr. *The most powerful of its type, L13000*. Tech. rep. Liebherr, 2021. URL: <https://www.liebherr.com/external/products/products-assets/65ddddd8-9f35-49db-be08-3190d90f2c49-2/liebherr-195-1r-13000-1.0-td-195-02-defisr07-2022.pdf>.
- [77] Accel. *MOBILE CRANE / CRAWLER CRANE*. Tech. rep. Accel, 2023. URL: <https://accel.a-tems.com/mobile-crane-crawler-crane/>.
- [78] L. Fingersh. *Wind Turbine Design Costand Scaling Model*. Tech. rep. NREL, 2006. URL: <https://www.nrel.gov/docs/fy07osti/40566.pdf>.
- [79] S. Johnson. *A design-driven wind blade manufacturing model to identify opportunities to reduce wind blade costs*. Tech. rep. NREL, 2023. URL: <https://doi.org/10.1016/j.renene.2023.118945>.
- [80] Sarens. *Sarens Giant Cranes*. 2023. URL: https://www.sarens.com/pdf_brochures/equipment_giant.pdf.
- [81] W. Kenton. “Operating Expense (OPEX) definition and Examples”. In: *Investopedia* (Aug. 2023). URL: https://www.investopedia.com/terms/o/operating_expense.asp.
- [82] G. Katsouris and A.J. Marina. *Cost Modelling of Floating Wind Farms*. Tech. rep. ECN-E-15-078. ECN Wind Energy, 2016. URL: <https://publications.ecn.nl/ECN-E--15-078>.
- [83] Y. Liu et al. “Developments in semi-submersible floating foundations supporting wind turbines: A comprehensive review”. In: *Renewable & Sustainable Energy Reviews* 60 (July 2016), pp. 433–449. DOI: 10.1016/j.rser.2016.01.109. URL: <https://doi.org/10.1016/j.rser.2016.01.109>.
- [84] M. Leimeister, A. Kolios, and M. Collu. “Critical review of floating support structures for offshore wind farm deployment”. In: *Journal of physics* 1104 (Oct. 2018), p. 012007. DOI: 10.1088/1742-6596/1104/1/012007. URL: <https://doi.org/10.1088/1742-6596/1104/1/012007>.
- [85] PivotBuoy and WavEC Offshore Renewables. *D5.4 Benchmark of PivotBuoy Compared to Other Floating Systems*. Tech. rep. H2020-LC-SC3-RES-11-2018. PivotBuoy, 2021. URL: <https://pivotbuoy.eu/wp-content/uploads/2021/06/D5.4-Benchmark-of-PivotBuoy-versus-other-floating-systems-v1.1.pdf>.
- [86] Petrobangla. *Offshore Model Production Sharing Contract*. Tech. rep. Petrobangla, 2019. URL: <https://www.lawinsider.com/dictionary/abandonment-costs>.
- [87] TNO. *Offshore wind farm decommissioning*. Tech. rep. TNO.
- [88] M. Sølvik, B. Nergård, and M.C. Ramstad. *Tool development for LCOE calculation for floating offshore wind*. 2022. URL: <https://hdl.handle.net/11250/3002197>.

- 
- [90] C. Moné. Tech. rep. National Renewable Energy Laboratory, 2015. URL: <https://www.nrel.gov/docs/fy16osti/64281.pdf>.
- [91] N.O. Jensen. *A note on wind generator interaction*. English. Risø-M 2411. Risø National Laboratory, 1983. ISBN: 87-550-0971-9.
- [92] M. Bastankhah and F. Porté-Agel. “A new analytical model for wind-turbine wakes”. In: *Renewable Energy* 70.C (2014), pp. 116–123. DOI: 10.1016/j.renene.2014.01.. URL: <https://ideas.repec.org/a/eee/renene/v70y2014icp116-123.html>.
- [93] S. Ott and M. Nielsen. *Developments of the offshore wind turbine wake model Fuga*. English. DTU Wind Energy E 0046. Denmark: DTU Wind Energy, 2014.